TIDAL DISTORTION OF A NEUTRON STAR IN THE VICINITY OF A BLACK HOLE

by

M NAIDOO

submitted in part fulfilment of the requirements
for the degree of

MASTER OF SCIENCE

in the subject

APPLIED MATHEMATICS

at the

UNIVERSITY OF SOUTH AFRICA

SUPERVISOR: PROF NT BISHOP

JOINT SUPERVISOR: PROF WM LESAME

NOVEMBER 2007

Contents

Abstract

We will consider the scenario of the co-rotation of a fluid star (in specific, a neutron star) and a black hole. The neutron star (or primary) is assumed to have constant angular velocity. The tidal effects on the primary are investigated. First, the *centrally condensed approximation* is applied, where both bodies are considered as point sources. In the second treatment, the primary is treated as an incompressible and homogeneous fluid mass, which in addition to its own gravity is subject to centrifugal and Coriolis forces, derived from fluid motions. The black hole (or secondary) is treated as a rigid sphere and can be regarded as a point mass. The equilibrium figure is derived. The problem is then adapted to include vorticity and a pseudo-Newtonian potential. The coalescence of neutron star - black hole binaries and their importance to gravitational wave detection is also discussed.

keywords: tidal distortion - binary stars - neutron star - black hole - virial method - Roche ellipsoid.

1 Introduction

1.1 Previous Work on Binary Systems

The problem of the tidal influence of a gravitating source on a satellite was first formulated in (1847 - 1850) by the French Mathematician Edouard Albert Roche (1820 - 1883). Roche considered the effect of a neighbouring mass on a self gravitating uniformly homogeneous body of idealized fluid subject to the action of its own gravity, centrifugal forces and Coriolis forces. He showed that there was an upper limit to the orbital angular velocity ($\mathbf{\Omega}$) above which there were no possible equilibrium figures. This limit sets in turn a lower limit on the orbital radius (R) (for the circular Keplerian orbit) below which no figures are possible. The lower limit on R is called the *Roche limit*. The effect of the neighbouring mass is referred to as the *tidal force*. The name has come from its application to the tides on the Earth. The earth tends to be elongated along the line toward (and away from) the centre of the moon. The rigidity of the Earth's crust is strong enough to prevent bulging in response to the tidal force. However a fluid does not show the same rigidity and where the Earth is covered with water, we find that a tidal effect is noticeable. This effect is what we call ocean tides. The tides are

strongest at the side facing the moon and naturally magnified if the three bodies : the Sun, the Moon and the Earth lie in approximately the same straight line (Full Moon and New Moon) We expect that these effects will be more pronounced for a gaseous sphere (such as a neutron star, modelled as an ideal fluid) in the vicinity of a far more massive body (a black hole).

The roots of the Roche formulation go back much further, though, to Isaac Newton in his *Philosophiae Naturalis Principia Mathematica*[1] which appeared in 1687. It is here that we see the first investigation of the gravitational equilibrium of homogeneous uniformly rotating masses. Newton considered two slender canals of homogeneous fluid, one along the polar radius of the earth, and the other along an equatorial radius. Newton concluded that the two columns would have to be balanced, i.e. be in equilibrium. For this to happen, the weight of the equatorial column must equal the weight of the polar column. According to Todhunter's *History of the Mathematical Theories of Attraction and Figure of the Earth*, Newton's calculation found that 'the centrifugal force at the equator is to the force at the attraction there as 1 to 289' (2nd ed. of *Principia*). He then concluded that 'the resultant attraction on the equatorial canal must be greater than that along the polar canal in the ratio of 289 to 288 in order that there be relative equilibrium.'

[1]Mathematical Principles of Natural Philospohy (Latin)

He argued that proceeding along any given radius inside the earth, the attraction varies as the distance and the centrifugal force varies as the distance; hence the ratio of the latter to the former is constant along the equatorial radius; so that the effect of the centrifugal force may be considered equivalent to removing $\frac{1}{289}$ of the force of attraction. His next step was to compare the attraction of an oblate ellipsoid of revolution on a particle at its pole with the attraction of the same body on a particle at its equator, the ellipticity assumed to be very small. From this comparison, Newton's calculations led him to conclude that if the earth were homogeneous and its shape the same as if it were entirely fluid, the ellipticity, ϵ, must be $\frac{5}{4}$ of the ratio of the centrifugal force to the attraction at the equator, that is,

$$\epsilon = \frac{5}{4}\frac{1}{290} \approx \frac{1}{230}. \tag{1}$$

Newton's predictions contradicted the prevailing astronomical evidence of the time. His predictions were contrary to those of Cassinis, who held that the Earth would be prolate, and so led to the development of two different schools of thought.

We know now that the Earth is oblate, as Newton predicted, but with ellipticity of $\frac{1}{294}$ and we can say with confidence that the Earth is not homogeneous. Newton did consider that if the Earth, instead of being of uniform

density, were denser towards the centre than towards the surface, the ellipticity would be increased. Here Newton was wrong. Fifty years later Clairaut, in his *Figure de la Terre*[2], points out Newton's mistake. If we were to assume the original fluidity of the Earth, the ellipticity is decreased by increasing the density of the central part, supposed spherical and making it solid. The result of Newton, though, remains very important in theory of the subject. As written in Todhunter, 'Newton's investigations in the theories of Attraction and of the Figure of the Earth may justly be considered worthy of his name. The propositions on Attraction are numerous, exact and beautiful; they reveal his ample mathematical power. The treatment of the Figure of the Earth is, however still more striking; inasmuch as the successful solution of a difficult problem in natural philosophy is much rarer than profound researches in abstract mathematics.'

Maclaurin extended Newton's result in 1742 to the case when the ellipticity caused by the rotation cannot be considered small. Although Maclaurin did not establish that a rapidly rotating figure will necessarily take the figure of an oblate spheroid he did show :

1. 'that the force which results from the attraction of the spheroid and

[2]Figures of the Earth (French)

those extraneous powers compounded together always act in a right line perpendicular to the surface of the spheroid,

2. that the columns of the fluid sustain or balance each other at the centre of the spheroid, and

3. that any particle in the spheroid is impelled equally in all directions.'

Later, Thomas Simpson, in 1743, noted that for any rotational angular velocity, $\mathbf{\Omega}$, there are two and only two possible 'oblata' resulting from Maclaurin's relations. In the limit $\Omega \to 0$, one solution tends to a spheroid of small eccentricity ($\epsilon \to 0$) and in the limit $\Omega \to \infty$ the second solution tends to a highly flattened spheroid ($\epsilon \to 1$).

These Maclaurin's spheroids remained unchallenged as the only admissible solutions to the problem of the equilibrium of uniformly rotating masses. The investigations of Jacobi (1834) led him to conclude, 'ellipsoids with three unequal axes can very well be figures of equilibrium; and that one can assume an ellipse of arbitrary shape for the equatorial section and determine the third axis (which is also the least of the three axes) and the angular velocity of rotation such that the ellipsoid is a figure of equilibrium,' as noted in Todhunter (1873).

In 1856-7, Dirichlet considered the conditions required for a configuration to have, at every instant, an ellipsoidal figure and in which the motion (in an inertial frame) is a linear function of the coordinates. Dirichlet formulated the general equations governing this problem but only provided solutions to the case where the bounding surface is a spheroid of revolution. This work was edited and published posthumously by Dedekind, who investigated further the admissible figures of equilibrium under the general conditions of Dirchlet's formulation. These led to solutions referred to as the *ellipsoids of Dedekind*. Although these figures are congruent to the Jacobi ellipsoids, they are stationary in an inertial frame and the prevailing internal motions maintain their ellipsoidal figures.

Riemann, later, gives the complete solution of the stationary figures admissible under Dirichlet's general assumptions. He shows that ellipsoidal figures of equilibrium are only possible for each of three cases :

1. The rotation is uniform with no internal motions.

   This leads to sequences of Maclaurin and Jacobi.

2. The directions of $\mathbf{\Omega}$ and vorticity ξ coincide with the principal axis of the ellipsoid.

   These 'Riemann sequences' of ellipsoids are obtained for each of which

the ratio $f = \xi/\Omega$ remains constant.

In the limit for $f = 0$ we obtain the special case of the Jacobian sequence, and in the limit $f \to \infty$ we have the Dedekind sequence.

3. The directions of $\mathbf{\Omega}$ and ξ lie in a principal plane of the ellipsoid.

   Three new classes of ellipsoids are obtained for this case. They are specified according to their domain of occupancy. in the (a_1, a_2, a_3)-space, where the (a_1, a_2, a_3) refer to the axes corresponding to the semi-axes of the ellipsoid.

Riemann extended his investigation, by attempting to determine the stability of the figures by using an energy criterion, but his criterion is shown to be false by Lebovitz (Chandrasekhar, 1969).

A number of questions remained unsolved in the partial solution of Dirichlet's general problem, together with the question of the relation between the Riemann ellipsoids and the Maclaurin spheroids. This situation remained for about a century mainly due to all subsequent investigations over the next seventy-five years following a flawed diversion. A 'spectacular discovery' by Poincaré in 1885 led to an unexpected turn of investigations which remained undiverted for over 75 years. It is not necessary to elaborate on this turn of events.

Chandrasekhar's text, *Ellipsoidal Figures of Equilibrium* (1969), provides the most comprehensive review of the analytical works of Maclaurin, Jacobi, Dedekind and Riemann in the equilibrium configurations of rapidly self-gravitating fluid systems. Through his pioneering work employing the tensor virial method, he has provided exact solutions for equilibrium configurations in the incompressible limit. Most of our modern knowledge of these exact triaxial solutions are owed to him. We will include his analysis in a later chapter, in particular for the Roche problem, where we complete some of the details in the calculation. Chandrasekhar's text, apart from its historical review, is based mainly on the series of papers published during the years 1961-1969, which he and Lebovitz authored separately and in collaboration. This text remains the definitive text in the theory and modern day investigation into the equilibrium structures and stability properties of stars perturbed by rotation or tidal fields in close binary systems. The configurations in Chandrasekhar (1969), however, are uniform in density, have figures of equilibrium described by perfect spheroids or ellipsoids, and have simple internal flow linear in the coordinates. It is clear that these models cannot represent realistic astrophysical systems. For rotating stars or galaxies, the density is not uniform and can be highly centrally condensed. Furthermore the internal flow of these self-gravitating systems is non-linear. Also, the equilibrium configuration cannot be represented by perfect quadratic sur-

faces. However, the simplified analytical models in Chandrasekhar (1969) provide some useful general tools to understand the structure and global properties of rotating stars.

Closely following Chandrasekhar's work, Aizenman (1968), extended the classical problem of Roche to the case where motions of uniform vorticity exist within the ellipsoid. He shows that the introduction of such motions lead to the introduction of new types of equilibrium configurations, which he chooses to call the Roche-Riemann ellipsoids. Aizenman's investigation shows that internal motions of uniform vorticity can maintain the equilibrium and the stability of an ellipsoid at points within the Roche Limit. He also raises the question, as did Chandrasekhar, of the behaviour of a Roche ellipsoid when it crosses the Roche Limit. He supposes that the ellipsoid develops internal motions as it moves towards the secondary and that it would branch off the Roche sequence and become a type-S_+ ellipsoid. He suggests further that 'some type of tumbling' occurs.

We can classify the study of the tidal encounters by the different stellar models. The problem is greatly simplified by treating the star as incompressible as is the case in Chandrasekhar (1969). Thus the complicated non-linear partial differential equations governing the evolution of the stellar gas can

be reduced to a set of ordinary differential equations. These are then easy to solve analytically and numerically. This approach has been taken by numerous other researchers using both Newtonian and relativistic tidal fields and for different kinds of orbits of the star (eg. Nduka 1971; Fishbone 1973; Mashoon 1975; Luminet and Carter 1986; Kosovichev and Novikov 1992). This simplification is highly unrealistic when considering tidal effects, as the compressibility can play a major role (Carter and Luminet 1982).

Models allowing for the compressibility of the star were put forward by Lattimer and Schramm (1976) and then by Carter and Luminet (1983, 1985), who proposed what is called the *affine model*. In the decades following Chandrasekhar's work on incompressible binary systems, several powerful numerical schemes enabled binary systems to be constructed without using the ellipsoidal approximation. These include constructions of configurations for both incompressible and compressible binary systems, to obtain deformed self-gravitating stars (see eg. Eriguchi and Hachisu 1983 ; Hachisu and Eriguchi 1984a, 1984b ; Hachisu 1986). Constructing consistent models of stationary configurations of compressible stars such as binary systems with arbitrary spins is still a difficult problem, even with the advances in numerical schemes. Including full general relativity also remains difficult. The models of Hachisu and Eriguchi (1984) and Hachisu (1986) investigated only *synchronised* bi-

nary systems and this was only in Newtonian gravity. Shibata (1997) was able to investigate compressible synchronised binary configurations in post-Newtonian gravity up to highly deformed configurations.

For configurations whose spins are different from the orbital angular velocities, there are only approximate solutions by Lai, Rasio and Shapiro (1993a, 1994a, 1994b). They employed triaxial ellipsoidal polytropes for deformed binary states in Newtonian gravity and discussed their evolutions using approximate equilibria. Using an ellipsoidal energy variational method, formally equivalent to the hydrostatic limit of the affine method used by Carter and Luminet, they presented a new analytical study of the figure of equilibrium for compressible, self-gravitating Newtonian fluids. They considered both uniformly and non-uniformly rotating configurations, with their solutions reducing to those of Chandrasekhar when taken in the incompressible limit. The method replaces the full set of coupled hydrodynamic equilibrium equations (partial differential equations in two or three dimensions) with two or three coupled algebraic equations for the principal axes of the configuration. The most important result obtained through their energy variational method is the identification of a turning point prior to the Roche limit along a binary equilibrium sequence. This turning point is referred to as the secular instability limit r_{sec}. This important instability was not identified

in Chandrasekhar's tensor virial treatment of the problem. The results of Chandrasekhar indicate the onset of instability only at the Roche Limit. He concluded that the Roche solutions remain stable, secularly and dynamically, all the way to the Roche limit, and on reaching that limit, then only become secularly unstable. However, this would be in conflict with Chandrasekhar's own result of the existence of minimum E and J before the Roche limit is reached. The secular instability would lead to energy and angular momentum loss through gravitational radiation, resulting in orbital decay of the system.

Taniguchi and Nakamura (1996) determined the innermost stable circular orbit (ISCO) of black hole-neutron star systems by using a pseudo-Newtonian potential to mimic general relativistic effects. We will follow this work in Chapter 4, completing much of the detailed calculation.

A close binary system such as a black hole (BH) and neutron star (NS) binary (BHNS) must emit gravitational waves (GW). The gravitational waves carry away the angular momentum and energy from the system resulting in their separation decreasing quasi-adiabatically, with the orbit of the system becoming circular. The time scale in which the binary separation decreases is longer than the orbital period (Shapiro and Teukolsky 1983) and so the

evolution of the system due to GW emission can be approximated well by quasi-stationary states until just before the final stage.

Several scenarios exist for the final states of BH-star systems (Kidder, Will and Wiseman 1992, Lai, Rasio and Shapiro 1993a). Studies based on the tidal approximation (the configuration of a Newtonian star around a BH in its relativistic tidal field), classify the fate into two cases (Shibata 1996; Wiggins and Lai 2000; Ishii, Shibata and Mino 2005; Faber et al. 2006). One possibility is the inspiraling on a dynamical time scale as a result of the tidal or the general relativistic (GR) effect. The NS will be swallowed into the BH horizon without tidal disruption before the orbit reaches the innermost stable circular orbit (ISCO) (Wiggins and Lai 2000; Ishii, Shibata and Mino 2005).

The other scenario is Roche lobe overflow, where there is mass transfer from the neutron star to the black hole or the environment. This would be possible if the NS is able to approach a state in which the Roche lobe is filled up without suffering from dynamical instability. Even after Roche overflow, the neutron star and the black hole may remain in a stable binary configuration or at least some amount of matter may orbit around the BH longer than the dynamical time scale (Kochanek 1992, Bildsten and Cutler

1992).

The latter case has been studied with great interest since the outcome of such merging process of compact binary systems may be possible sources of astrophysically important phenomena such as γ-ray bursts (see e.g. Paczýnski 1986). Furthermore, coalescing binary systems are expected to be sources of GW detectable by the ground based interferometric detectors of GW currently coming online : LIGO/VIRGO/TAMA/GEO (see e.g. Bradaschia et al. 1990; Abramovici et al. 1992 ; Thorne 1994). This has provided motivation for the extensive investigations into compact binaries over the last few years.

It is important to obtain stationary states of close binary star systems as they will provide models for compact binary systems just prior to coalescence. Relativistic astrophysicists have tried to solve equilibrium configurations of highly deformed close binary star systems by devising numerical schemes for the binaries. The expected observational data of the GW detectors will be compared against theoretical results. These will provide a large amount of information about the macroscopic quantities of mass and spin of the neutron star as well as microscopic characters such as the equation of state (EOS) and the viscosity (Cutler, et al. 1993; Shibata 1997 ; Baumgarte et al. 1997a,

1998a, 1998b ; Bonazzola, Gourgoulhon and Marck 1997).

In order to simulate coalescing binary systems, initial data first needs to be produced that satisfy the Einstein constraint equations and that are as physically relevant as possible. In the second step, the initial configurations are evolved forward in time. Most of the initial data for coalescing binaries depend on the quasiequilibrium (QE) hypothesis. This assumes that the objects are on exact closed circular orbits, which can only be an approximation since no closed orbits can exist for those systems in general relativity. However, for large separations this is a good approximation (Grandclément 2006). Considerable effort has gone into the study of binary neutron stars (BNS) using this approximation, by Baumgarte et al. 1998a, 1998b; Usui, Uryū and Eriguchi 2000; Uryū and Y. Eriguchi 2000; Gourgoulhon et al. 2001. The QE approach has also been applied to the binary black hole system (BBH) (Pfeiffer, Teukolsky and Cook 2000; Gourgoulhon, Grandclément and Bonazzola 2002; Grandclément, E. Gourgoulhon and S. Bonazzola 2002 and Caudill et al. 2006).

More recently the evolution of BNS mergers have included both fully relativistic gravitation as well as physically realistic equations of state (Shibata, Taniguchi and Uryū 2005; Shibata and Taniguchi 2006). With recent

progress also in the evolution of systems of BBH (Pretorius 2006; Baker et al. 2006; Campanelli et al. 2006) it seems timely to turn interest more towards the study of the NSBH system.

To date, investigations of NSBH binaries have been performed within the framework of Newtonian gravity in either some or all aspects of the calculation for both quasiequilibrium calculations and dynamical simulations. Investigations of NSBH binaries in a fully relativistic framework have only been initiated recently. Studies for quasiequilibrium models have been done by Baumgarte, Skoge, and Shapiro 2004; Taniguchi et al. 2005; Taniguchi et al. 2006 and Grandclément 2006. Dynamical simulations have been conducted by Faber et al 2006b; Sopuerta, Sperhake, and Laguna 2006; Löffler, Rezzolla, and Ansorg 2006; Shibata and Uryū, 2006.

Whilst the quasiequilibrium approximation is a good one for large separation, it becomes less accurate as the distance between the compact objects decreases. Eventually the approximation breaks down necessitating the use of full dynamical simulations. Recently, Bishop et al. (2005), made a first step in this direction in a relativistic context. Their approach showed that the initial spurious GW signal resulting from the approximations in the calculation of the initial data are rapidly radiated away. As a result, the NSBH

relaxes to a quasi-equilibrium state.

Subsequent investigations conducted by Faber et al. (2006a), found that an accretion disc can be formed from the tidal disruption of the compact star and that, although short-lived, this could provide energy to power a gamma-ray burst. Taniguchi et al. (2005) extended these results to consider the case in which the NS is irrotational. The effect of the spin of the neutron star was found to have only a minor effect on the location of the tidal break-up which plays an important role in the form of the gravitational waves produced. Whilst Sopuerta, Sperhake and Laguna (2006), treated the problem in full general relativity, the hydrodynamics of their neutron star was frozen. For large black hole-to-neutron star mass ratios the approximation is valid if in addition the dynamical timescales related with the deformation of the neutron star are much bigger than the orbital timescales.

These studies are important first steps in the study of the dynamics of mixed binary systems in General Relativity (GR). However these studies were unable to include binaries with comparable mass. From a computational point of view such an investigation would require the solution of the full Einstein equations, of accurate hydrodynamical techniques and the direct inclusion of the black hole's apparent horizon within the computational

domain. This remains a difficult problem.

1.2 Plan of Dissertation

The work is organised as follows. As an introductory investigation into tidal deformation of a neutron star in the vicinity of a black hole, a model where both components of the binary are considered to be point sources is introduced (and hence we may employ Newtonian Gravity) in the next chapter. The method used may be referred to as the Centrally Condensed Approximation. The gravitational force is taken to be Newtonian with contributions to the potential coming from both the fluid star and the black hole. The orbit is assumed to be circular.

In the chapter that follows, the figures of equilibrium are derived following the computational method first used in the 1960's by Chandrasekhar (1969) .The method is referred to as the *Virial Method*. Essentially, the *Virial Method*, is the method of moments applied to the solution of hydrodynamical problems in which the gravitational field of the prevailing distribution of matter is taken into account. Specifically we will take the virial equations of the second order where we multiply the hydrodynamic equations throughout by x_j and integrate over the entire volume. We provide the detailed calcula-

tion for the derivation of Roche ellipsoids outlined in Chandrasekhar (1969). Here we employ Newtonian Gravity also.

Next, we refine the model to include viscosity and a pseudo-Newtonian potential in Chapter 4. The detailed calculations are completed for the investigations in the study, *Newtonian Models for black hole-gaseous star binary systems*, conducted by Taniguchi and Nakumura (1996). The calculations follow closely those done by Chandrasekhar (1969) and that of Aizenman (1968) and extend their respective work to include general relativity. To mimic the general relativistic effects of gravitation, Taniguchi and Nakumura generalise the so-called pseudo-Newtonian potential first proposed by Paczyńsky & Wiita (1980). This potential fits the effective potential of the Schwarzschild black hole quite well.

Other advances in NSBH studies in the 'post-Chandrasekhar era' are also discussed in Chapter 4. In particular, we take a look at the various numerical results of Uryū and Eriguchi (1998a, 1998b, 1999, 2000). The computational results in (Uryū and Eriguchi, 1999) show that the binary systems reach the Roche(-Riemann) limit states or the Roche lobe filling states without suffering from hydrodynamical instability due to tidal force, for a large parameter range of the mass ratio and the polytropic index. The

stable Roche(-Riemann) limits or Roche lobe filling states are expected to survive even when GR is introduced. Their results show that Roche overflow will occur instead of merging of a black hole and a star. This contrasts with results prior to their investigations. We conclude the chapter with a discussion on the status quo of investigations surrounding the subject, and on future research arising from the topic.

In chapter 5 we consider the population synthesis of compact binaries, in particular for NSBH binaries. Over the last three decades, population synthesis studies (Lattimer and Schramm 1976; Narayan, Piran and Shemi 1991; Tutukov and Yungelson 1993; Lipunov, Postnov and Prokhorov 1997; Portegies Zwart and Yungelson 1998; Belczýnski and Bulik 1999; Kalogera et al. 2001) have indicated that the merger rate of NSBH binaries is comparable to that of DNS binaries, and is of the order 10^{-6} to 10^{-5} per year per galaxy. There remains some controversy about the rates of NSBH mergers, with Bethe and Brown (1998) predicting the rates of NSBH mergers to be 5 times more frequent than those of double neutron star (DNS) binaries. Pfahl, Podsiadlowski and Rappaport (2005) calculate the number of NSBH in the Galaxy to be a hundredth that of DNS. Currently, no black hole-neutron star binary systems have been discovered as yet, whilst the count of observed DNS stand at 8 (Stairs 2004). In this chapter, we will also discuss the expected

detection of astrophysical phenomena predicted to be the result of merging compact binaries, such as NSBH, DNS and BBH. GW detectors are currently coming on line, and detection is imminent. These would confirm theoretical predictions such as rates of formation of NSBH and give information on the macroscopic and microscopic characters of neutron stars. We discuss the various gravitational detectors currently online, together with their various sensitivities. We also take a look at the gravitational wave detectors planned to be operational in the next decade. A discussion on the nature of gravitational waves as compared to electromagnetic waves is given.

In the final chapter we summarise our work and discuss prospects for further research in this area.

Some of the detailed calculation omitted from the main body of work for the sake of brevity, is included in the appendices, which also include an explanation of symbols and abbreviations used.

2 Centrally Condensed Approximation

Compact Binaries are also considered to be strong sources of gravitational waves. The GW signals emanating from their inspiral and merger cover a wide frequency band $\sim 10^{-4} - 10^{-1}$ Hz for supermassive black hole binaries of $\sim 10^4 - 10^7 M_\odot$ (Arun 2006) to $\sim$ 1000Hz for NSNS binaries. In this range compact binaries provide potential sources for detection by ground-based interferometers.

Now, we may separate the entire inspiral of compact binaries into three different phases, each requiring different techniques to model.

The first phase can be regarded as the initial *quasi-equilibrium inspiral phase*. During this first stage , which is by far of the longest duration, there is the quasi-adiabatic decrease in the separation between the stars as a result of energy being carried away by gravitational radiation.The frequency and amplitude of the emitted gravitational radiation increases as the separation between the components of the binary decreases. The gravitational radiation tends to circularise binary orbits. However, general relativity does not admit strictly circular orbits, as the emission of gravitational radiation will lead to loss of energy and angular momentum, and hence to a shrinking of the orbit.

The separation, though, decreases very slowly, on a timescale much larger than the orbital period. Hence, we may approximate the orbit as quasi-circular. As our interest is in close binaries, we will focus on these quasi-circular orbits. The inspiral signals are thought to provide information on the spins and masses of the compact objects (Poisson and Will 1995). Quasi-circular orbits correspond to turning points of the energy function (Cook 1994), with a minimum corresponding to a stable quasi-circular orbit, and a maximum corresponding to an unstable orbit. The transition from stable to unstable orbits defines the innermost stable circular orbit (ISCO), which occurs at the saddle point. Post-Newtonian methods (Blanchet et.al., 1995; Damour, Jaranowski and Schäfer, 2000) provide very accurate models for the early inspiral phase, with large binary separations. Numerical relativity may be required for the late quasi-adiabatic inspiral phase, just outside of the ISCO, where finite-size and relativistic effects may become large enough for post-Newtonian point-mass techniques to break down.

At the innermost stable circular orbit (ISCO) these quasi-circular orbits become unstable and the inspiral gradually enters the second phase which is referred to as the *plunge and merger phase*. The merger and coalescence of the compact binary happens on a dynamical timescale. The GW signal associated with the merger is thought to carry information on the structure

and equation of state (EOS) of the neutron star (Faber and Rasio 2000; Faber and Rasio 2002). The plunge and merger phase is generally accepted to require a fully self-consistent numerical relativity simulation.

The *ringdown phase*, where the merged object settles down to equilibrium, is the final stage of the evolution. For the final phase, the merged object may be approximated as a distorted equilibrium object. In this case perturbative techniques may be applied (Price and Pullin, 1994; Baker et.al., 2001, 2002).

For NSBH mergers with massive enough BHs ($M \gtrsim 100 M_{\odot}$), the NS is expected to plunge into the BH as a whole. In these cases not much information on the EOS of the NS will be carried by the GW signal. The NS behavior remains point-like throughout the merger and disruption will never be observed by a distant observer Only the merger of the NSBH binaries with a stellar-mass BH will allow for the NS to disrupt outside the innermost stable circular orbit (ISCO). It is this scenario which will enrich the GW signal with information on the physics of the NS matter. For NSNS binaries, the GW signals from the inspiral is expected to be accessible to ground-based interferometers, which cover the frequency range 40 - 1000Hz. However the signals from their final mergers will probably be lost in the high-frequency noise level (Vallisneri 2000; Faber et al. 2002). In contrast, the GW merger

signals for many NSBH binaries are expected to lie well within the sensitivity band of LIGO, at frequencies $\sim$ 100 - 500 Hz. Whilst extensive studies have been conducted on DNS and BBH, far less attention has been spent on NSBH binaries.

As discussed above, relativistic binaries emit gravitational radiation, causing them to slowly spiral toward each other, and hence they do not follow strictly circular orbits. The term innermost stable circular orbit is hence a misnomer. The minimum in the equilibrium energy identifies the onset of a secular instability, while the onset of dynamical instability may be more relevant for the binary inspiral (Lai, Rasio and Shapiro 1993b). Lombardi, Rasio and Shapiro (1997) show that the two instabilities coincide in irrotational binaries. Ori and Thorne (2000) and Buananno and Damour (2000), suggest that the passage through the ISCO may proceed quite gradually, so that a precise definition of the ISCO may be less meaningful than the above turning method suggests (see also Duez et.al. (2002)). Invariably, dynamical evolution calculations will have to simulate the approach to the ISCO and investigate these issues.

Now, a neutron star in the vicinity of a black hole will experience tidal distortion. According to Berti, Iyer and Will (2007), for black holes, tidal

effects are negligible at the separations in question. For neutron stars, tidally induced distortions must be taken into account. The size of the neutron star as encoded in the compactness factor m_{NS}/r_{NS}, where m_{NS} and r_{NS} represent the mass and radius respectively, plays a role in the tidal deformation experienced by the neutron star. Mora and Will (2004) also note that tidal effects need to be taken into account carefully in an accurate diagnostic for neutron star binaries, with the modest size of the deformation supporting their use of Newtonian theory to calculate them. This only becomes problematic for the largest neutron stars near the very endpoint of their inspiral. Baumgarte, Skoge and Shapiro (2004) also conclude that it is appropriate to neglect the effects of tidal distortion or internal structure in calculations of neutron stars inspiral onto supermassive black holes, but state that these factors become important for neutron stars orbiting *stellar* mass black holes.

We will consider the scenario of the co-rotation of a fluid star (in specific, a neutron star) and a black hole. In this binary, the primary (the fluid star) is assumed to be homogeneous and have constant angular velocity, whilst the secondary (the black hole) can be considered as a point mass. The orbit may be assumed to be circular.

Over half of all stars in the sky are actually multiple star systems and,

of the binaries, about half again are close enough to one another for mass exchange between the components to occur at some point in their evolution (Motl, Tohline and Frank 2002). Newton was the first to show the gravitational field of a spherical body with mass m, is equivalent to that of a point mass, m. This *point-mass approximation* is generally more valid than might be at first thought (Hilditch, 2001). A typical star can be considered to consist of a core and a "stellar envelope". Stars are generally "*centrally condensed*" objects, with some 85 - 90 % of a star's mass contained within the inner 50% of its radius, at least on the zero-age main sequence (Kippenhahn an Wiegert, 1991). Hence, for many stars the point-mass approximation may be considered as sufficient. In addition, as stars evolve, they become even more centrally condensed.

Chandrasekhar, in his investigations entitled *The Equilibrium of Stellar Envelopes and the Central Condensation of Stars* (1932), defines the stellar envelope as "the outer parts of a star which, though only consisting of a small fraction of the total mass M of the star, nevertheless occupy a good fraction of the radius R of the star." He goes on to define a star as highly "centrally condensed" if 90% of the mass of the star is contained within the inner 10% of the radius of the star. In using this "*centrally condensed*" approach, he introduces two simplifications :

1. that the mass contained in the envelope can be neglected in comparison to the mass of the star as a whole,

2. that there are no sources of energy in the stellar envelope.

These assumptions, in fact, define the stellar envelope. For our binary system, we assume that the distance between the two bodies is large compared to the radius of either. With this further assumption, the mass of the star is then considered to be concentrated at its centre in such a way that the total mass can be approximated as a point mass. Hence both bodies in our binary are considered as point sources.

In the unperturbed state, the potential at the surface of the star is

$$\phi_{NS} = -\frac{Gm_{NS}}{r_{NS}} \tag{2}$$

(with ϕ normalised so that $\phi = 0$ at infinity). In the centrally condensed approximation for tidal distortion or disruption, it is assumed that at the boundary of the star, the above potential, ϕ_{NS}, remains the same for both the perturbed and unperturbed states, with the potential field generated by the point mass sources at the centre of the star and black hole. The problem has cylindrical symmetry, and we use cylindrical polar coordinates (ρ, θ, z) with origin at the centre of the fluid star.

Then the potential field is

$$\phi = -\frac{Gm_{NS}}{\sqrt{\rho^2 + z^2}} - \frac{Gm_{BH}}{\sqrt{\rho^2 + (z_0 - z)^2}} \tag{3}$$

Thus, we need to determine the location of the contour value of ϕ_{NS} for the potential field given by equation (3). There are 3 possible cases as illustrated in Figures (1) - (3).

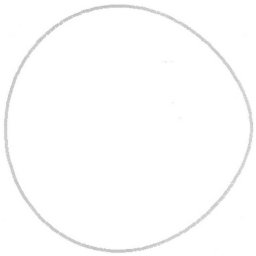

Figure 1: Distortion

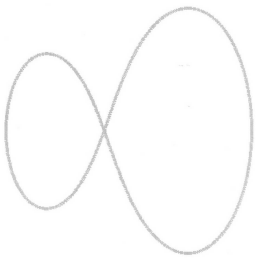

Figure 2: Critical Case

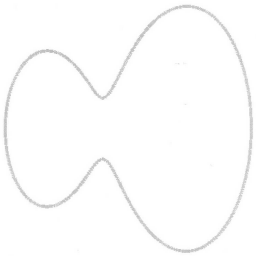

Figure 3: Disruption

Of particular interest is the critical case, and we derive an analytic formula to characterise it. In this case there is a point on the z-axis at which :

$$\phi = \phi_{NS} \tag{4}$$

$$\nabla\phi = 0 \tag{5}$$

with ϕ given by (3).

From the first condition (4), we equate (2) and (3) :

$$-\frac{Gm_{NS}}{\sqrt{\rho^2+z^2}} - \frac{Gm_{BH}}{\sqrt{\rho^2+(z_0-z)^2}} = -\frac{Gm_{NS}}{r_{NS}} \tag{6}$$

Applying the second condition (5) gives :

$$\frac{m_{NS}G}{z^2} - \frac{m_{BH}G}{(z_0-z)^2} = 0 \tag{7}$$

Solving equation (7) and keeping the solution with $z < z_0$,

$$\begin{aligned} z &= \left[\frac{m_{NS} - (m_{NS}m_{BH})^{\frac{1}{2}}}{m_{NS} - m_{BH}}\right] z_0 \\ &= \left[\frac{1 - \left(\frac{m_{BH}}{m_{NS}}\right)^{\frac{1}{2}}}{1 - \left(\frac{m_{BH}}{m_{NS}}\right)}\right] z_0 \end{aligned}$$

$$\therefore z = \frac{z_0}{1 + \left(\frac{m_{BH}}{m_{NS}}\right)^{\frac{1}{2}}} \tag{8}$$

Substituting (8) into (6), we find the critical value of z_0 to be

$$z_c = r_{NS}\left[1 + \left(\frac{m_{BH}}{m_{NS}}\right)^{\frac{1}{2}}\right]^2 \tag{9}$$

For $z_0 > z_c$, tidal distortion occurs, while for $z_0 < z_c$ there is tidal disruption.

We can test equation (9) by generating the equipotential from equation (3).

First, we normalise our equations by taking :

$$\begin{aligned} G.m_{NS} &= 1 \\ p &= \frac{m_{NS}}{m_{BH}} = \frac{1}{Q} \end{aligned} \tag{10}$$

Then equations (2), (3) and (9) may be written as :

$$\phi = -\frac{1}{\sqrt{\rho^2 + z^2}} - \frac{Q}{\sqrt{\rho^2 + (z_0 - z)^2}} \tag{11}$$

p	Q	z_c/r_{NS}
0.1	10	17.3246
	9	16
	7	13.2915
	6	11.8990
0.2	5	10.4721
0.25	4	9
0.3	$\frac{10}{3}$	7.9848
0.4	2.5	6.6623
0.5	2	5.8284

Table 1: Critical radii for given mass ratios

$$\phi_{NS} = -\frac{1}{r_{NS}} \tag{12}$$

$$z_c/r_{NS} = \left(1+Q^{\frac{1}{2}}\right)^2 \tag{13}$$

respectively.

In the table above a NSBH with $m_{BH} = 14M_\odot, m_{NS} = 1.4M_\odot, r_{NS} = 10km$, corresponds to the first row of entries in the table above. Hence, we can calculate the critical radius for the onset of tidal disruption to be $z_c \approx 173km$. In Figure (4) we produce the Roche figures for the critical states as given in

Table (1) for $Q = 4, Q = 7, Q = 9, Q = 10$ (from top to bottom, respectively).

All these figures correspond to the case illustrated in Figure (2).

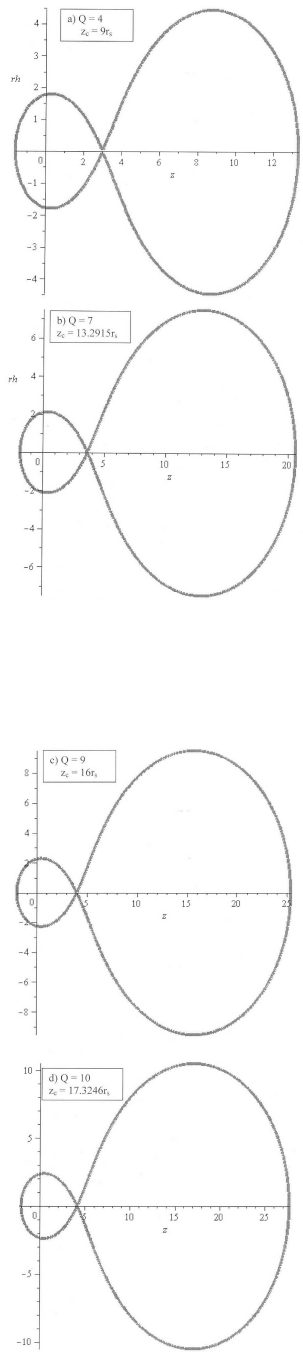

Figure 4: Critical states for $Q = 4, Q = 7, Q = 9, Q = 10$

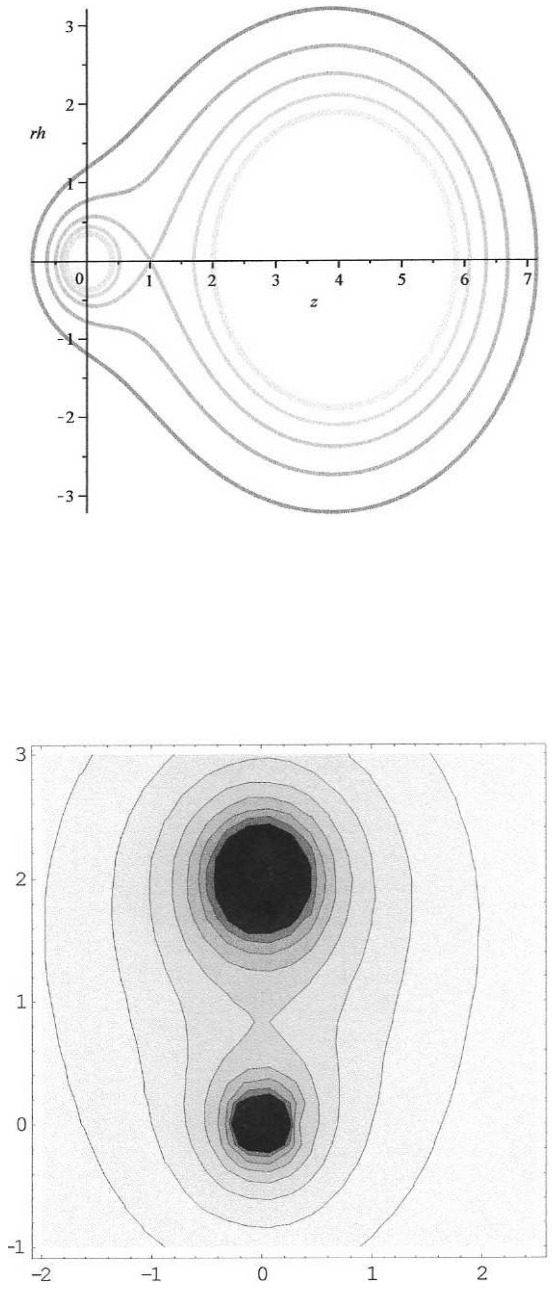

Figure 5: Contour Plots for ϕ

By using equation (3), we can show the Roche figures for the NHBS binary using different contour values for ϕ. In general we will obtain figures as illustrated in Figure (5), depending on the chosen parameters and contour steps taken.

We illustrate the use of contour plots by taking an example. Taking $p = 0.1$ and $z_0 = 7$, we start with $\phi = -1.5$ and take equal steps of -0.25 up to $\phi = -3$. In this example we use the normalisation given by equations (10) - (13). The result is illustrated in Figure (6).

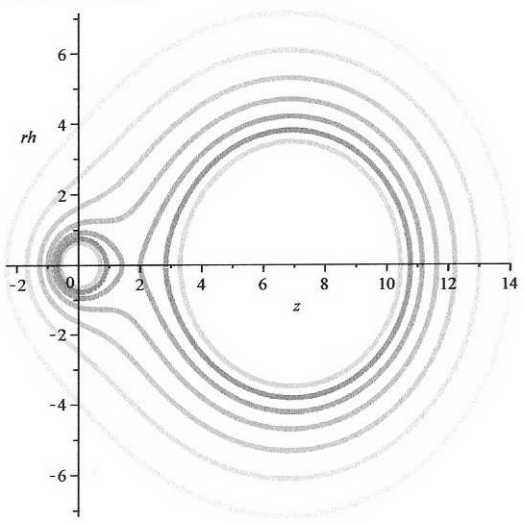

Figure 6: Roche figures for $p = 0.1$ and $z_0 = 7$

For a NSBH close binary with $m_{BH} = 10M_{\odot}, m_{NS} = 1.4M_{\odot}, z_0/r_{NS} = (200/15)$, we obtain the Roche Figure in Figure (7). We see that this figure corresponds to that of Figure (3) and hence we can conclude that this scenario is one of disruption, i.e. the neutron star is tidally disrupted by the black hole.

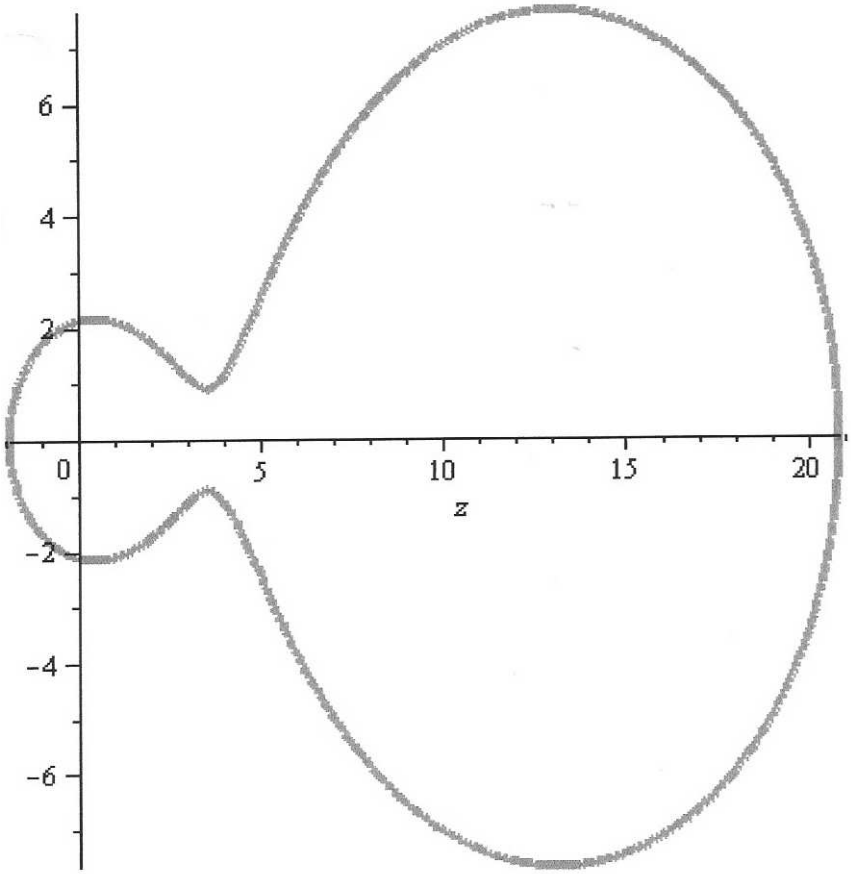

Figure 7: Roche figure for $m_{BH} = 10M_{\odot}, m_{NS} = 1.4M_{\odot}, r_{NS} = 15km, z_0 = 200km$

We note from Mora and Will (2004) that "in reality, the bodies in our binary system cannot be treated as purely point masses. They may be rotating (spinning), and thus subject to a number of effects, including rotational kinetic energy, rotational flattening, and spin-orbit and spin-spin interactions. Furthermore, there will be tidal deformations. These effects will not only make direct contributions to the energy and angular momentum of the system, they may also modify the equations of motion." The interesting case in the merger of NSBH binaries is the case for tidal disruption. For a highly condensed star, disruption is unlikely to take place with the star being swallowed whole in the merger. From Shapiro and Teukolsky (1983) we note that for objects that are more and more centrally condensed, the allowed range of rotation is severely limited by the condition of no mass shedding at the equator. Furthermore, centrally condensed objects in uniform orbit lose mass before they are rotating (spinning) fast enough to encounter "interesting stabilties." For a more realistic NSBH binary we need to adapt our equations.

3 Deriving the Figure of Equilibrium

The *Virial Method* within Newtonian gravity, first used by Chandrasekhar, in the 1960's is essentially the method of moments applied to the solution of hydrodynamical problems in which the gravitational field of the prevailing distribution of matter is taken into account. Virial equations of the second order : where we multiply the hydrodynamic equations throughout by x_j and integrate over the entire volume. The tensor form of the virial equation had been known as early as 1900 by Rayleigh (1903). It was only a half century later that its usefulness in hydromagnetic and hydrodynamic problems was realised. The power of the tensor virial equation to provide information on equilibrium and stability of hydromagnetic systems was demonstrated by Parker (1957) and Chandrasekhar (1960, 1961). Chandrasekhar and Lebovitz (1961) applied the tensor virial method to a series of astrophysical scenarios in the 1960's. Of interest to us will be the discussions on rotating, self-gravitating fluids, in particular, the derivation for the equilibrium figure of the Roche Ellipsoid.

3.0.1 Assumptions

The black hole (BH) is considered as a point mass m_{BH} with gravitational potential $\phi_{BH}(r)$ For the neutron star (NS) we assume incompressibility and homogeneity. For the gravitational force we employ Newtonian gravity. The gravitational potential

$$\phi = \phi_{NS} + \phi_{BH} \tag{14}$$

consists of a contribution from the fluid star, ϕ_{NS}, and from the black hole, ϕ_{BH}.

The former can be expressed as:

$$\phi_{NS}(\mathbf{r}) = -G \int_V \frac{\rho(\mathbf{r})}{\mid \mathbf{r} - \mathbf{r}' \mid} \, d^3\mathbf{r}' \tag{15}$$

where G is the gravitational constant and the integration is performed over the stellar interior V,

r is the distance from the centre of mass of the neutron star to the fluid element whose potential is being measured,

r' is the distance from the centre of mass of the the neutron star to each fluid element of the neutron star.

For the latter potential we assume that the potential at a point $\mathbf{r}$ on the fluid star is given by:

$$\phi_{BH}(\mathbf{r}) = -\frac{Gm_{BH}}{(\mathbf{r} - \mathbf{r}_{BH})} \tag{16}$$

where m_{BH} is the mass of the black hole and $\mathbf{r}_{BH}$ is the distance from the BH to the fluid element of the neutron star whose potential is being measured. The orbit is assumed circular. We take a rotating frame of reference of angular velocity relative to the inertial frame coincident with the orbital angular velocity, Ω, of the binary system .

3.0.2 The Basic equations

The Hydrodynamic equations governing the motions of the fluid referred to in an inertial frame of reference are the Euler equations:

$$\rho\frac{du_i}{dt} = -\frac{\partial P}{\partial x_i} + \rho\frac{\partial \mathfrak{B}}{\partial x_i} \tag{17}$$

where

u_i is the fluid velocity,

P is the pressure,

$$\frac{d}{dt} = \frac{\partial}{\partial t} + u_j\frac{\partial}{\partial x_j} \tag{18}$$

and the gravitational effect at a point $\mathbf{x}$, due to a distribution of matter with density $\rho(\mathbf{x})$ is given by the Newtonian potential :

$$\mathfrak{B} = G \int_V \frac{\rho \mathbf{x}'}{\mid \mathbf{x} - \mathbf{x}' \mid} d\mathbf{x}' \tag{19}$$

where G denotes the constant of gravitation.

We choose a co-ordinate system in which the origin is at the centre of mass of the primary, the x_1-axis points to the centre of mass of the secondary, and the x_3-axis is parallel to the direction of Ω. For a frame of reference rotating with the angular velocity, Ω, equation (17) becomes :

$$\rho \frac{du_i}{dt} = -\frac{\partial P}{\partial x_i} + \rho \frac{\partial \mathfrak{B}}{\partial x_i} + \frac{1}{2} \rho \frac{\partial}{\partial x_i} \mid \mathbf{\Omega} \times \mathbf{x} \mid^2 + 2\rho \epsilon_{ilm} \Omega_m u_l \tag{20}$$

where

$$\frac{1}{2} \mid \mathbf{\Omega} \times \mathbf{x} \mid^2 \tag{21}$$

and

$$\mathbf{u} \times \mathbf{\Omega} = \epsilon_{ilm} \Omega_m u_l \tag{22}$$

represent the centrifugal potential and the Coriolis acceleration, respectively.

To take account of the tidal potential we must include the potential $\mathfrak{B}'$, generated by the black hole. In our chosen co-ordinate system, the equation

governing the fluid elements of the neutron star is :

$$\rho\frac{du_i}{dt} = -\frac{\partial P}{\partial x_i} + \rho\frac{\partial}{\partial x_i}\left\{\mathfrak{B} + \mathfrak{B}' + \frac{1}{2}\Omega^2\left[\left(x_1 - \frac{m_{BH}R}{m_{NS}+m_{BH}}\right)^2 + x_2^2\right]\right\} + 2\rho\Omega\epsilon_{il3}u_l \quad (23)$$

where R is the distance between the centres of mass of the black hole and the neutron star and so the term containing R is the centre of mass adjustment.

3.0.3 Definitions and Results used

The mass of a neutron star is :

$$m_{NS} = \int_V \rho(x,t)d\mathbf{x} \quad (24)$$

This is constant, so :

$$\frac{d}{dt}\int_V \rho(\mathbf{x},t)d\mathbf{x} = \frac{dm_{NS}}{dt} = 0 \quad (25)$$

Hence for any attribute Q($\mathbf{x}$,t) of a fluid element :

$$\frac{d}{dt}\int_V Q(\mathbf{x},t)\rho(\mathbf{x},t)d\mathbf{x} = \int_V \rho(\mathbf{x},t)\frac{\partial Q}{\partial t}d\mathbf{x} \quad (26)$$

For our frame of reference whose origin is at the centre of mass,

$$I_i = \int_V \rho(\mathbf{x},t)x_i d\mathbf{x} = 0 \quad (27)$$

The moment of inertia tensor is :

$$I_{ij} = \int_V \rho x_i x_j d\mathbf{x} \tag{28}$$

I_{ij} is clearly symmetric in its lower indices and its trace is the scalar moment of inertia :

$$I_{ii} = I \tag{29}$$

The prevailing distribution of pressure p leads to the moments :

$$\Pi = \int_V P d\mathbf{x} \tag{30}$$

$$\Pi_i = \int_V P x_i d\mathbf{x}, etc. \tag{31}$$

The total kinetic energy of the motions of the system is :

$$\mathfrak{I} = \frac{1}{2} \int_V \rho \mid \mathbf{u} \mid^2 d\mathbf{x} \tag{32}$$

where

$$\mid \mathbf{u} \mid^2 = u_1^2 + u_2^2 + u_3^2 \tag{33}$$

is the square of the velocity of the fluid element at x.

The corresponding kinetic energy tensor is :

$$\mathfrak{I}_{ij} = \frac{1}{2}\int_V \rho u_i u_j d\mathbf{x} \tag{34}$$

Associated with the gravitational potential, (19), is the potential energy :

$$\mathfrak{W} = -\frac{1}{2}\int_V \rho \mathfrak{B} d\mathbf{x} \tag{35}$$

We shall need the tensor generalisations,$\mathfrak{B}_{ij}$ and $\mathfrak{W}_{ij}$, with

$$\mathfrak{B} = \mathfrak{B}_{ii} \tag{36}$$

$$\mathfrak{W} = \mathfrak{W}_{ii} \tag{37}$$

The generalisations are provided by :

$$\mathfrak{B}_{ij} = G\int_V \rho(\mathbf{x}')\frac{(x_i - x_i')(x_j - x_j')}{\mid \mathbf{x} - \mathbf{x}' \mid^3} d\mathbf{x}' \tag{38}$$

and

$$\mathfrak{W}_{ij} = -\frac{1}{2}\int_V \rho \mathfrak{B}_{ij} d\mathbf{x} \tag{39}$$

From this last equation we now get :

$$\mathfrak{W}_{ij} \;=\; -\frac{1}{2}G\int_V\int_V \rho(\mathbf{x})\rho(\mathbf{x}')\frac{(x_i - x_i')(x_j - x_j')}{\mid \mathbf{x} - \mathbf{x}' \mid^3} d\mathbf{x}' d\mathbf{x}$$

$$= -G \int_V \int_V \rho(\mathbf{x})\rho(\mathbf{x}') \frac{x_i(x_j - x_j')}{\mid \mathbf{x} - \mathbf{x}' \mid^3} d\mathbf{x}' d\mathbf{x}$$

$$= +G \int_V \int_V d\mathbf{x}\rho(\mathbf{x}) x_i \frac{\partial}{\partial x_j} \left[\frac{\rho(\mathbf{x}')}{\mid \mathbf{x} - \mathbf{x}' \mid} d\mathbf{x}' \right]$$

$$= \int_V \rho(\mathbf{x}) x_i \frac{\partial}{\partial x_j} \int_V G \left[\frac{\rho(\mathbf{x}')}{\mid \mathbf{x} - \mathbf{x}' \mid} d\mathbf{x}' \right]$$

Hence we can write :

$$\mathfrak{W}_{ij} = \int_V \rho(\mathbf{x}) x_i \frac{\partial \mathfrak{B}}{\partial x_j} \tag{40}$$

and

$$\mathfrak{W}_{ii} = \int_V \rho(\mathbf{x}) x_i \frac{\partial \mathfrak{B}}{\partial x_i} \tag{41}$$

From the theory of the Interior Potential of Homoeiodal Shells, as outlined in Appendix A, we have the following results :

$$\frac{\mathfrak{W}_{ij}}{\pi G \rho} = -2A_i L_{ij} \tag{42}$$

$$L_{ij} = \delta_{ij} a_i^2 \tag{43}$$

With the A_i defined as

$$A_i = \frac{L}{a_i^2} - \frac{1}{a_i} \left(\frac{\partial L}{\partial a_i} \right) \tag{44}$$

the B_{ij} are in turn defined by :

$$a_i^2 A_i - a_j^2 A_j = \left(a_i^2 - a_j^2 \right) B_{ij} \tag{45}$$

The a_i's represent the semi-axes of the ellipsoid and L is given by equation (176) in the Appendix A.

3.1 Obtaining the figure of Equilibrium

3.1.1 Deriving the Basic equation

Our hydrodynamic equation, (equation 23), is :

$$\rho\frac{du_i}{dt} = -\frac{\partial P}{\partial x_i}+\rho\frac{\partial}{\partial x_i}\left\{\mathfrak{B}+\mathfrak{B}'+\frac{1}{2}\Omega^2\left[\left(x_1-\frac{m_{BH}R}{m_{NS}+m_{BH}}\right)^2+x_2^2\right]\right\}+2\rho\Omega\epsilon_{il3}u_l \tag{46}$$

Now, treating the secondary as a rigid sphere, allows us to Taylor expand the tide-generating potential $\mathfrak{B}$', of the mass m_{BH} over the primary :

$$\mathfrak{B}' = \frac{Gm_{BH}}{R} \tag{47}$$

and

$$r = \sqrt{(R-x_1)^2+x_2^2+x_3^2} \tag{48}$$

So, we get

$$\mathfrak{B}' = \frac{Gm_{BH}}{R}\left(1+\frac{x_1}{R}+\frac{2x_1^2-x_2^2-x_3^2}{2R^2}+\cdots\right) \tag{49}$$

where R is the constant separation distance of the centres of mass of each of the bodies.

We will make the approximation of ignoring all higher terms which have

not been written down explicitly in the equation above. The equation of motion, equation (23) then becomes :

$$\begin{aligned}\rho\frac{du_i}{dt} &= \frac{\partial P}{\partial x_i}+\rho\frac{\partial}{\partial x_i}\left[\mathfrak{B}+\frac{1}{2}\Omega^2\left(x_1^2+x_2^2\right)+\mu\left(x_1^2-\frac{1}{2}x_2^2-\frac{1}{2}x_3^2\right)\right] \\ &\quad +\rho\frac{\partial}{\partial x_i}\left[\left(\frac{Gm_{BH}}{R^2}-\frac{m_{BH}R}{m_{NS}+m_{BH}}\Omega^2\right)x_1\right]+2\rho\Omega\epsilon_{il3}u_l \qquad (50)\end{aligned}$$

Next we let Ω^2 have the 'Keplerian' value. Then,

$$\begin{aligned}\Omega^2 &= \frac{G(m_{NS}+m_{BH})}{R^3} \\ &= \mu\left(1+\frac{m_{NS}}{m_{BH}}\right)\end{aligned} \qquad (51)$$

where we have used the abbreviation :

$$\mu=\frac{Gm_{BH}}{R^3} \qquad (52)$$

So

$$\begin{aligned}\frac{Gm_{BH}}{R^2}-\frac{m_{BH}R}{m_{NS}+m_{BH}}\Omega^2 &= \frac{Gm_{BH}}{R^2}-\frac{m_{BH}R}{(m_{NS}+m_{BH})}\,\frac{G(m_{NS}+m_{BH})}{R^3} \\ &= 0\end{aligned}$$

reducing our equation (50) to

$$\rho\frac{du_i}{dt} = -\frac{\partial P}{\partial x_i}+\rho\frac{\partial}{\partial x_i}\left[\mathfrak{B} + \frac{1}{2}\Omega^2\left(x_1^2 + x_2^2\right) + \mu\left(x_1^2 - \frac{1}{2}x_2^2 - \frac{1}{2}x_3^2\right)\right]+2\rho\Omega\epsilon_{il3}u_l \tag{53}$$

3.1.2 The Virial Equations

We now proceed with obtaining the virial equations of the second order by multiplying equation (53) by x_j and integrating over the entire volume V.

The l.h.s. of equation (53) then becomes, using equation (26), as :

$$\begin{aligned} \int_V \rho \frac{du_i}{dt} x_j d\mathbf{x} &= \int_V \rho [\frac{d}{dt}(u_i x_j) - u_i u_j] d\mathbf{x} \\ &= \frac{d}{dt} \int_V \rho u_i x_j d\mathbf{x} - \int_V \rho u_i u_j d\mathbf{x} \end{aligned} \tag{54}$$

since

$$\begin{aligned} \frac{d}{dt}(u_i x_j) &= \frac{du_i}{dt} x_j + u_i \frac{dx_j}{dt} \\ &= \frac{du_i}{dt} x_j + u_i u_j \end{aligned}$$

From equation (34), equation (54) becomes :

$$\int_V \rho \frac{du_i}{dt} x_j d\mathbf{x} = \frac{d}{dt} \int_V \rho u_i x_j d\mathbf{x} - 2\mathfrak{I}_{ij} \tag{55}$$

Now for the first term on the r.h.s. of equation (53), the virial method will give us :

$$- \int_V x_j \frac{\partial P}{\partial x_i} d\mathbf{x} \tag{56}$$

which may be written as

$$-\int \left[\int_a^b x_j \frac{\partial P}{\partial x_i} dx_i\right] d^2x \tag{57}$$

where a, b are x_i values on the boundary. Then

$$\begin{aligned}\int_a^b x_j \frac{\partial P}{\partial x_i} dx_i &= x_j \left[P\right]_a^b - \int_a^b \frac{\partial x_j}{\partial x_i} P dx_i &(58)\\ &= 0 - \int_a^b \delta_{ij} P dx_i &(59)\end{aligned}$$

Hence, using equation (30) we can write equation (57) as :

$$-\int_V x_j \frac{\partial P}{\partial x_i} d\mathbf{x} = \delta_{ij}\Pi \tag{60}$$

For last term on the right hand side of equation (53), the virial method gives :

$$2\epsilon_{il3}\Omega \int_v \rho u_l x_j d\mathbf{x} \tag{61}$$

For the second term on the r.h.s of equation(53), we first note that eq.(40) gives :

$$\int_V \rho x_j \frac{\partial \mathfrak{B}}{\partial x_i} d\mathbf{x} = \mathfrak{W}_{ij} \tag{62}$$

Next, we note that for the 3rd and 4th terms on the r.h.s. of (53) :

$$\begin{aligned}
& \rho\frac{\partial}{\partial x_i}\left[\frac{1}{2}\Omega^2\left(x_1^2+x_2^2\right)+\mu\left(x_1^2-\frac{1}{2}x_2^2-\frac{1}{2}x_3^2\right)\right] \\
= \;& \rho\left[\frac{1}{2}\Omega^2\left(\delta_{1i}2x_1\delta_{2i}2x_2\right)+\mu\left(\delta_{1i}2x_1-\frac{1}{2}\delta_{2i}2x_2-\frac{1}{2}\delta_{3i}2x_3\right)\right] \\
= \;& \rho\left[\Omega^2\left(\delta_{1i}+\delta_{2i}\right)x_i+\mu\left(2\delta_{1i}-\delta_{2i}-\delta_{3i}\right)x_i\right] \\
= \;& \rho\left[\Omega^2\left(\delta_{1i}+\delta_{2i}+\delta_{3i}\right)x_i-\mu\left(\delta_{1i}+\delta_{2i}+\delta_{3i}\right)x_i-\Omega^2\delta_{3i}x_i+3\mu\delta_{3i}x_i\right] \\
= \;& \rho\left[\left(\Omega^2-\mu\right)\left(\delta_{1i}+\delta_{2i}+\delta_{3i}\right)-\Omega^2\delta_{3i}+3\mu\delta_{1i}\right]x_i
\end{aligned}$$

Then, taking the virial equation of the second order we get :

$$\begin{aligned}
& \int_V\left[\rho\left[\left(\Omega^2-\mu\right)\left(\delta_{1i}+\delta_{2i}+\delta_{3i}\right)-\Omega^2\delta_{3i}+3\mu\delta_{1i}\right]x_i\right]x_j d\mathbf{x} \\
= \;& \int_V\rho\left[\left(\Omega^2-\mu\right)\left(\delta_{1i}+\delta_{2i}+\delta_{3i}\right)-\Omega^2\delta_{3i}+3\mu\delta_{1i}\right]x_i x_j d\mathbf{x} \qquad (63) \\
= \;& \left[\left(\Omega^2-\mu\right)\left(\delta_{1i}+\delta_{2i}+\delta_{3i}\right)-\Omega^2\delta_{3i}+3\mu\delta_{1i}\right]I_{ij} \qquad (64)
\end{aligned}$$

Collecting our results from equations (55),(60),(61), (62) and (64), the virial method of multiplying our hydrodynamic equation (53) throughout by x_j and integrating over the entire volume, produces the virial equation of the second order as :

$$\begin{aligned}
& \frac{d}{dt}\int_v\rho u_i x_j d\mathbf{x} \\
= \;& 2\mathfrak{I}_{ij}+\mathfrak{W}_{ij}+\left[\left(\Omega^2-\mu\right)\left(\delta_{1i}+\delta_{2i}+\delta_{3i}\right)-\Omega^2\delta_{3i}+3\mu\delta_{1i}\right]I_{ij}+2\epsilon_{il3}\Omega\int_v\rho u_l x_j d\mathbf{x}
\end{aligned} \qquad (65)$$

3.1.3 The Roche Ellipsoids

We are now ready to derive the equilibrium figure of a Roche ellipsoid from the the virial equation of the second order, equation (65). For the steady state equation

$$\frac{d}{dt}\int_v \rho u_l x_j d\mathbf{x} = 0 \tag{66}$$

Thus our equation (65) becomes :

$$2\mathfrak{I}_{ij}+\mathfrak{W}_{ij}+\left[\left(\Omega^2-\mu\right)\left(\delta_{1i}+\delta_{2i}+\delta_{3i}\right)-\Omega^2\delta_{3i}+3\mu\delta_{1i}\right]I_{ij}+2\epsilon_{il3}\Omega\int_v \rho u_l x_j d\mathbf{x} = 0 \tag{67}$$

So, when no fluid motions are present in our frame of reference and hydrostatic equilibrium prevails, this equation reduces to :

$$\mathfrak{W}_{ij}+\left[\left(\Omega^2-\mu\right)\left(\delta_{1i}+\delta_{2i}+\delta_{3i}\right)-\Omega^2\delta_{3i}+3\mu\delta_{1i}\right]I_{ij} = -\delta_{ij}\Pi \tag{68}$$

The diagonal elements of equation (68) then give :

$$\mathfrak{W}_{11}+\left(\Omega^2+2\mu\right)I_{11} = -\Pi \tag{69}$$

$$\mathfrak{W}_{22}+\left(\Omega^2-\mu\right)I_{22} = -\Pi \tag{70}$$

$$\mathfrak{W}_{33}-\mu I_{33} = -\Pi \tag{71}$$

Next, we let

$$p = \frac{m_{NS}}{m_{BH}} \tag{72}$$

so that

$$\Omega^2 = (1+p)\mu \tag{73}$$

Then,

$$\mathfrak{W}_{11} + \left(\Omega^2 + 2\mu\right) I_{11} = \mathfrak{W}_{22} + \left(\Omega^2 - \mu\right) I_{22} = \mathfrak{W}_{33} - \mu I_{33} \tag{74}$$

may be written as

$$(3+p)\mu a_1^2 - 2A_1 a_1^2 = p\mu a_2^2 - 2A_2 a_2^2 = \mu a_3^2 - 2A_3 a_3^2 \tag{75}$$

where Ω^2 and μ are measured in units of $\pi G\rho$ and we have used equations (42) and (43): From the first and third equations of (75),

$$\begin{aligned} (3+p)\mu a_1^2 - 2A_1 a_1^2 &= \mu a_3^2 - 2A_3 a_3^2 & (76)\\ \left[(3+p)a_1^2 + a_3^2\right]\mu &= 2(a_1^2 A_1 - a_3^2 A_3) \\ \left[(3+p)a_1^2 + a_3^2\right]\mu &= 2(a_1^2 - a_3^2)B_{13} & (77) \end{aligned}$$

where from equation (45), we have B_{ij} defined as :

$$(a_i^2 A_i - a_j^2 A_j) = (a_i^2 - a_j^2)B_{ij} \tag{78}$$

From the second and third equations of (75),

$$p\mu a_2^2 - 2A_2 a_2^2 = \mu a_3^2 - 2A_3 a_3^2 \tag{79}$$

$$\begin{aligned}\left(pa_2^2 + a_3^2\right)\mu &= 2\left(A_2 a_2^2 - A_3 a_3^2\right) \\ \left(pa_2^2 + a_3^2\right)\mu &= 2\left(a_2^2 - a_3^2\right) B_{23} \end{aligned} \tag{80}$$

Dividing equation (77) by (80) we get :

$$\frac{(3+p)a_1^2 + a_3^2}{pa_2^2 + a_3^2} = \frac{(a_1^2 - a_3^2)B_{13}}{(a_2^2 - a_3^2)\,B_{23}} \tag{81}$$

This equation determines the equilibrium figure of a Roche ellipsoid. Data for selected equilibrium figures are given in Table (2) and these are illustrated in Figure (8). The figures in Figure (8)correspond to alternate entries in Table (2) with the topmost figure corresponding with the first entry in the table and the bottom figure corresponding with the penultimate entry.

a_2/a_1	a_3/a_1	Ω^2 $\times 10^{-2}$
0.932	0.914	2.26
0.841	0.809	4.79
0.707	0.669	7.48
0.578	0.545	8.82
0.530	0.500	8.99
0.514	0.485	9.01
0.497	0.469	9.00
0.480	0.454	8.97
0.429	0.407	8.72
0.341	0.326	7.75

Table 2: Selected equilibrium figures from Chandrasekhar (1969)

Figure 8: Equilibrium Figures of a Roche Ellipsoid

4 Advances in Compact Binaries

The last decade and a half has seen an intensification in the study of compact binaries. The motivation has been primarily due to the proposals of the construction of the various gravitational wave detectors, many of which are currently online. Most analytical studies built on the seminal work of Chandrasekhar in the 1960's. Lai, Rasio and Shapiro adapted the model of Chandrasekahar and his colleague Aizenmann to include compressible models. A brief report on their work is included in the first section in this chapter. Next, the work of Taniguchi and Nakamura is discussed in more detail. Their work attempts to tackle the difficult problem of considering general relativity in the NSBH problem by including a pseudo-Newonian potential. Their arguments are closely followed with much of the detailed calculation omitted, completed here. In their paper, Taniguchi and Nakamura present only numerical results for various parameters of NSBH binaries. Using this data, the figures are produced here here for some of the NSBH binaries. Uryū and Eriguchi constructed equilibrium sequences for compact binaries. Their results are briefly discussed here with their simulations for various configurations included. Finally, there is a discussion on the most recent advances in the study of neutron star-black hole binaries, in particular the attempts

to include full general relativity.

4.1 Ellipsoidal Figures of Equilibrium : Compressible Models

In a series of papers, Lai, Rasio and Shapiro (1993a, 1994a, 1994b) use an energy variational method to present a new analytical study of the figure of equilibrium for compressible, self-gravitating Newtonian fluids. They appear to be the first to apply an energy variational method to determine the equilibrium and stability properties of a binary stellar configuration. Both uniformly and non-uniformly rotating configurations were considered . The ellipsoidal energy variational method is formally equivalent to the hydrostatic limit of the affine model used by Carter and Luminet (1985). In the model of Carter and Luminet, a time-dependent matrix relates the positions of all the fluid elements linearly to their initial positions in a spherical star. Lai, Rasio and Shapiro use a similar method to replace the full set of coupled hydrodynamic equilibrium equations (partial differential equations in two or three dimensions) with two or three coupled algebraic equations for the principal axes of the configuration. The affine model proves to be very useful for calculating numerically the approximate dynamical evolution of stellar mod-

els. The approach by Lai, Rasio and Shapiro, using the energy variational method is more convenient and simple to use in the study of equilibrium configurations and the associated stability limits.

The model of a point source and a corotating star is referred to as a Roche type binary configuration. The other configuration of the binary which tends to settle into a state in which the fluid star rotates with zero vorticity in the inviscid limit, is called the irrotational Roche-Riemann (IRR) binary configuration (Kochanek 1992 ; Bildsten and Cutler 1992). These two types of configurations correspond to the models of ellipsoidal equilibria for binary systems first studied by Roche and by Aizenman, extended to more realistic models in which deformation and compressibility of the fluid are fully taken into account (Chandrasekhar 1969 and Aizenman 1968).

For given masses, m_{NS} and m_{BH}, Lai, Rasio and Shapiro construct one-parameter sequences of equilibrium configurations parameterised by the binary separation, r. If the distances of the centres of mass m_{NS} and m_{BH} to that of the binary are r_{cm} and r'_{cm} respectively and the ratio of the masses is written as

$p = \frac{m_{NS}}{m_{BH}}$, then $r = r_{cm} + r'_{cm} = (1 + p)r_{cm}$.

Three critical radii are identified as the separation of the masses decrease. The final fates of NS-BH systems depend on which critical state is first approached. In order to find these critical states, certain physical quantities such as the total angular momentum, J, and the total energy, E, are first expressed as functions of r, i.e. $J(r)$ and $E(r)$, respectively. The turning point of each physical quantity, then corresponds to the point at which some instability sets in. At the turning points of $J(r)$ and $E(r)$, corresponding to minima in the case of the Roche-type binaries, secular instability sets in at that critical radius, $r = r_{sec}$. The rotation of the gaseous star from this point, then changes secularly. The dynamic instability is expected to occur at a radius, $r = r_{dyn}$ having smaller separation r than that where secular instability sets in i.e. $r_{dyn} < r_{sec}$. At the dynamical instability point, the two components are thought to coalesce or merge. The difference in separation between these two radii is very small and so hydrodynamic instability is also considered to set in at the turning points of the physical quantities $J(r)$ and $E(r)$. The radius corresponding to this point, r_{sec}, is therefore regarded as the radius where the instability of orbital motion sets in.

The IRR type binaries are not subjected to the influence of the viscosity and so there is no secular instability limit. In the IRR case, the turning point

corresponds to the dynamical instability limit, $r = r_{dyn}$. The third critical distance for the BH-NS binary sequence is the Roche(-Riemann) limit, denoted as $r = r_R$, corresponding to the minimum separation of two components or to the Roche lobe filling state, where the matter fills up its Roche lobe. This limit is determined through computing sequences by changing the parameter r to smaller values until the inner edge of the fluid star forms a cusp. The Roche lobe filling state corresponds to the configuration with such a cusp. The smallest value of r is the Roche limit $r = r_R$ of the sequence.

The results of Lai, Rasio and Shapiro, in which the ellipsoidal approximation of the polytropic star has been used, show that the relation $r_R < r_{dyn}$ is always satisfied for the IRR binary systems. This means that the IRR binary systems are always dynamically unstable at the Roche-Riemann limit. In the case of the Roche binary systems, the conditions $r_R < r_{sec}$ is always satisfied for all polytropic indices n and all mass ratios $p = M_{NS}/M_{BH}$. Lai, Rasio and Shapiro show that the relation,

$$r_R < r_{dyn} < r_{sec} \tag{82}$$

is also satisfied for almost realistic values of n and $p = M_{NS}/M_{BH}$, eg. $0.1 \lesssim p$ for $n = 1$ or $0.5 \lesssim p$ for $n = 1.5$. The results of Lai, Rasio and Shapiro show that for other parameters it is possible for r_R to appear at a

larger separation than r_{dyn}.

4.2 Innermost Stable Circulating Orbit of Coalescing Neutron Star-Black Hole Binary

Taniguchi and Nakamura (1996) determined the innermost stable circular orbit of black hole-neutron star systems by using a pseudo-Newtonian potential to mimic general relativistic effects. They also included vorticity in their model. We follow this work, completing much of the detailed calculation.

4.2.1 Obtaining the figure of Equilibrium

We begin the construction of figures of equilibrium for a neutron star in the vicinity of a black hole by stipulating the following conditions for our model:

1. for the neutron star
    - internal motions are linear in the coordinates with a uniform vorticity $\zeta_{\mathbf{k}}$ in the rotating frame
    - assume to be homogeneous ellipsoid with semi-axes a_1, a_2 and a_3
    - assume incompressibility for the equation of state
    - take own gravitational potential V_1 as Newtonian

- take mass m_{NS} and density ρ_1

2. for the black hole

   - consider as point mass, m_{BH},
   - assume its own gravitational potential V_2 is spherically symmetric : $V_2(r)$,
   - assume $V_2(r)$ of pseudo-Newtonian form, approximating general relativistic effects.

3. the neutron star rotates about the black hole with their separation distance remaining a constant R
4. the distance R is much larger than a_1, a_2 and a_3.
5. the angular velocity of rotation about the centres, $\mathbf{\Omega}$, is constant.

For the coordinate system :

- the origin is at the centre of mass of the primary
- x_1 axis points toward the secondary
- x_3 axis coincides with the direction of the angular velocity $\mathbf{\Omega}$ of the binary

If we are to take the internal motions to be linear in the coordinates, then

$$u_i = Q_{ij} x_j \tag{83}$$

The quantities Q_{ij} are determined such that the internal motions associated with $\zeta_{\mathbf{k}}$, preserve the ellipsoidal boundary.

If there are no motions normal to the surface, then $Q_{ii} = 0$. i.e.

$$Q_{11} = Q_{22} = Q_{33} = 0 \tag{84}$$

We then would have (cf. Chandrasekhar, 1966) :

$$Q_{ij} = -\epsilon_{ijk} \left(\frac{a_i^2}{a_i^2 + a_j^2} \right) \zeta_k \tag{85}$$

From (85) we then get :

$$u_1 = -\left(\frac{a_1^2}{a_1^2 + a_2^2} \right) \zeta_3 x_2 + \left(\frac{a_1^2}{a_1^2 + a_3^2} \right) \zeta_2 x_3 \tag{86}$$

$$u_2 = -\left(\frac{a_2^2}{a_2^2 + a_3^2} \right) \zeta_1 x_3 + \left(\frac{a_2^2}{a_2^2 + a_1^2} \right) \zeta_3 x_1 \tag{87}$$

$$u_3 = -\left(\frac{a_3^2}{a_3^2 + a_1^2} \right) \zeta_2 x_1 + \left(\frac{a_3^2}{a_3^2 + a_2^2} \right) \zeta_1 x_2 \tag{88}$$

Restricting the vorticity of the primary to be uniform and parallel to the

rotation axis, the equations above reduce to

$$\begin{aligned} u_1 &= -\left(\frac{a_1^2}{a_1^2+a_2^2}\right)\zeta_3 x_2 \\ &= -\left(\frac{a_1^2}{a_1^2+a_2^2}\right)\zeta x_2 \end{aligned} \tag{89}$$

$$\begin{aligned} u_2 &= \left(\frac{a_2^2}{a_2^2+a_1^2}\right)\zeta_3 x_1 \\ &= \left(\frac{a_2^2}{a_2^2+a_1^2}\right)\zeta x_1 \end{aligned} \tag{90}$$

$$u_3 = 0 \tag{91}$$

where

$$\zeta_k = (\zeta_1, \zeta_2, \zeta_3) = (0, 0, \zeta_3) = (0, 0, \zeta) \tag{92}$$

and the Q_{ij}'s are written as

$$\begin{aligned} Q_{12} &= -\left(\frac{a_1^2}{a_1^2+a_2^2}\right)\zeta \\ \\ Q_{21} &= \left(\frac{a_2^2}{a_2^2+a_1^2}\right)\zeta \end{aligned} \tag{93}$$

Now, the neutron star, m_{NS} orbits around the centre of mass of the binary,

at radius , r_{cm}, given by:

$$r_{cm} = \frac{m_{BH}R}{m_{NS} + m_{BH}} \tag{94}$$

The neutron star is under the influence of a centrifugal potential,

$$\frac{1}{2} \mid \mathbf{\Omega} \times \mathbf{r} \mid^2 \tag{95}$$

We may write

$$\mid \mathbf{\Omega} \times \mathbf{r} \mid^2 = (\mathbf{\Omega}.\mathbf{\Omega})(\mathbf{r}.\mathbf{r}) - (\mathbf{\Omega}.\mathbf{r}).(\mathbf{\Omega}.\mathbf{r}) \tag{96}$$

Using

$$\mathbf{\Omega} = (\mathbf{\Omega_1}, \mathbf{\Omega_2}, \mathbf{\Omega_3}) = (\mathbf{0}, \mathbf{0}, \mathbf{\Omega_3}) = (\mathbf{0}, \mathbf{0}, \mathbf{\Omega}) \tag{97}$$

and

$$\begin{aligned} \mathbf{r} &= (r_{cm} - x_1, x_2, x_3) \\ &= \left(\frac{m_{BH}R}{m_{NS} + m_{BH}} - x_1, x_2, x_3 \right) \end{aligned} \tag{98}$$

we can then write

$$\mid \mathbf{\Omega} \times \mathbf{x} \mid^2 = \Omega^2 \left[\left(\frac{m_{BH}R}{m_{NS} + m_{BH}} - x_1 \right)^2 + x_2^2 + x_3^2 \right] - \Omega^2 x_3^2$$

$$\therefore \frac{1}{2} \mid \mathbf{\Omega} \times \mathbf{x} \mid^2 = \frac{1}{2}\Omega^2 \left[\left(\frac{m_{BH} R}{m_{NS} + m_{BH}} - x_1 \right)^2 + x_2^2 \right] \tag{99}$$

For the Coriolis acceleration, we have :

$$2(\mathbf{u} \times \mathbf{\Omega}) = 2 \begin{pmatrix} \mathbf{e_1} & \mathbf{e_2} & \mathbf{e_3} \\ u_1 & u_2 & u_3 \\ \Omega_1 & \Omega_2 & \Omega_3 \end{pmatrix}$$

$$= 2 \begin{pmatrix} \mathbf{e_1} & \mathbf{e_2} & \mathbf{e_3} \\ u_1 & u_2 & 0 \\ 0 & 0 & \Omega \end{pmatrix}$$

$$\therefore 2(\mathbf{u} \times \mathbf{\Omega}) = 2\epsilon_{il3} u_l \Omega \tag{100}$$

We now turn our attention to the interaction potential $V_2(r)$.

First, we note that r is given by :

$$r = \left[(R - x_1))^2 + x_2^2 + x_3^2 \right]^{\frac{1}{2}} \tag{101}$$

which we can write as :

$$r = \left[R^2 - 2Rx_1 + x_1^2 + x_2^2 + x_3^2 \right]^{\frac{1}{2}}$$

$$
\begin{aligned}
&= R\left[1 - 2\frac{x_1}{R} + \frac{x_1^2 + x_2^2 + x_3^2}{R^2}\right]^{\frac{1}{2}} \\
&= R\,(1+\gamma)^{\frac{1}{2}} \qquad (102)
\end{aligned}
$$

where

$$
\gamma = \left[-2\frac{x_1}{R} + \frac{x_1^2 + x_2^2 + x_3^2}{R^2}\right] \qquad (103)
$$

We can assume that R is much larger than a_1, a_2 and a_3 and so the following approximations are valid :

$$
\begin{aligned}
r &= R\,(1+\gamma)^{\frac{1}{2}} \\
&= R\left(1 + \frac{1}{2}\gamma - \frac{1}{2\cdot 4}\gamma^2 + \frac{1\cdot 3}{2\cdot 4\cdot 6}\gamma^3 - \cdots\right) \\
&= R\left[1 - \frac{x_1}{R} + \frac{x_1^2 + x_2^2 + x_3^2}{2R^2} - \frac{1}{2\cdot 4}\frac{4x_1^2}{R^2} + O(x_i^3)\right] \\
\therefore r &\approx R - x_1 + \frac{x_2^2 + x_3^2}{2R}
\end{aligned}
\qquad (104)
$$

Using (104), the expansion of $V_2(r)$ becomes

$$
V_2 = (V_2)_0 - \left(\frac{\partial V_2}{\partial r}\right)_0 x_1 + \frac{1}{2R}\left(\frac{\partial V_2}{\partial r}\right)_0 \left(x_2^2 + x_3^2\right) + \frac{1}{2}\left(\frac{\partial^2 V_2}{\partial r^2}\right)_0 x_1^2 \qquad (105)
$$

where the subscript 0 denotes the derivatives at the origin of the coordinates. For our chosen coordinate system, with the angular velocity rotating with the frame of reference, the hydrodynamic equations governing the motion of the fluid elements of the neutron star, are given by:

$$\rho\frac{du_i}{dt} = -\frac{dP}{dx_i} + \rho\frac{\partial}{\partial x_i}\left\{V_1 + V_2 + \frac{1}{2} \mid \mathbf{\Omega} \times \mathbf{x} \mid^2 + 2(\mathbf{u} \times \mathbf{\Omega})\right\} \tag{106}$$

Collecting our results from (99) and (100), and substituting we get :

$$\begin{aligned}
\rho\frac{du_i}{dt} = & - \frac{\partial P}{\partial x_i} + \\
& \rho \frac{\partial}{\partial x_i}\left\{V_1 + V_2 + \frac{1}{2}\Omega^2\left[\left(\frac{m_{BH}R}{m_{NS}+m_{BH}} - x_1\right)^2 + x_2^2\right] + 2\epsilon_{il3}u_l\Omega\right\} \\
= & - \frac{\partial P}{\partial x_i} + \rho\frac{\partial V_1}{\partial x_i} + 2\epsilon_{il3}u_l\Omega \\
& + \rho\frac{\partial}{\partial x_i}\left\{V_2 + \frac{1}{2}\Omega^2\left[\left(\frac{m_{BH}R}{m_{NS}+m_{BH}} - x_1\right)^2 + x_2^2\right]\right\}
\end{aligned} \tag{107}$$

Using (105) and (133) we can expand and simplify the terms in the bracket in (107), noting that the constant terms will fall away due to the differentiation.

$$\frac{\partial}{\partial x_i}\left\{V_2 + \frac{1}{2}\Omega^2\left[\left(\frac{m_{BH}R}{m_{NS}+m_{BH}} - x_1\right)^2 + x_2^2\right]\right\}$$

$$= \frac{\partial}{\partial x_i}\left[-\left(\frac{\partial V_2}{\partial r}\right)_0 x_1 + \frac{1}{2R}\left(\frac{\partial V_2}{\partial r}\right)_0 \left(x_2^2 + x_3^2\right) \quad + \right.$$
$$\left. \frac{1}{2}\left(\frac{\partial^2 V_2}{\partial r^2}\right)_0 x_1^2 - \Omega^2 \frac{m_{BH} R}{m_{NS} + m_{BH}} x_1 + \frac{1}{2}\Omega^2 \left(x_1^2 + x_2^2\right)\right]$$

$$= \frac{\partial}{\partial x_i}\left[\frac{1}{2R}\left(\frac{\partial V_2}{\partial r}\right)_0 \left(x_2^2 + x_3^2\right) + \frac{1}{2}\left(\frac{\partial^2 V_2}{\partial r^2}\right)_0 x_1^2 \right.$$
$$\left. + \delta\left(\frac{\partial V_2}{\partial r}\right)_0 x_1 + \frac{1}{2}\Omega^2 \left(x_1^2 + x_2^2\right)\right] \tag{108}$$

where the constant δ is defined immediately after equation (133) on page 78.

We now apply the *Virial Method*, which is essentially the method of moments applied to the solution of hydrodynamical problems in which the gravitational field of the prevailing distribution of matter is taken into account.

Specifically we will take the virial equations of the second order where we multiply the hydrodynamic equations throughout by x_j and integrate over the entire volume of the neutron star. The term proportional to δ in Eq. (108) becomes proportional to $\int \rho_1 x_j d^3\mathbf{x}$ and therefore vanishes since we take the coordinate system to be comoving with respect to the centre of mass. We obtain :

$$\begin{aligned}
\frac{d}{dt}\int \rho_1 u_i x_j d^3\mathbf{x} &= 2\mathfrak{I}_{ij} + \mathfrak{W}_{ij} + \left\{\Omega^2 + \left(\frac{\partial^2 V_2}{\partial r^2}\right)_0\right\}\delta_{1i} I_{1j} \\
&\quad + \left\{\Omega^2 + \frac{1}{R}\left(\frac{\partial V_2}{\partial r}\right)_0\right\}\delta_{2i} I_{2j} + \frac{1}{R}\left(\frac{\partial V_2}{\partial r}\right)_0 \delta_{3i} I_{3j} \\
&\quad + 2\Omega\epsilon_{il3}\int \rho_1 u_l x_j d^3\mathbf{x} + \delta_{ij}\Pi,
\end{aligned} \tag{109}$$

where

$$\mathfrak{I}_{ij} \equiv \frac{1}{2}\int \rho_1 u_i u_j d^3\mathbf{x} : \text{Kinetic Energy Tensor}, \tag{110}$$

$$\mathfrak{W}_{ij} \equiv \int \rho_1 \frac{\partial V_1}{\partial x_i} x_j d^3\mathbf{x} : \text{Potential Energy Tensor}, \tag{111}$$

$$I_{ij} \equiv \int \rho_1 x_i x_j d^3\mathbf{x} \quad : \text{Moment of Inertia Tensor}, \tag{112}$$

and

$$\Pi \equiv \int P d^3\mathbf{x}. \tag{113}$$

In the steady state :

$$\frac{d}{dt}\int_v \rho u_l x_j d\mathbf{x} = 0 \tag{114}$$

And so (109) can be written as :

$$\begin{aligned} -\delta_{ij}\Pi, \;=\; & 2\mathfrak{I}_{ij} + \mathfrak{W}_{ij} + \left[\Omega^2 + \left(\frac{\partial^2 V_2}{\partial r^2}\right)_0\right]\delta_{1i}I_{1j} \\ & + \left[\Omega^2 + \frac{1}{R}\left(\frac{\partial V_2}{\partial r}\right)_0\right]\delta_{2i}I_{2j} + \frac{1}{R}\left(\frac{\partial V_2}{\partial r}\right)_0 \delta_{3i}I_{3j} \\ & + 2\Omega\epsilon_{il3}\int \rho_1 u_l x_j d^3\mathbf{x} \end{aligned} \tag{115}$$

Substituting for $u_i = Q_{ij}x_j$,in (109) we obtain :

$$\begin{aligned} Q_{ik}Q_{jl}I_{kl} + \mathfrak{W}_{ij} \;+\; & \left[\Omega^2 + \left(\frac{\partial^2 V_2}{\partial r^2}\right)_0\right]\delta_{1i}I_{1j} + \left[\Omega^2 + \frac{1}{R}\left(\frac{\partial V_2}{\partial r}\right)_0\right]\delta_{2i}I_{2j} \\ + \; & \frac{1}{R}\left(\frac{\partial V_2}{\partial r}\right)_0 \delta_{3i}I_{3j} + 2\Omega\epsilon_{il3}Q_{lk}I_{kj} = -\delta_{ij}\Pi, \end{aligned} \tag{116}$$

Now, only Q_{12} and Q_{21} are non-zero, so we obtain the following equations from (116) :

$$Q_{12}^2 I_{22} + \mathfrak{W}_{11} + \left[\Omega^2 + \left(\frac{\partial^2 V_2}{\partial r^2}\right)_0\right] I_{11} + 2\Omega Q_{21} I_{11} \;=\; -\Pi, \quad (117)$$

$$Q_{21}^2 I_{11} + \mathfrak{W}_{22} + \left[\Omega^2 + \frac{1}{R}\left(\frac{\partial V_2}{\partial r}\right)_0\right] I_{22} - 2\Omega Q_{12} I_{22} \;=\; -\Pi, \quad (118)$$

and

$$\mathfrak{W}_{33} + \frac{1}{R}\left(\frac{\partial V_2}{\partial r}\right)_0 I_{33} \;=\; -\Pi. \quad (119)$$

Substituting equation (119) into equations (117) and (118) gives:

$$\begin{aligned} & Q_{12}^2 I_{22} + \mathfrak{W}_{11} + \left[\Omega^2 + \left(\tfrac{\partial^2 V_2}{\partial r^2}\right)_0\right] I_{11} + 2\Omega Q_{21} I_{11} \\ = \quad & \mathfrak{W}_{33} + \tfrac{1}{R}\left(\tfrac{\partial V_2}{\partial r}\right)_0 I_{33} \end{aligned} \quad (120)$$

and

$$\begin{aligned} & Q_{21}^2 I_{11} + \mathfrak{W}_{22} + \left[\Omega^2 + \tfrac{1}{R}\left(\tfrac{\partial V_2}{\partial r}\right)_0\right] I_{22} - 2\Omega Q_{12} I_{22} \\ = \quad & \mathfrak{B}_{33} + \tfrac{1}{R}\left(\tfrac{\partial V_2}{\partial r}\right)_0 I_{33} \end{aligned} \quad (121)$$

Taking the gravitational potential of the neutron star to be Newtonian, we now use results for the interior potential of homoeiodal shells from the Appendix A.

For the tensors $\mathfrak{W}_{\rm ij}$ and I_{ij} we have :

$$\mathfrak{W}_{ij} = -2A_i I_{ij} \tag{122}$$

$$I_{ij} = \delta_{ij} a_i^2 \tag{123}$$

where we have normalised by taking Ω^2 to be measured in units of $\pi G\rho$ and the A_i's are given by :

$$A_i = a_1 a_2 a_3 \int_0^\infty \frac{du}{\Delta\left(a_i^2+u\right)}, \tag{124}$$

and

$$\Delta^2 = \left(a_1^2+u\right)\left(a_2^2+u\right)\left(a_3^2+u\right). \tag{125}$$

Then equations, (120) and (121), become :

$$\left(\frac{a_1^2}{a_1^2+a_2^2}\right)^2 \zeta^2 a_2^2 - 2A_1 a_1^2 + \left[\Omega^2 + \left(\frac{\partial^2 V_2}{\partial r^2}\right)_0\right] a_1^2 + 2\Omega\left(\frac{a_2^2}{a_1^2+a_2^2}\right)\zeta a_1^2$$
$$= -2A_3 a_3^2 + \frac{1}{R}\left(\frac{\partial V_2}{\partial r}\right)_0 a_3^2 \tag{126}$$

$$\left(\frac{a_2^2}{a_1^2+a_2^2}\right)^2 \zeta^2 a_1^2 - 2A_2 a_2^2 + \left[\Omega^2 + \frac{1}{R}\left(\frac{\partial V_2}{\partial r}\right)_0\right] a_2^2 - 2\Omega\left(\frac{a_1^2}{a_1^2+a_2^2}\right)\zeta a_2^2$$
$$= -2A_3 a_3^2 + \frac{1}{R}\left(\frac{\partial V_2}{\partial r}\right)_0 a_3^2 \tag{127}$$

From our results in the previous chapter we may use equations (44) and (45) for A_{ij} and B_{ij} respectively:

$$a_i^2 A_i - a_j^2 A_j \;=\; \left(a_i^2 - a_j^2\right) B_{ij}, \tag{128}$$

Using these results and writing

$$f_R = \frac{\zeta}{\Omega} \tag{129}$$

we can rewrite our equations as

$$\left\{\left[1 + 2\frac{a_2^2}{a_1^2 + a_2^2} f_R + \left(\frac{a_1 a_2}{a_1^2 + a_2^2} f_R\right)^2\right]\Omega^2 + \left(\frac{\partial^2 V_2}{\partial r^2}\right)_0\right\} a_1^2 - \frac{1}{R}\left(\frac{\partial V_2}{\partial r}\right)_0 a_3^2 = 2\left(a_1^2 - a_3^2\right) B_{13} \tag{130}$$

and

$$\left\{\left[1 + 2\frac{a_1^2}{a_1^2 + a_2^2} f_R + \left(\frac{a_1 a_2}{a_1^2 + a_2^2} f_R\right)^2\right]\Omega^2 + \frac{1}{R}\left(\frac{\partial V_2}{\partial r}\right)_0\right\} a_2^2 - \frac{1}{R}\left(\frac{\partial V_2}{\partial r}\right)_0 a_3^2 = 2\left(a_2^2 - a_3^2\right) B_{23} \tag{131}$$

$$p = \frac{m_{NS}}{m_{BH}} \tag{132}$$

For a circular orbit, assuming that $\frac{\partial P}{\partial x_i} = 0$ the force balance at the center of the NS gives

$$\begin{aligned} r_{cm}\Omega^2 &= -\left(\frac{\partial V_2}{\partial r}\right)_0 (1+\delta) \\ \left(\frac{m_{BH}R}{m_{NS}+m_{BH}}\right)\Omega^2 &= -\left(\frac{\partial V_2}{\partial r}\right)_0 (1+\delta) \end{aligned} \tag{133}$$

where the constant δ is the quadrupole term of the interaction potential (Lai, Rasio and Shapiro 1993b).

We can then rewrite Ω :

$$r_{cm}\Omega^2 = -\left(\frac{\partial V_2}{\partial r}\right)_0 (1+\delta)$$

$$\therefore \Omega^2 = -\left(\frac{p+1}{R}\right)\left(\frac{\partial V_2}{\partial r}\right)_0 (1+\delta) \tag{134}$$

Dividing Eq.(130) by Eq.(131), and using eqn(134) we get

$$\frac{\left[(1+p)(1+\delta)\left\{1+2\frac{a_2^2}{a_1^2+a_2^2}f_R+\left(\frac{a_1a_2}{a_1^2+a_2^2}f_R\right)^2\right\}-R\left(\frac{\partial^2 V_2}{\partial r^2}\right)_0/\left(\frac{\partial V_2}{\partial r}\right)_0\right]a_1^2+a_3^2}{\left[(1+p)(1+\delta)\left\{1+2\frac{a_1^2}{a_1^2+a_2^2}f_R+\left(\frac{a_1a_2}{a_1^2+a_2^2}f_R\right)^2\right\}-1\right]a_2^2+a_3^2}$$

$$= \frac{(a_1^2-a_3^2)\,B_{13}}{(a_2^2-a_3^2)\,B_{23}} \tag{135}$$

These are the equilibrium figures for type-S Roche-Riemann Ellipsoids.

4.2.2 Finding the ISCO

Both the total energy and the total angular momentum of the NSBH binary are decreasing functions of time as gravitational waves carrying energy and angular momentum are emitted. At some separation of the binary, the total angular momentum reaches its minimum. This point is regarded as the ISCO. The true minimum point of the total energy coincides with that of the total angular momentum. (If only terms to the quadrupole order are included, this coincidence fails. The difference, though, is as small as the numerical accuracy.) Taniguchi and Nakumaura (1996) give the total angular momentum of the system as the sum of the orbital and the spin angular momentum :

$$J_{tot} = m_{NS} r_{cm}^2 \Omega + m_{BH}(R - r_{cm})^2 \Omega + I\Omega + \frac{2}{5} m_{NS} \frac{a_1^2 a_2^2}{a_1^2 + a_2^2} \zeta \qquad (136)$$

or in the alternate form

$$= \frac{m_{NS} m_{BH}}{m_{NS} + m_{BH}} R^2 \Omega \left\{ 1 + \frac{1}{5}(1+p) \frac{1}{R^2} \left(a_1^2 + a_2^2 + 2 \frac{a_1^2 a_2^2}{a_1^2 + a_2^2} f_R \right) \right\} \qquad (137)$$

The first term in the braces of the right hand side of equation(137) comes from the orbital angular momentum of the binary system and the second

does from the spin angular momentum of the primary.

The orbital angular velocity can be obtained from equations (131) and (134).

First, we rewrite equation (134) as :

$$\frac{\Omega^2}{(1+p)(1+\delta)} = -\frac{1}{R}\left(\frac{\partial V_2}{\partial r}\right)_0 \tag{138}$$

Now, substituting for the term appearing on the right side of equation (138)

in the equation (131), we obtain :

$$\left\{\left[1+2\frac{a_1^2}{a_1^2+a_2^2}f_R+\left(\frac{a_1a_2}{a_1^2+a_2^2}f_R\right)^2\right]\Omega^2-\frac{\Omega^2}{(1+p)(1+\delta)}\right\}a_2^2 \\ +\frac{\Omega^2}{(1+p)(1+\delta)}a_3^2=2\pi\rho_1\left(a_2^2-a_3^2\right)B_{23} \tag{139}$$

Multiplying throughout by $(1+p)(1+\delta)$, we get :

$$\left\{(1+p)(1+\delta)\left[1+2\frac{a_1^2}{a_1^2+a_2^2}f_R+\left(\frac{a_1a_2}{a_1^2+a_2^2}f_R\right)^2\right]\Omega^2-\Omega^2\right\}a_2^2 \\ +\Omega^2a_3^2=2\pi\rho_1\left(a_2^2-a_3^2\right)B_{23}(1+p)(1+\delta) \tag{140}$$

The orbital angular velocity Ω can then be written as :

$$\frac{\Omega^2}{\pi\rho_1}=\frac{2(1+p)(1+\delta)\left(a_2^2-a_3^2\right)B_{23}}{\left[(1+p)(1+\delta)\left\{1+2\frac{a_1^2}{a_1^2+a_2^2}f_R+\left(\frac{a_1a_2}{a_1^2+a_2^2}f_R\right)^2\right\}-1\right]a_2^2+a_3^2}. \tag{141}$$

This quantity may be normalised with:

$$\tilde{\Omega}=\frac{\Omega}{\sqrt{\pi\rho_1}} \tag{142}$$

Now, the density of the primary is given as :

$$\rho_1 = \frac{m_{NS}}{\frac{4}{3}\pi\bar{a}^3}$$

where $\bar{a}$ is the mean radius of the primary.

$$\therefore \bar{a} = (a_1 a_2 a_3)^{\frac{1}{3}} \tag{143}$$

To mimic the general relativistic effects of the gravitation Taniguchi and Nakumura generalise the so-called pseudo-Newtonian potential first proposed by Paczyńsky & Wiita (1980). It is shown that the potential fits the effective potential of the Schwarzschild black hole quite well. The generalised pseudo-Newtonian potential used is defined by

$$V_2(r) = \frac{m_{BH}}{r - r_{pseudo}}, \tag{144}$$

$$r_{pseudo} = r_s \left\{1 + g(p)\right\}, \tag{145}$$

$$g(p) = \frac{7.49p}{6(1+p)^2} - \frac{10.4p^2}{3(1+p)^4} + \frac{29.3p^3}{6(1+p)^6}, \tag{146}$$

$$r_s \equiv \frac{2GM_{tot}}{c^2}, \tag{147}$$

$$M_{tot} = m_{NS} + m_{BH}, \tag{148}$$

where $p = m_{NS}/m_{BH}$ and $g(p)$ is the special term to fit the ISCO's of the hybrid second post-Newtonian calculations by Kidder, Will, & Wiseman(1982). This generalized pseudo-Newtonian potential agrees with the

pseudo-Newtonian potential proposed by Paczyńsky & Wiita, in the case $p = 0$.

The angular momentum is normalised as :

$$\tilde{J} = \frac{J_{tot}}{m_{NS} m_{BH} (r_s / M_{tot})^{1/2}} \tag{149}$$

For a given mass ratio p and mean radius $\bar{a}/m_{NS}$, circulation parameter f_R and axial ratio a_3/a_1, we are able to determine the axial ratio a_2/a_1 using Eq.(140). Then, by using the axial ratios (a_2/a_1, a_3/a_1), we are able to calculate the orbital angular velocity by Eq.(141). The total angular momentum is calculated by Eq.(137). By finding the minimum of the total angular momentum, we are able to locate the ISCO.

The Roche ellipsoids (REs) are obtained for the case of $f_R = 0$ in the above equation, i.e. when the viscosity inside the primary is so effective that no internal motion exists. The irrotational Roche-Riemann ellipsoids (IRREs) are obtained in the inviscid limit with $\mathcal{C} = 0$, $f_R = -2$. Substituting the Newtonian potential as an interaction potential, Eqs.(135) and (141) agree with the equations derived by Chandrasekhar (1969) in the REs ($f_R = 0$) case and those by Aizenman (1968) in the RREs case.

In Table 3 † indicates the point of the ISCO and ‡ indicates the point of

$p = 0.1$

$\bar{a}/m_{NS} = 3$

Roche Sequences					Irrotational Roche-Riemann Sequences				
a_3/a_1	a_2/a_1	$\tilde{\Omega}^2$	$\tilde{J}$	R/r_s	a_3/a_1	a_2/a_1	$\tilde{\Omega}^2$	$\tilde{J}$	R/r_s
					0.992	0.992	2.42(-3)	2.70	3.26 †
0.990	0.992	2.39(-3)	2.71	3.27 †					
0.950	0.959	9.94(-3)	2.85	2.35	0.950	0.949	1.17(-2)	2.89	2.27
0.900	0.914	1.80(-2)	3.02	2.08	0.900	0.896	2.04(-2)	3.06	2.03
0.850	0.868	2.51(-2)	3.16	1.96	0.850	0.843	2.76(-2)	3.19	1.93
0.800	0.821	3.12(-2)	3.26	1.88	0.800	0.789	3.35(-2)	3.29	1.86
0.750	0.772	3.65(-2)	3.35	1.84	0.750	0.735	3.84(-2)	3.37	1.82
0.700	0.722	4.10(-2)	3.42	1.80	0.700	0.682	4.23(-2)	3.43	1.79
0.650	0.672	4.47(-2)	3.48	1.78	0.650	0.629	4.53(-2)	3.48	1.77
0.600	0.621	4.75(-2)	3.52	1.76	0.600	0.577	4.74(-2)	3.51	1.76
0.550	0.569	4.93(-2)	3.56	1.75	0.550	0.526	4.86(-2)	3.54	1.76
					0.525	0.501	4.89(-2)	3.55	1.76 ‡
0.500	0.517	5.02(-2)	3.58	1.75 ‡					

Table 3: Equilibrium Sequences of the REs and the IRREs with $p = 0.1$ and $\bar{a}/m_{NS} = 3$.

the Roche limit where the Roche limit is defined by the distance of closest approach for equilibrium to be possible. The values in the parentheses show the power of 10. $\tilde{\Omega}$ and $\tilde{J}$, are normalised according to equations (142) and (149) respectively.

The figures of contours of equal density, corresponding to the entries for the Roche ellipsoids are given in Figure 9, with (a) corresponding to the first row of entries, ending with (k) corresponding to the last row. In all the figures the axis units are normalized so that the mean radius $\bar{a} = 1$. The four figures from top to bottom in Figure 10 corresponds to the 2nd, 5th, 8th and 11th entries respectively for Irrotational Roche-Riemann Sequences in Table 3. Figure 11 illustrates the surface shape for the Roche-type binary given in case (k) in Figure 9. We illustrate, in Figure 12, the z-y plane for the parameter $a_3/a_1 = 0.95$ for both the (a)Roche and (b)Roche Riemann case.

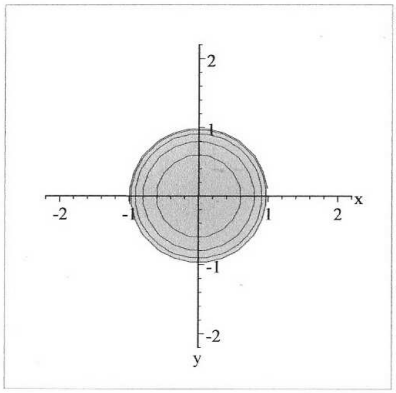

9 (a)

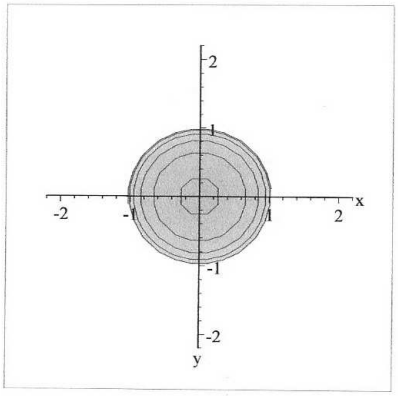

9 (b)

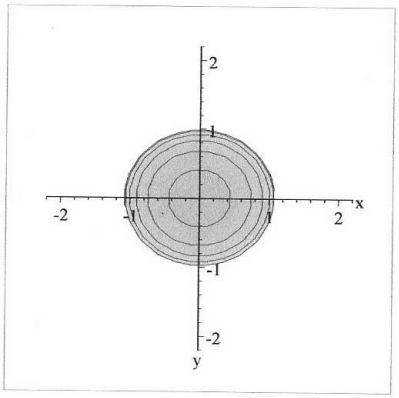

9 (c)

Figure 9: Equilibrium Sequences for Roche-type binaries

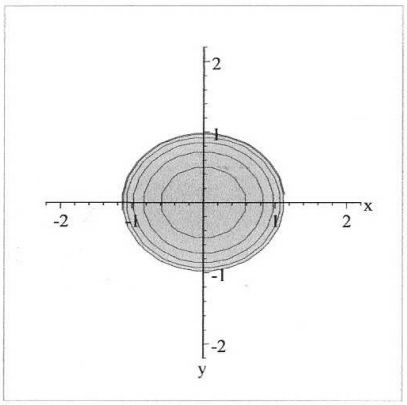

9 (d)

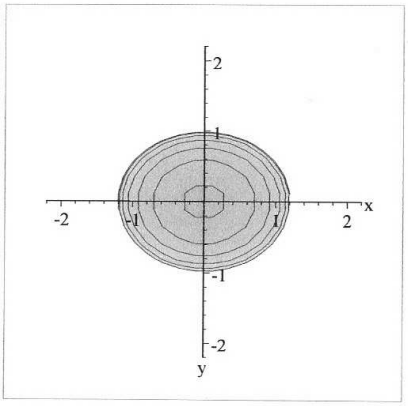

9 (e)

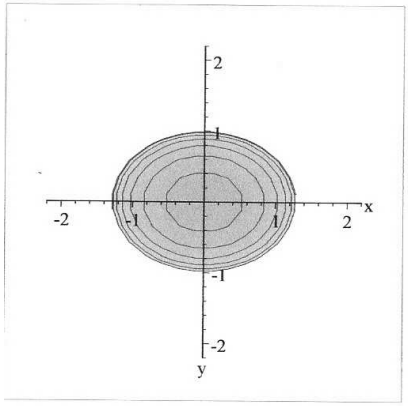

9 (f)

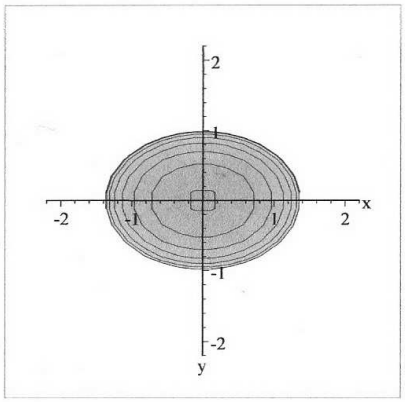

9 (g)

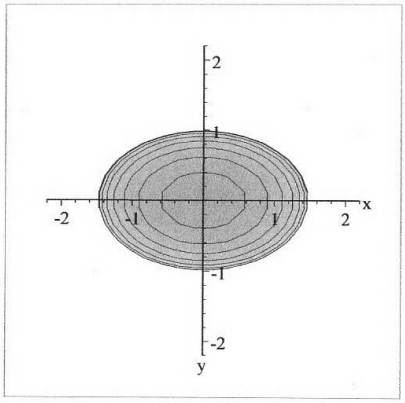

9 (h)

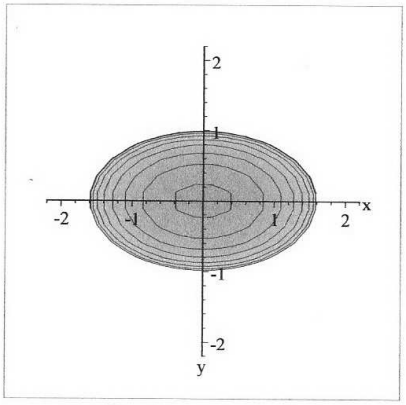

9 (i)

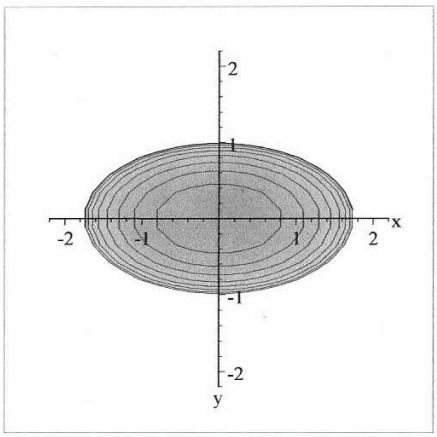

9 (j)

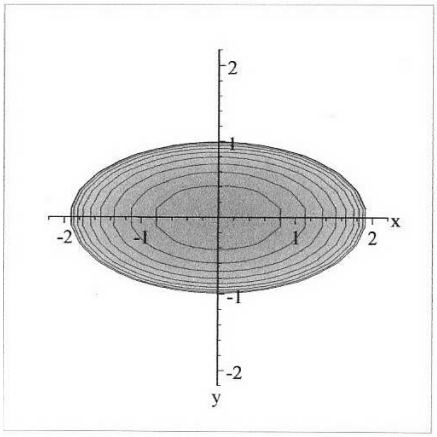

9 (k)

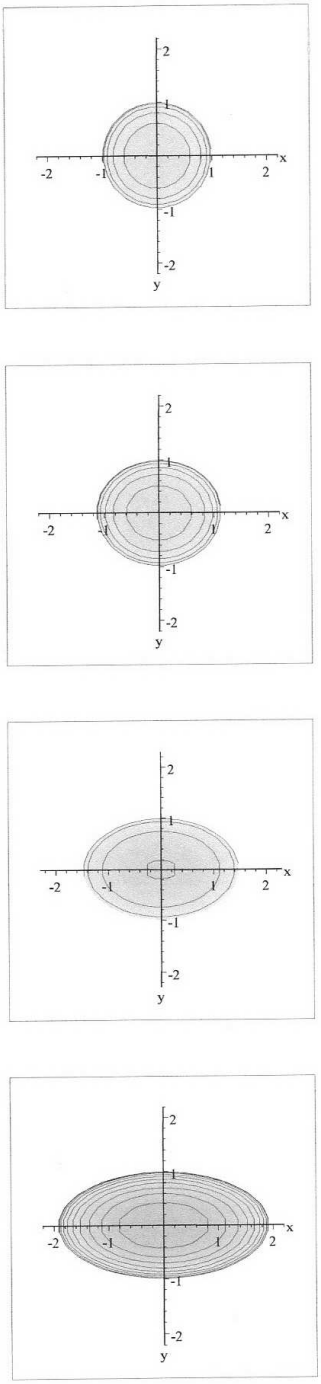

Figure 10: Equilibrium Sequences for IRR-type binaries

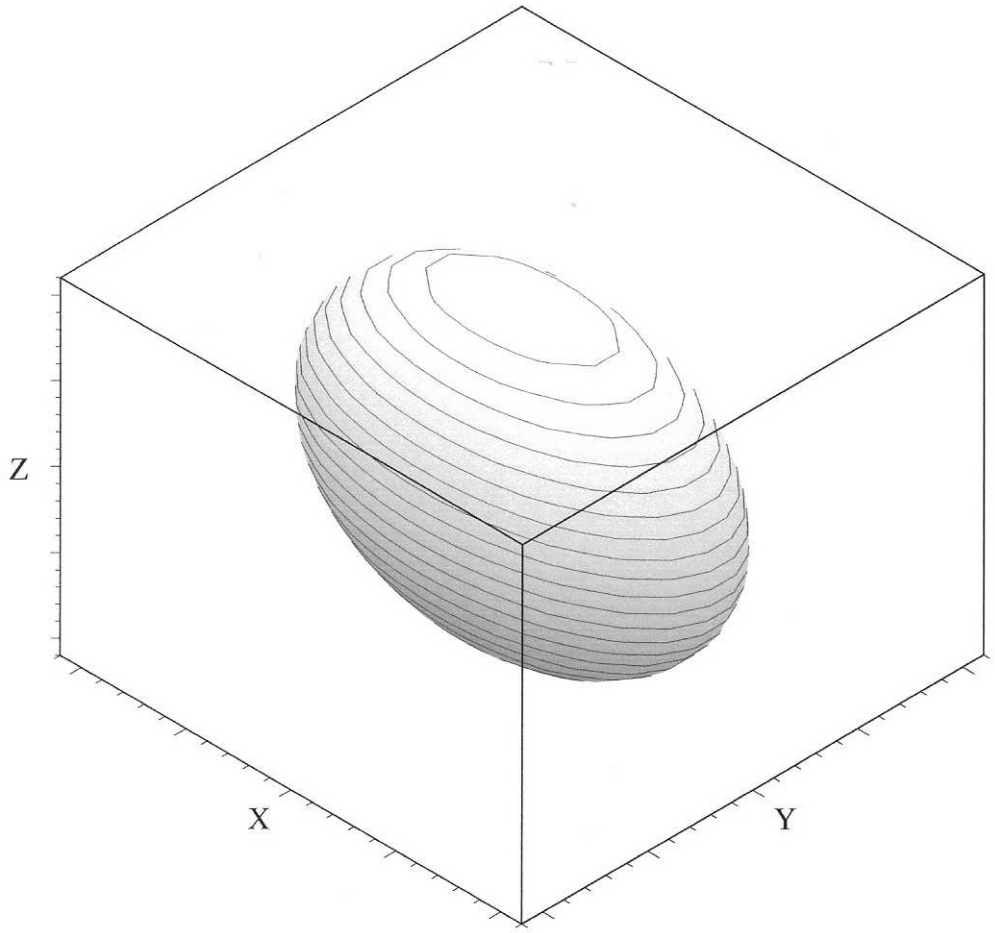

Figure 11: Surface Shape for Roche-type binary

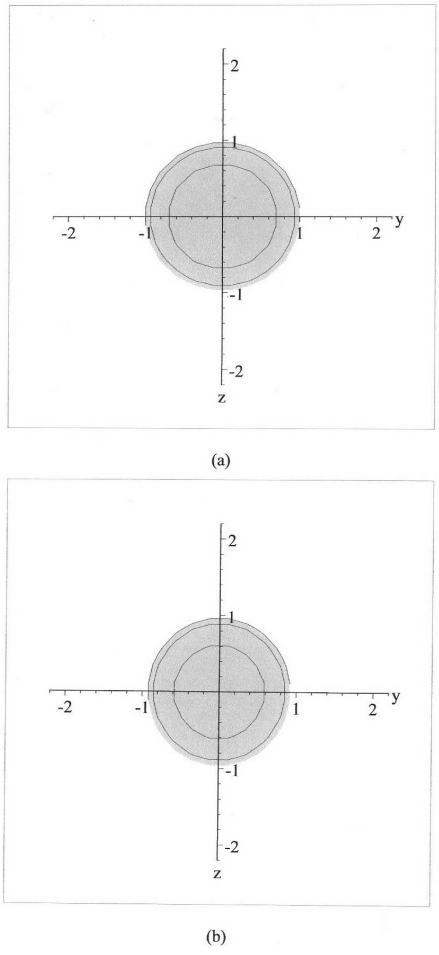

Figure 12: Equilibrium Sequences for Roche-type binaries

4.3 Newtonian Models for Black Hole-Gaseous Star Close Binary Systems

Kōji Uryū and Yoshiharu Eriguchi use numerically exact stationary configurations in the framework of Newtonian gravity to investigate circularly orbiting black hole-gaseous star close binary systems, including NSBH binaries (Uryū and Eriguchi, 1999). The fluid star or neutron star is assumed to be a polytrope, with equation of state satisfying the polytropic relation : $p = K\rho^{1+1/n}$. The black hole is taken as a point source. Two ideal situations are considered. Firstly the star is taken to be rotating synchronously, which corresponds to a rotating star under the influence of viscosity(Roche type binary configuration). The second scenario, for the inviscid limit, is of an irrotationally rotating star(irrotational Roche-Riemann (IRR) binary configuration). The final stages of black hole-gaseous star close binary systems can then be discussed by taking the stationary sequences of binary systems with small separations.

The orbit of a binary system becomes circular as a result of the gravitational wave emission leading to the separation of two components decreasing. Several different possibilities exist for the final states of such BH-star systems (see e.g. Kidder, Will and Wiseman 1992, Lai, Rasio and Shapiro 1993a).

One possibility is inspiraling on a dynamical time scale as a result of the tidal or the general relativistic (GR) effect. The Schwarzschild solution for a test particle around the BH field is well known, resulting in an innermost stable circular orbit (ISCO). Another possibility is Roche lobe overflow with mass overflow from the fluid star to the black hole or the environment.

The computational results in (Uryū and Eriguchi, 1999) show that the binary systems reach the Roche(-Riemann) limit states or the Roche lobe filling states without suffering from hydrodynamical instability due to tidal force for a large parameter range of the mass ratio and the polytropic index. Furthermore, the stable Roche(-Riemann) limits or Roche lobe filling states are expected to survive even under the general relativistic effect. The results show that Roche overflow will occur instead of merging of a black hole and a star. This contrasts to the results of Lai, Rasio and Shapiro. The results of Uryū and Eriguchi, show that for a wide parameter range r_R appears earlier than r_{sec} or r_{dyn} as the separation decreases. The reason for this is that those configurations around the critical radii, in particular at r_R, cannot be expressed well by the ellipsoidal approximation even for fairly stiff equations of state because of a large deformation of the stellar envelope due to compressibility (Uryū and Eriguchi 1998a, , 1998b). If the Roche(-Riemann) limit appears for a larger separation than the other hydrodynamical insta-

bility limit, then the final stage of the evolution of binary systems would be drastically different from the scenario suggested by Lai, Rasio and Shapiro. This means that Roche lobe overflow or the mass transfer from the star to the black hole instead of unstable plunge of the star to the black hole is more likely to occur.

As stated previously, the Roche limit is determined by computing sequences, changing the parameter R to smaller values. The deformation of the envelope due to the tidal force becomes large, and, in particular, that around the inner parts near the BH becomes larger than that of other parts. With this significant deformation of the envelope, a cusp is formed at the inner edge and hence the sequence is terminated at a larger separation $r = r_R$ than that for the ellipsoidal approximation.

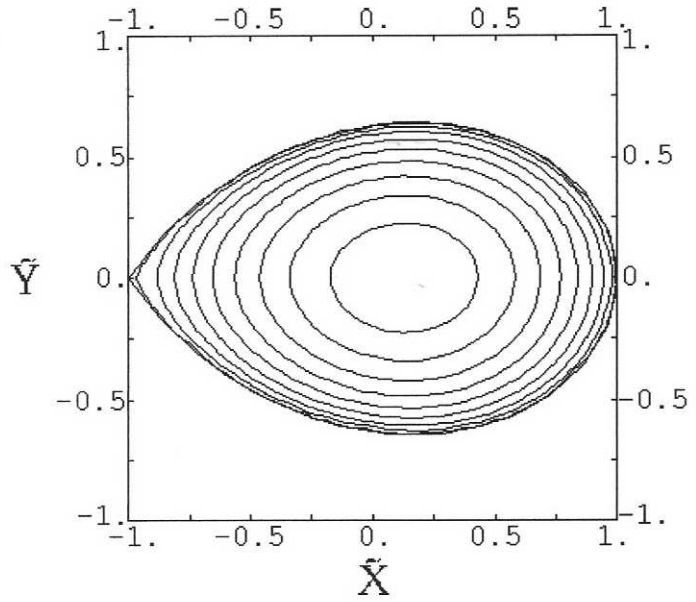

Figure 13: Contours of the density in the equatorial $\tilde{X}$-$\tilde{Y}$ plane for Roche type binary, where the axes have been normalised. [Uryu and Eriguchi(1998a)]

This can be seen clearly in Figures 13 and 14. These are equilibrium figures obtained by Uryū and Eriguchi (1998a) for Roche binary system with $M_{NS}/M_{BH} = 0.1$ and $n = 0.5$ at the Roche Limit r_R. The $\tilde{X}\tilde{Y}\tilde{Z}$-coordinates are the Cartesian coordinates where the $\tilde{X}$ axis intersects the inner and the outer edges of the star and the rotational center. $\tilde{X}$-$\tilde{Y}$ plane is the equatorial plane. The $\tilde{Z}$ axis is parallel to the rotational axis. The origin of the $\tilde{X}\tilde{Y}\tilde{Z}$-coordinates is at the geometrical center of the star. The coordinates are

normalised by

$$R_0 = (R_{out} - R_{in})/2 \tag{150}$$

where R_{out} and R_{in} are distances from the rotational axis to the outermost and innermost edges of the star respectively. The difference between two subsequent density contours for each quantity is 1/10 of the difference between maximum to minimum value.

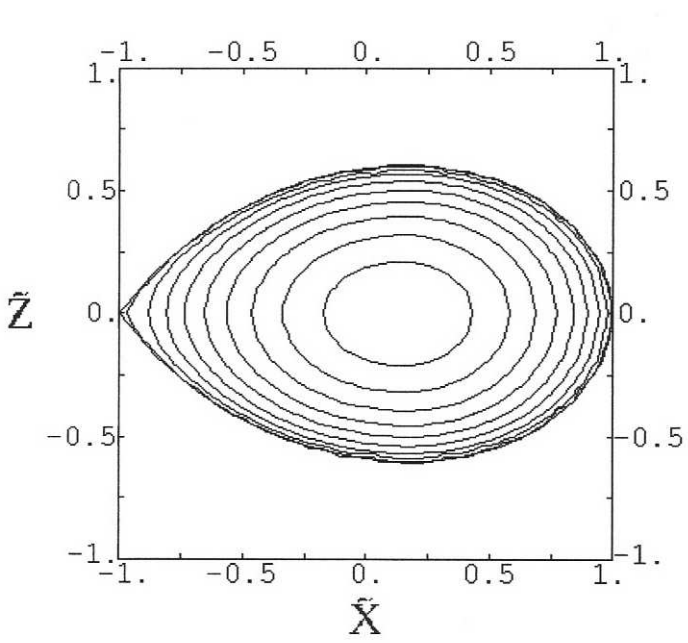

Figure 14: Contours of the density in the meridional $\tilde{X}$-$\tilde{Z}$ plane for Roche type binary, where the axes have been normalised. [Uryu and Eriguchi(1998a)]

Figure 16 is the corresponding figures for the IRR-type binary at the Roche Limit, $r = r_R$, $p = 0.1$ and $n = 0.5$. Comparing each of these figures,

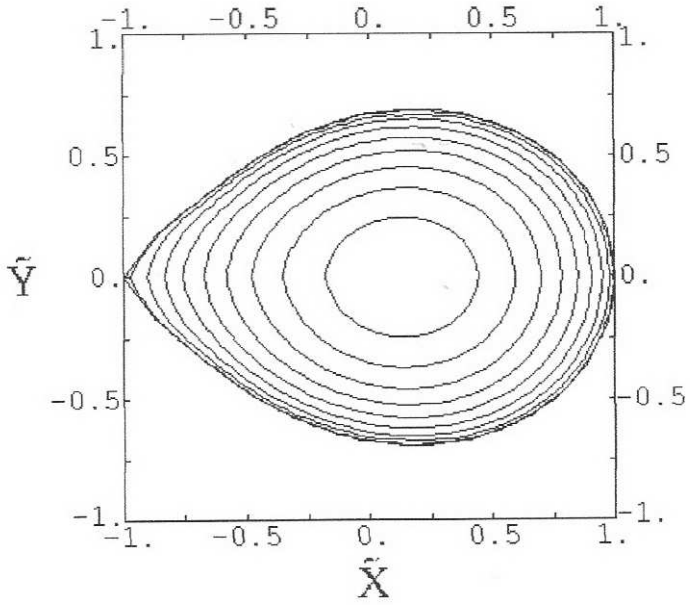

Figure 15: Contours of the density in the equatorial plane for IRR-type binary, with $p = 0.1$ and $n = 0.5$. [Uryu and Eriguchi(1998a)]

a difference is detected in the shape, with the Roche-type being more prolate and the IRR-type less prolate.

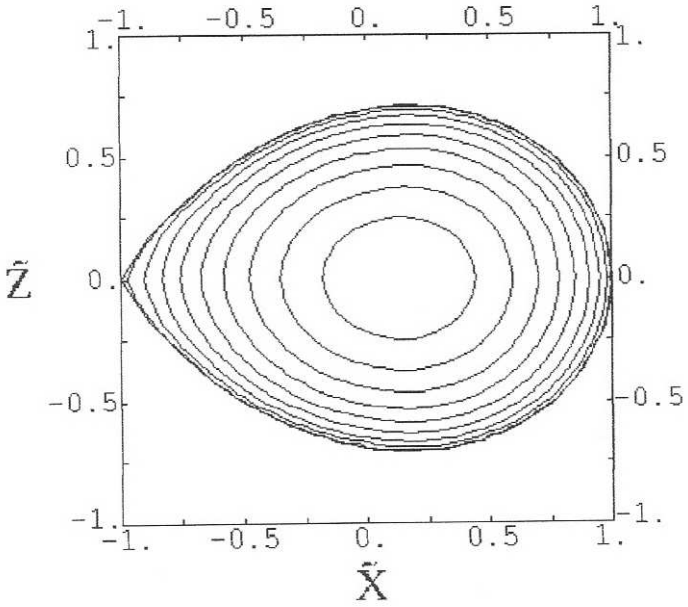

Figure 16: Contours of the density in the meridional $\tilde{X}$-$\tilde{Z}$ plane for IRR-type binary, with $p = 0.1$ and $n = 0.5$. [Uryu and Eriguchi(1998a)]

The difference in shape between the Roche-type and IRR type is more clearly seen in the comparison for the figures in the $\tilde{Y}$-$\tilde{Z}$ plane for the Roche type (Figure 17) and the IRR-type (Figure 18) binaries.

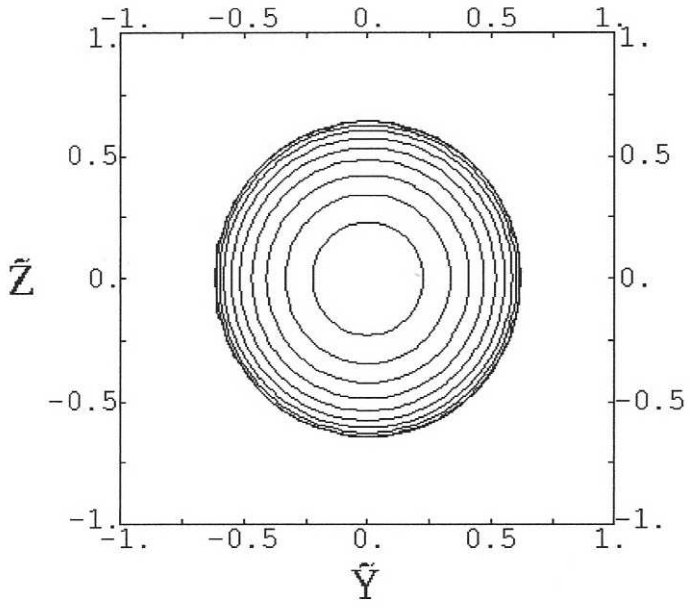

Figure 17: Contours of the density in the meridional $\tilde{Y}$-$\tilde{Z}$ plane for Roche type binary, with $p = 0.1$ and $n = 0.5$. [Uryu and Eriguchi(1998a)]

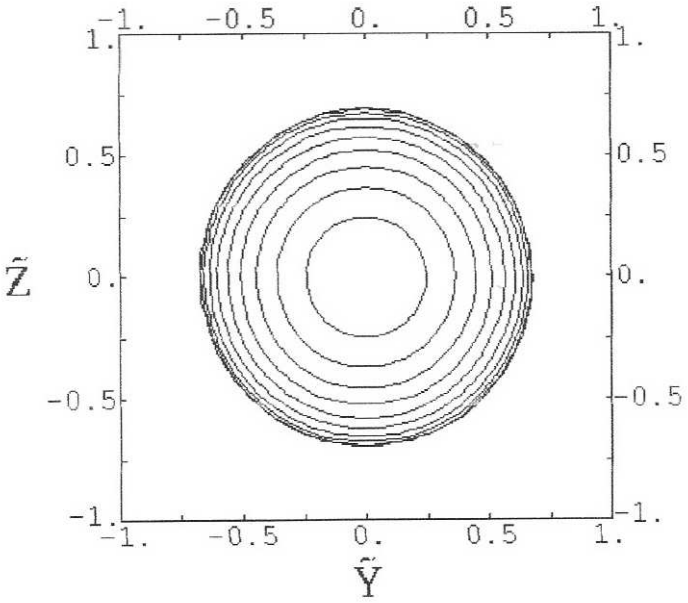

Figure 18: Contours of the density in the meridional $\tilde{Y}$-$\tilde{Z}$ plane for the IRR-type binary, with $p = 0.1$ and $n = 0.5$. [Uryu and Eriguchi(1998a)]

In a subsequent paper, Uryū and Eriguchi (2000) include the shape of the surface of the model for the gaseous component of the IRR binary system with $r = r_R$, $p = 0.1$ and $n = 0.5$. We include this figure here as Figure 19 .

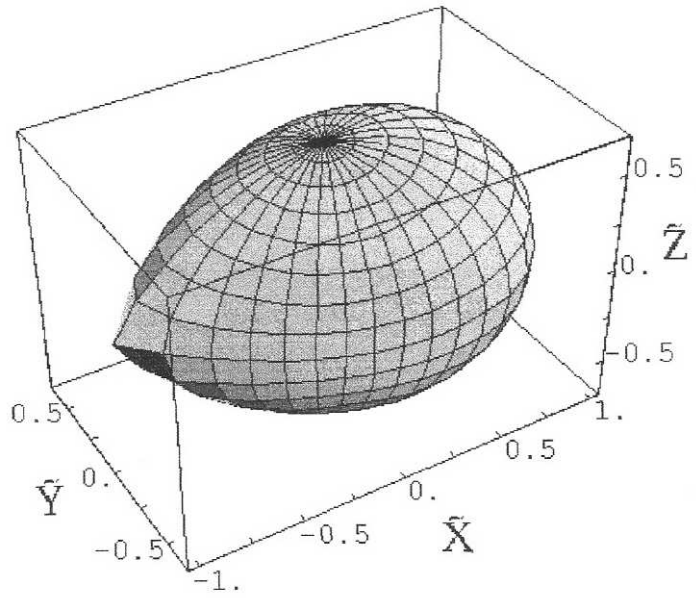

Figure 19: Surface shape of the gaseous component of the IRR binary system with $n = 0.5$ and $M_{NS}/M_{BH} = 0.1$ polytropes. [Uryu and Eriguchi(2000)]

In the same paper, Uryū and Eriguchi show that the gaseous component, the neutron star (NS), becomes highly deformed for larger mass ratios. We include these figures here as Figures 20-22 for the IRR binary system $r = r_R$, $p = 0.5$ and $n = 1$. The density distributions in the equatorial and meridional planes show that the inner edges of the neutron stars become cusp-like. These configurations correspond to the smallest separations and are dynamically stable models. As in the polytropes with $p = 0.1$, these figures show that the configurations for the IRR system become slightly prolate.

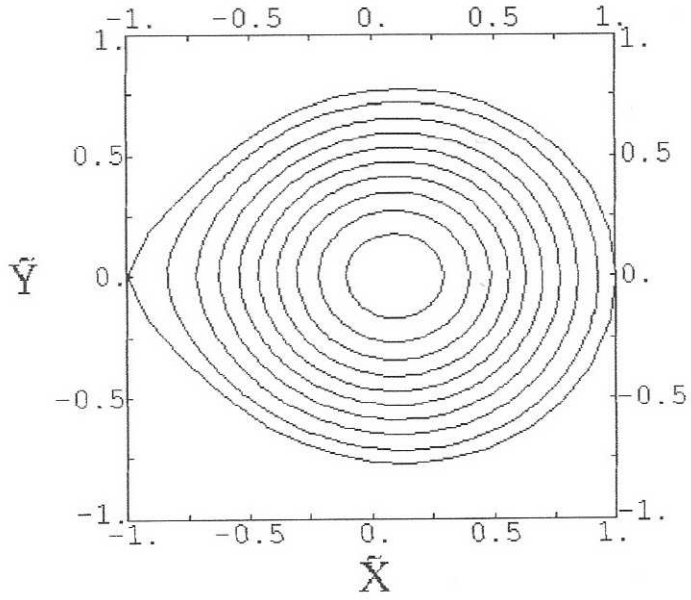

Figure 20: Density distribution in the equatorial plane for IRR-type binary ($p = 0.5$ and $n = 1$) [Uryu and Eriguchi(2000)]

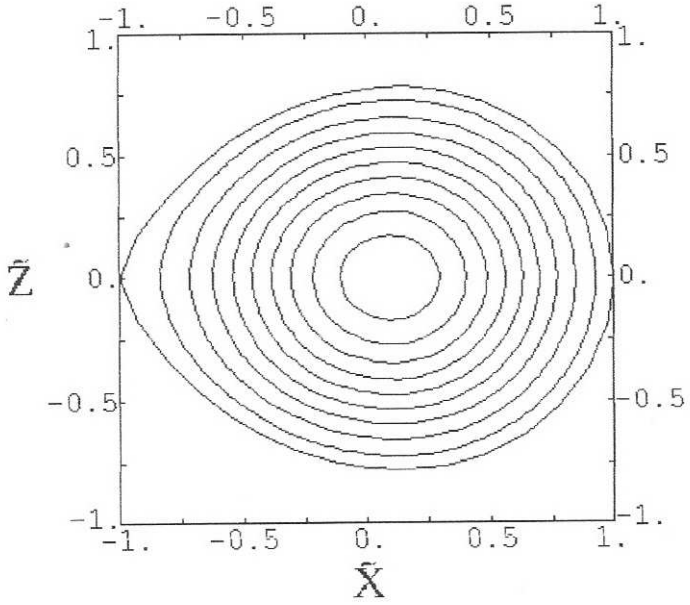

Figure 21: Density distribution in the meridional $\tilde{X}$-$\tilde{Z}$ plane for IRR-type binary ($p = 0.5$ and $n = 1$) [Uryu and Eriguchi(2000)]

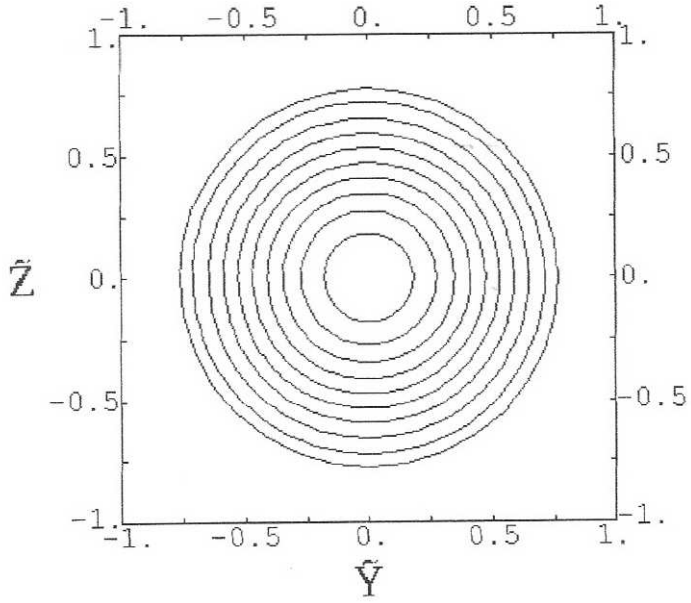

Figure 22: Density distribution in the meridional $\tilde{Y}$-$\tilde{Z}$ plane for IRR-type binary ($p = 0.5$ and $n = 1$) [Uryu and Eriguchi(2000)]

4.4 Black Hole- Neutron Star Binaries in Full General Relativity

Most of the attention in the study of compact binaries, has been on double binaries : Binary Neutron Stars, (BNS or NSNS), and Binary Black Holes, (BBH or BHBH). Both fully general realitivistic gravitation as well as physically realistic equations of state have been included in recent treat-

ments of NSNS mergers (Shibata, Tanigichi and Uryū, 2005 and Shibata and Taniguchi,2006). Progress on the numerical evolution of merging BHBH binaries has been rapid, with Pretorius (2005) performing the stable merger of two equal mass black holes, through the implementation of generalised harmonic coordinates. The study of NSBH binaries has enjoyed less attention, albeit that they are expected to represent a significant proportion of compact mergers visible in gravity waves and NSBH mergers are predicted to be one of the most likely progenitors for short gamma-ray bursts (SGRBs). For the research that has been conducted on NSBH binaries, the majority has been performed in Newtonian gravity. The scenario based on the tidal approximation studies may be incorrect as gravitational radiation reaction and gravititional effects of NS to the orbital motion are ignored.

The reason that research into NSBH binaries has lagged behind those of double binaries is simply the high costs of computer simulations, together with the high costs of developing the appropriate computational infrastucture. This necessitates the development of a framework which admits the use of approximations, thus dratically reducing the computational resources needed. Stationary states of NSBH binary systems provide models just prior to coalescence. Relativistic astrophysicists have tried to solve equilibrium configurations of highly deformed close binary star systems by devising nu-

merical schemes for the binaries. The expected observational data of the GW detectors will be compared against the theoretical results for the ISCO. These will provide a large amount of information about the macroscopic quantities of mass and spin of the neutron star as well as microscopic characters such as the EOS and the viscosity (Cutler, et al. 1993; Shibata 1997 ; Baumgarte et al. 1997, 1998a, 1998b ; Bonazzola, Gourgoulhon and Marck 1997).

Simulating coalescing binary systems, requires that initial data be produced that both satisfy the Einstein constraint equations and are as physically relevant as possible. The initial configurations are then evolved forward in time. Most of the initial data for coalescing binaries depend on the quasiequilibrium (QE) hypothesis, which assumes that the objects are on exact closed circular orbits. Whilst no closed orbits can exist for those systems in general relativity, this is a good approximation for large separations (Grandclément 2006). Research into binary neutron stars (BNS) using this approximation, have been done by Baumgarte et al. 1998a, 1998b; Usui, Uryū and Eriguchi 2000; Uryū and Y. Eriguchi 2000; Gourgoulhon et al. 2001. The QE approach has also been applied to the binary black hole system (BBH) by Pfeiffer, Teukolsky and Cook 2000; Gourgoulhon, Grandclément and Bonazzola 2002; Grandclément, E. Gourgoulhon and S. Bonazzola 2002 and Caudill 2006. Whilst the quasiequilibrium approximation is a good one

for large separation, it becomes less accurate as the distance between the compact objects decrease. Eventually the approximation breaks down necessitating the use of full dynamical simulations. Recently, Bishop et al. (2005), made a first step in this direction in a relativistic context. Their approach showed that the initial spurious GW signal resulting from the approximations in the calculation of the initial data are rapidly radiated away. As a result, the NSBH relaxes to a quasi-equilibrium state with an approximate orbital motion of the NS which has been followed only for a small fraction of an orbit. They have developed and implemented a numerical relativity code(within the characteristic framework) for evolving a star in close orbit around a Schwarzschild black hole. The conservative formulation of the hydrodynamics, provides procedures for determining initial data. The study does not take into account variations of the initial matter data, such as the shape or size of the star, which would occur if tidal distortion were allowed.

A similar approach to Bishop et al., (2005), is used by Sopuerta, Sperhake and Laguna, (2006). They treat the problem in full general relativity, by 'freezing' the hydrodynamics of their neutron star. For large black hole-to-neutron star mass ratios the approximation is valid if in addition the dynamical timescales related with the deformation of the neutron star are much bigger than the orbital timescales. In their *hydro-without-hydro* ap-

proximation they freeze most of the hydrodynamical degrees of freedom and evolve only a finite number of them with their attention focussed on the radiation-reaction effects in the orbit. The reduction of the degrees of freedom avoids the use of hyrodynamical computations. In this approximation scheme, the internal and external motions, which are generally coupled, are separated. The former motion consists of the evolution of the parameters describing the deformations of the matter distributions due to the tidal deformations, for instance. The latter motion consists of the orbital motion of a reference point in the matter distribution (a relativistic generalisation to the Newtonian concept of centre of mass).

First simulations of a head-on collision of a neutron star and a black hole of comparable mass in full General Relativity have been conducted by Löffler, Rezzolla, and Ansorg (2006). They do not set any limitations on the mass ratio between the black hole and the neutron star, nor on the position of the black hole, whose apparent horizon is entirely contained within the computational domain. For a prototypical binary system with mass ratio 6, they find that although a tidal disruption is evident, the neutron star is accreted promptly and entirely into the black hole. They also discuss a new approach for obtaining initial data for mixed binary systems and include an extraction of the gravitational wave signal produced in their study.

Taniguchi et al. (2007a, 2007b) have pursued a systematic approach to developing increasingly realistic models of BHNS binaries in quasiequilibrium circular orbits. Their first studies (Faber et al. 2006; Baumgarte, Skoge, and Shapiro 2004; Taniguchi et al. 2005) assumed extreme mass ratios, i.e. $m_{BH} \gg m_{NS}$. From a computational point of view, this is a very natural first step. However, binaries with comparable masses are much more interesting from the perspective of ground-based gravitational wave observations and for the launching of SGRBs. They have extended their results to the case of comparable-mass BHNS binaries Taniguchi et al. (2006, 2007a, 2007b). They adopt a polytropic equation of state and focus on irrotational neutron star configurations as well as approximately nonspinning black holes. In order to ascertain the ISCO they try to locate turning points along both the binding energy and total angular momentum curves. They also identify the formation of cusps on the neutron star surface, indicating the onset of tidal disruption. By comparing critical binary separations for different mass ratios and neutron star compactions they distinguish those regions of parameter space that will lead to a tidal disruption of the neutron star from those that will result in the plunge into the black hole of a neutron star more or less intact, albeit distorted by tidal forces. They also estimate the energy spectrum of the outgoing gravitational radiation emitted during the inspiral

phase for these binaries.

Other recent work includes that of Tsokaros and Uryū (2007) and Shibata and Taniguchi (2007). Tsokaros and Uryū (2007) present a new numerical method to construct binary black hole - neutron star initial data. The method uses three spherical coordinate patches. Shibata and Taniguchi (2007) systematically perform the merger simulation of black hole-neutron star (BH-NS) binaries in full general relativity, focusing on the case where the NS is tidally disrupted. BH-NS binaries in a quasicircular orbit are prepared with initial conditions in which the BH is modeled by a nonspinning moving puncture. They investigate the binary for varying mass ratios and separation differences. They also present gravitational waveforms during the inspiral, tidal disruption of the NS, and subsequent evolution of the disrupted material. The amplitude of gravitational waves is found to decrease quickly after the onset of tidal disruption.

5 Observation and Detection

5.1 Population Synthesis

Currently no black hole-neutron star binary systems have been confirmed. So far, 8 double neutron stars (DNS) have been observed (Stairs 2004). Over the last three decades, population synthesis studies (Lattimer and Schramm 1976; Narayan, Piran and Shemi 1991; Tutukov and Yungelson 1993; Lipunov, Postnov and Prokhorov 1997; Portegies Zwart and Yungelson 1998; Belczýnski and Bulik 1999; Kalogera et al. 2001) have indicated that the rate of NSBH mergers is comparable to that of double neutron star binaries, and is on the order of 10^{-6} to 10^{-5} per year per galaxy. However, there is some controversy about the rates at which NSBH mergers do occur. Bethe and Brown (1998) argued that NSBH should merge about an order of magnitude more frequently than DNS, while a recent study by Pfahl et al. (2005) comes to the conclusion that the number of NSBH systems in the Galaxy should be below 1 % of the number of double neutron star systems.

In order for NSBH binaries to become both an astronomical and physical reality, evidence must be obtained that these configurations can be and have been produced. The current situation is not too dissimilar to what it was

with neutron stars, after their theoretical possibilty had been proposed by in 1934, by Zwicky and Baade in their paper *Supernovae and Cosmic Rays*. The first theoretical model was only published in 1939 by Oppenheimer and Volkoff, whilst the discovery of pulsars by Bell and Hewish took place in 1967. Hulse and Taylor (1975) discovered the first binary pulsar B1913+16 in 1975. This last discovery has, in turn, provided the first evidence for the existence of gravitational radiation (Taylor and Weisberg 1982). This DNS has also become valuable in testing general relativity in the strong-field regime (Taylor and Weisberg 1989).

Authors	NS + NS	NS + BH	BH + BH
	$[\mathrm{yr}^{-1}]$	$[\mathrm{yr}^{-1}]$	$[\mathrm{yr}^{-1}]$
Tutukov and Yungelson (1993)	3×10^{-4}	2×10^{-5}	1×10^{-6}
van den Heuvel and Lorimer (1996)		8×10^{-6}	
Lipunov et al. (1997)	3×10^{-5}	2×10^{-6}	3×10^{-7}
Portegies Zwart and Yungelson (1998)	2×10^{-5}	10^{-6}	
Bethe and Brown (1998)	10^{-5}	2×10^{-4}	
Nelemans et al. (2001)	2×10^{-5}	4×10^{-6}	
Voss and Tauris (2003)	2×10^{-6}	6×10^{-7}	10^{-5}
O'Shaughnessy et al. (2005)	7×10^{-6}	1×10^{-6}	1×10^{-6}
de Freitas Pacheco et al. (2006)	2×10^{-5}		

Table 4: Population synthesis calculations of merger rates of compact binaries by various groups.

5.2 Gravitational Waves

According to the theory of general relativity, as formulated by Einstein (1916, 1918), the force of gravity is due to curvature of spacetime caused by the presence of massive objects. The curvature is more pronounced the greater the mass of the object, which in turn increases the gravity. The motion of massive objects in spacetime produces changes to the curvature and if this motion occurs in a paticular way, ripples in the curvature of spacetime can be produced, which are referred to as gravitational waves. These waves are produced for accelerating masses, provided that the motion is not spherically or cylindrically symmetrical. The finite speed of light and gravitational influence is crucial to the existence of gravitational radiation. Mathematically, for gravitational radiation to occur, the second time derivative of the quadrupole moment (or the l-th time derivative of the l-th multipole moment) of the stress-energy tensor (of an isolated system) must be non-zero. For this reason we do not expect gravitational radiation from an isolated non-spinning object moving at constant speed nor from a spherical star pulsating spherically. However, two masses orbiting each other will produce gravitational radiation. From any standard text on gravitation such as (Misner, Thorne and Wheeler 1973), the quadrupole approximation to the Einstein

field equations give :

$$h \approx (G/c^4)\ddot{Q}/r \tag{151}$$

where $\ddot{Q}$ is the second time derivative of the source's quadrupole moment and r is the distance of the source from the Earth. We also see from (Misner, Thorne and Wheeler 1973) that : The corresponding power loss for two orbiting masses M_1 and M_2 with separation R is given by

$$P = \frac{dE}{dt} = -\frac{32G^4}{\pi c^5}\frac{(M_1 M_2)^2 (M_1 + M_2)}{R^5} \tag{152}$$

For the Earth-Sun system, this power loss is only about 300 watts. Compare this with the electromagnetic radiation of the sun of about 3.86×10^{26} watts or to the kinetic energy of the Earth orbiting the Sun of about 2.7×10^{33} joules. The scenario is very different for close compact binaries such as a NSBH binary.

Electromagnetic radiation forms the basis for much of our present understanding of the universe. Gravitational waves are set to revolutionise that understanding in that they are significantly different from electromagnetic waves. The following table compares them in an astronomical context.

Electromagnetic Waves	**Gravitational Waves**
typical sources of electromagnetic waves are stellar athmospheres, accretion discs and clouds of interstellar dust, none of which emit significant gravitational waves.	sources are collisions and mergers of black holes and other compact objects and emit very little electromagnetic radiation; the cores of supernovae which are hidden from electromagnetic view by dense layers of surrounding stellar gas.
propagate through spacetime as oscillating fields of coexisting electric and magnetic fields.	propagate as oscillations of the 'fabric' of spacetime itself.
are almost always incoherent superpositions of emission from individual electrons, atoms, or molecules.	produced by coherent, bulk motions of huge amounts of mass-energy - either material mass, or the energy of vibrating, nonlinear spacetime curvature.

wavelengths of electromagnetic waves are small compared to their sources (gas clouds, stellar atmospheres, accretion disks, ...), so from the waves we can make pictures of the sources.	wavelengths of cosmic gravitational waves are comparable to or larger than their coherent, bulk-moving sources, so we cannot make pictures from them. Instead, the gravitational waves are like sound; they carry, in two independent waveforms, a stereophonic, symphony-like description of their sources.
easily absorbed, scattered, and dispersed by matter.	travel nearly unscathed through all forms and amounts of intervening matter.
frequencies range from about 10^7 Hz *upwards* by around 20 orders of magnitude.	frequencies should range from around 10^4 Hz *downwards* by about 20 orders of magnitude.
information brought to us by electromagnetic waves show us the thermodynamic state of optically thin concentrations of matter.	gravitational waves will show us details of the bulk motion of dense concentrations of energy.

The frequency range of the gravitational waves may be broken into four frequency bands :

- The **Extremely Low Frequency Band** (ELF)

  range : 10^{-15} to 10^{-18} Hz.

  The measured anisotropy of the cosmic microwave background radiation places strong limits on gravitational wave strengths and may, in fact, have detected waves.

  The only waves expected in this band are relics of the big bang.

- The **Very Low Frequency Band** (VLF).

  range : 10^{-7} to 10^{-9} Hz.

  The only expected strong sources in this band are processes in the very early universe such as the big bang, phase transitions of the vacuum states of quantum fields, and vibrating or colliding defects in the structure of spacetime, such as monopoles, cosmic strings, domain walls, textures, and combinations thereof.

- The **Low-Frequency Band** (LF).

  range : 10^{-4} to 1 Hz. Joseph Taylor and others have achieved remarkable gravity-wave sensitivities by the timing of millisecond pulsars.

The Laser Interferometer Space Antenna, LISA will operate in this frequency range.

This is the band of massive black holes (M 1000 to 10^8M.) in the distant universe, and of other hypothetical massive exotic objects (naked singularities, soliton stars), as well of as binary stars (ordinary, white dwarf, neutron star, and black hole)

- The **High-Frequency Band** (HF).

  range : 1 to 10^4 Hz.

  Earth-based gravitational-wave detectors such as LIGO, VIRGO and TAMA operate in this frequency range. This is the band of stellar-mass black holes (M 1 to 1000M. and of other conceivable stellar-mass exotic objects (naked singularities and boson stars) in the distant universe, as well as of supernovae, pulsars, and coalescing and colliding neutron stars. Early universe processes should also have produced waves at these frequencies, as in the ELF, VLF, and LF bands.

5.3 Gravitational Wave Detection by Interferometers

From general relativity, a gravitational wave has two linear polarisations. These polarisations each have an associated gravitational-wave field which

oscillates in time and propagates at the speed of light. As each wave passes through any object it produces tidal forces. For objects that are comparitively small in relation to the wavelength of these waves, the forces have quadrapolar patterns relative to the object's center. These patterns are shown in Figure 12.

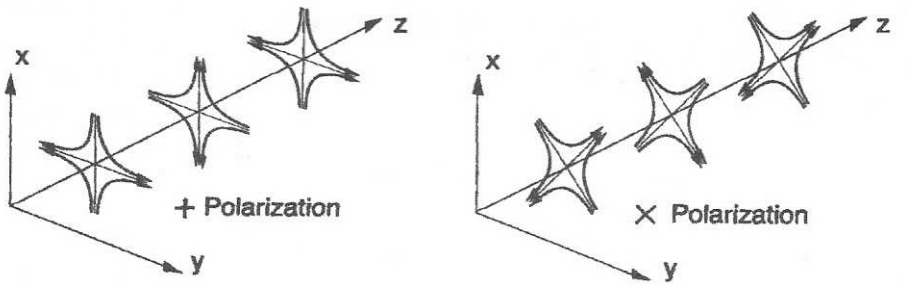

Figure 23: The lines of force associated with the two polarizations of a gravitational wave. [From Ref. Abramovici et. al. (1992)]

From the force patterns characterised by the orientation of the axis, the polaristaions have derived the names 'plus'(+) and 'cross' (×). Each of the gravitational wave fields are in turn named h_+ and $h_\times$.

The Weber bar, a large, solid piece of metal with electronics attached to detect any vibrations was the first type of gravitational wave detector. Passing gravitational waves "ring up" the bar at its resonant frequency, which would basically amplify the wave naturally. Nearby supernova may be strong

enough to be seen without resonant amplification. Modern forms of the Weber bar are still operated, cryogenically cooled, with superconducting quantum interference devices to detect the motion. However they are not sensitive enough to detect anything but extremely powerful gravitational waves.

Currently, gravitational wave detectors consist of a laser interferometer with four masses hanging from vibration-isolated supports with an optical system to monitor the separations between the masses. Figure 12 illustrates such a detection sytem.

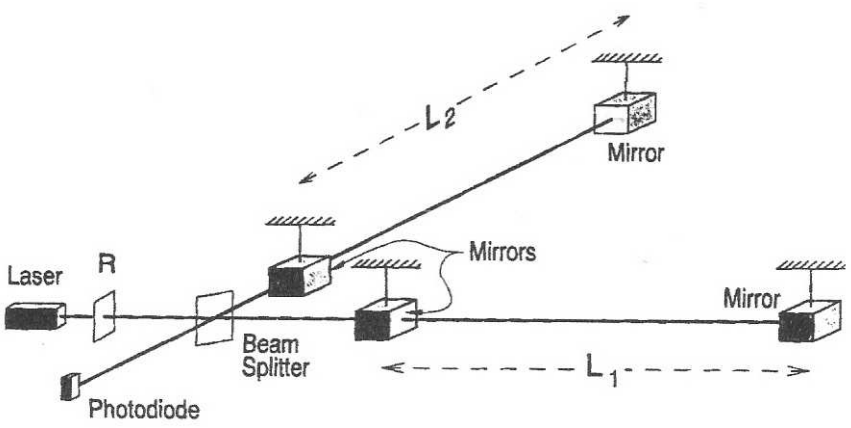

Figure 24: Schematic diagram of a laser interferometer gravitational wave detector. [From Ref. Abramovici et. al. (1992)]

The device consists of two long arms at right angles to each other meeting each other in such a manner as to form an 'L shape'. A mass is placed at each end of the long arms of the 'L shape', whilst two masses are placed

near each other at the corner of the 'L'. The arm lengths are approximately equal, with $L_1 \simeq L_2 = L$. As a gravitational wave (with high frequencies in comparison to the masses' $\sim$ 1Hz pendulum frequency) passes through the detector, the masses are pushed back and forth relative to each other. This results in a change in the arm-length difference, i.e. $\Delta L \equiv L_1 - L_2$. Through laser interferometry that change is monitored. The variations in the output of the photodiode (the output of the interferometer) is directly proportional to ΔL. If the gravitaional waves are arriving from above or below the device and the axes of the + polarisation coincide with the arm's directions, then it is the waves' + polarisation that will drive the massses. We may then write :

$$\frac{\Delta L(t)}{L} = h_+(t). \tag{153}$$

In general, though, it is more likely that the interferometer's output is a linear combination of the two wave fields :

$$\frac{\Delta L(t)}{L} = F_+ h_+(t) + F_\times h_\times \equiv h(t). \tag{154}$$

$h(t)$ is referred to as the gravitational wave-strain acting on the detector. Reliable detection of gravitational waves requires the operation of at least two detectors in coincidence - if the signals coincide with those of a distant detector, local perturbations can be ruled out. In order to obtain the full information about the gravitational waves (source position, polarization),

data from at least four detectors have to be compared. For a NSBH binary's inspiral and coalescence, two gravitational waves are produced, one for each polarisation. The waveform can be divided into three parts. The first, the *inspiral waveform* is emitted before tidal distortions become noticeable; the second, the *coalesence waveform* is emitted during distortion, disruption and/or merger; and the third, the *ringdown waveform* is due to the excitation of quasi-normal modes of the black hole.

5.4 Currently Operational Ground-based Laser Interferometers

- LIGO

  The Laser Interferometer Gravitational-Wave Observatory (LIGO) is a US Project consisting of two detectors (4km). LIGO operates two gravitational wave observatories in unison: the LIGO Livingston Observatory in Livingston, Louisiana and the LIGO Hanford Observatory, on the Hanford Nuclear Reservation located near Richland, Washington. These sites are separated by 3,002 kilometers. Since gravitational waves are expected to travel at the speed of light, this distance corresponds to a difference in gravitational wave arrival times of up to ten

milliseconds. Using triangulation, the difference in arrival times can restrict the location of the source of the wave in the sky. Each observatory supports an L-shaped ultra high vacuum system, measuring 4 kilometers on each side. Up to five interferometers can be set up in each vacuum system.

- VIRGO

  The VIRGO collaboration was set up between Italian and French research teams. The Virgo detector for gravitational waves consists mainly in a Michelson laser interferometer made of two orthogonal arms being each 3 kilometers long. Multiple reflections between mirrors located at the extremities of each arm extend the effective optical length of each arm up to 120 kilometers. The frequency range of Virgo extends from 10 to 6,000 Hz. This range as well as the very high sensitivity should allow detection of gravitational radiation produced by supernovae and coalescence of binary systems in the milky way and in outer galaxies, for instance from the Virgo cluster.

- GEO 600

  Of all the large interferometric gravitational-wave detectors, the German/British project GEO600 is the only one which uses dual recycling. GEO600, with an interferometric gravitational-wave detector of arm

length 600 m, is in northern Germany close to Hannover. GEO600 incorporates an externally modulated fourfold delay-line Michelson interferometer giving a round-trip optical length of 2400 m. Power recycling increases the light power inside the interferometer to a level of about 10 kW. The use of both power and signal recycling will yield a sensitivity of the same order of magnitude as the first stages of the other large-scale gravitational-wave detectors LIGO and VIRGO. High signal recycling factors allow the sensitivity to be increased at a chosen frequency while reducing the bandwidth of the detector. This gives an advantage over broad-band detectors in detecting narrow-band periodic sources such as pulsars. The 25 cm diameter mirrors will be suspended as double pendulums from a platform supported by vibration-reduction systems. The passive filtering properties of this system sufficiently reduce the seismic noise in the frequency range of interest, i.e. 50 - 1000 Hz. Between 2002 and 2006 GEO600 participated in several data runs in coincidence with the LIGO detectors and is now gradually approaching design sensitivity.

- TAMA 300

  The Japanese project has an interferometric gravitational-wave detector of arm length 300 m. TAMA operations began with much success

in 1999, soon achieving world's-best sensitivity and the longest accumulated data set during its runs in 2000 and 2001. With the start of the LIGO science run in 2002, TAMA aggressively joined the effort, helping to forge the international collaboration of coincidence analysis by scheduling operation time and sharing analysis methods and data.

5.5 Future Plans for Gravitational Wave Detectors

- Advanced LIGO

  As the initial LIGO interferometers start to put new limits on gravitational wave signals, the LIGO Lab, the LIGO Scientific Collaboration, and international partners are proposing Advanced LIGO to improve the sensitivity by more than a factor of 10. This new detector, to be installed at the LIGO Observatories, will replace the present detector once it has reached its goal of a year of observation, and will transform gravitational wave science into a real observational tool. It is anticipated that this new instrument will see gravitational wave sources possibly as often as daily, with excellent signal strengths, allowing details of the waveforms to be read off and compared with theories of neutron stars, black holes, and other highly relativistic objects. The

improvement of sensitivity will allow the one-year planned observation time of initial LIGO to be equaled in just several hours.

The change of more than a factor of 10 in sensitivity comes also with a change in the bandwidth of high sensitivity, and the ability to tune the instrument for specific astrophysical sources. This will allow Advanced LIGO to look at the inspiral, coalescence, and ringdown of pairs of black holes up to 50 solar masses, and to pinpoint periodic signals from the many known pulsars which radiate in the range from 500-1000 Hertz. A program of testing and practice installation will allow the new detectors to be brought on-line with a minimum of interruption in observation. The design of the instrument has come from scientists throughout the 40-institution, 400-person LIGO Scientific Collaboration, an international group which carries out both instrument development and scientific data analysis. Observations will start in 2013.

- LCGT

  The Large-scale Cryogenic Gravitational-wave Telescope, LCGT, is the next generation interferometer now under proposal in Japan. This powerful new instrument has a sensitivity comparable to the Advanced LIGO design and a far-reaching sky coverage complementary to that of other gravitational-wave detectors. The unique design of LCGT

is its use of a cryogenic system to suppress thermal noise. Sapphire was chosen for the substrate material because of its optical thermal conductivity and measured high Q values at low temperatures.

- LISA

  As the first dedicated space-based gravitational wave observatory, LISA will detect waves generated by binaries within our Galaxy, the Milky Way, and by massive black holes in distant galaxies. Although gravitational wave searches in space have previously been made, they were conducted for short periods by planetary missions that had other primary science objectives. Some current missions are using microwave Doppler tracking to search for gravitational waves. However, LISA will use an advanced system of laser interferometry for detecting and measuring them. And, LISA will directly detect the existence of gravitational waves, rather than inferring it from the motion of celestial bodies, as has been done previously. Additionally, LISA will make its observations in a low-frequency band that ground-based detectors can't achieve. Note that this difference in frequency bands makes LISA and ground detectors complementary rather than competitive. This range of frequencies is similar to the various types of electromagnetic wavelengths detected in astronomy, such as ultraviolet and infrared. Each

provides different information. In space, LISA won't be affected by the environmental noise that affects ground detectors on Earth's surface. Due to earthquakes and other vibrations, ground detectors can only make observations at frequencies above 1 hertz. However, other environmental factors will impact LISA. Such factors include the drift of the spacecraft, charging of the test masses, and buffeting by the solar wind. Making these small disturbances negligible is a technological challenge of the mission. Meeting this challenge will help to ensure the detection of gravitational waves. LISA is expected to be operational by 2015.

5.6 Gamma-Ray Bursts

The first gamma-ray burst(GRB) was detected on the 2nd of July 1967 by the US Vela nuclear test detection satellites. The discovery of GRBs was confirmed by many later space missions, including Apollo and the Soviet Venera probes. Many speculative theories about these events were presented, most of which involved nearby Galactic sources. However, there were no major new advancements until the launch in 1991 of the Compton Gamma Ray Observatory and its Burst and Transient Source Explorer (BATSE) instrument, an

extremely sensitive gamma-ray detector. Among the crucial pieces of information provided by this instrument were that gamma-ray bursts are isotropic (that is, not biased towards any particular direction on the sky such as the Galactic plane or Galactic center), ruling out nearly all Galactic origins; and that they fall into two apparently distinct categories, short-duration, hard-spectrum bursts ("short bursts") and long-duration, soft-spectrum bursts ("long bursts"). Short bursts are typically less than two seconds in duration and are dominated by higher-energy photons; long bursts are typically more than two seconds in duration and dominated by lower-energy photons. The separation is not absolute and the populations do overlap observationally, but the distinction suggested two different classes of progenitors. There is now almost universal agreement in the astrophysics community that the long-duration bursts are associated with the deaths of massive stars in a specific kind of supernova-like event commonly referred to as a collapsar.

While the astrophysical community has yet to settle on a single, universally favored model for the progenitors of the short-duration events, the general preferred model is the merger of two compact objects as a result of gravitational inspiral: two neutron stars, or a neutron star and a black hole.

A revolution in GRB astronomy is in progress today, largely as a result of

the successful launch of NASA's Swift satellite, which combines a sensitive gamma-ray detector with the ability to slew on-board X-ray and optical telescopes to the direction of a new burst in under one minute. Among the discoveries so far are the first discoveries of short burst afterglows and vast amounts of data on the behavior of GRB afterglows at early times in their evolution, even before the GRB itself (that is, the gamma-ray emission) has stopped, and the discovery of huge X-ray flares appearing from minutes to days after the end of the GRB. Additional discoveries are being made constantly, and as such, the study of GRBs is one of the most dynamic in all of astrophysics.

6 Conclusions

It has been nearly a century since the theory of relativity was first postulated by Einstein. Even before this theory was fully formulated (Einstein 1916, 1918), it became clear to Einstein and others that the theory would have to predict gravitational waves. Almost immediately after formulating the *General Theory of Relativity*, Einstein worked out the basic properties of those waves. Detection of these waves has been elusive, primarily due to the difficulty in creating the technology to do so. Over the next few years, the sensitivity of terrestrial-based detectors will reach levels of expected detection. Close binary systems such as the neutron star black hole binary, are considered as the primary targets for the forthcoming field of gravitational wave astronomy. For compact objects such as a neutron star and a black hole in a binary configuration, the emission of gravitational waves completely controls the orbital evolution, which eventually leads to the coalescence of the components. It is extremely difficult to complete analytical calculations of these gravitational waves and so numerical investigations remain the only viable option in the final stages of evolution. This is in itself is a challenging task. For a neutron star in the vicinity of a black hole, gravitational waves are generated due to the quadrupole moment of the star-black hole system

changing in time. By computing the stellar shape and structure along its motion due to the time-varying deformation, we can construct quasi-statically evolutionary sequences of the inspiraling neutron star. In so doing we can attempt to evolve the star until the last few moments before merger, where the nonlinear character of the gravitational and tidal effects become important. This will enable us to prepare initial conditions for numerical simulations of the merging of the binary neutron star black hole in full general relativity. Apart from this, the problem of tidal deformation in itself is an interesting problem. Analytical solutions exist for various binary configurations mainly in Newtonian gravity. Providing an analytical solution for the tidal deformation of a neutron star in the vicinity of a black hole, fully taking into account general relativistic effects, is unlikely to occur in the near future, if at all.

Appendices

A The Interior Potential of Homoeiodal Shells

A homoeoid is a shell bounded by two similar concentric ellipsoids in which strata of equal density are also ellipsoids that are concentric with and similar to the bounding ellipsoids.

We first state a theorem due to Newton and its corollary :

THEOREM 1 (NEWTON'S THEOREM) *The attraction at any internal point of a homogeneous homoeoid is zero.*

COROLLARY *The theorem is true for any heterogeneous homoeoid in which the strata of equal density are ellipsoids concentric with and similar to the bounding ellipsoids.*

The following theorem also follows from Newton's Theorem.

THEOREM 2 *The constant potential inside a homogeneous homoeoidal shell enclosed between the ellipsoids with the semi-axes a_i and qa_i, where*

$a_1 \leq a_2 \leq a_3$ *and* $q < 1$ *is given by*

$$\mathfrak{B} = \frac{1}{2} G\rho(1 - q^2) \int_S r^2 d\omega \tag{155}$$

where $\mathbf{r}$ *is the radius vector drawn from the centre to a point on the surface* (S) *of the outer bounding ellipsoid defined by*

$$\sum_{i=1}^{3} (\frac{x_i^2}{a_i^2}) = 1 \tag{156}$$

Proof. From Newton's Theorem, the potential is constant throughout the interior and equal to its value at the centre.

Now, consider an elementary cone of solid angle $\mathrm{d}\omega$, with its vertex at the centre, the contribution to $\mathfrak{B}$ by the frustrum of the cone intercepted by the homoeoid is

$$\int_{r_1}^{r_2} G\rho r d\omega dr = G\rho d\omega \left[\frac{r^2}{2}\right]_{r_1}^{r_2} = \frac{1}{2} G\rho(r_2^2 - r_1^2) dw \tag{157}$$

where, r_2^2 and r_1^2 are the radii of the outer and inner surfaces of the homoeoid in the direction of the cone.

Now, $r_1 = qr_2$

So, $\mathfrak{B} = \int_S \frac{1}{2} G\rho(r_2^2 - q^2 r_2^2) d\omega$

Hence,

$$\mathfrak{B} = \frac{1}{2} G\rho(1 - q^2) \int_S r^2 d\omega \tag{158}$$

which is the constant potential inside a homogeneous homoeoidal shell enclosed between the ellipsoids with the semi-axes a_i and qa_i.

The mass of our homoeiodal shell is given by :

$$M = \frac{4}{3}\pi a_1 a_2 a_3 (1 - q^3) \times \rho \tag{159}$$

giving

$$\rho = \frac{M}{\frac{4}{3}\pi a_1 a_2 a_3} . \frac{1}{(1 - q^3)} \tag{160}$$

hence

$$\mathfrak{B} = \frac{\frac{1}{2} GM}{\frac{4}{3}\pi a_1 a_2 a_3} . \frac{1 - q^2}{(1 - q^3)} \int_s r^2 d\omega \tag{161}$$

Now,

$$\begin{aligned} lim_{q \to 1} \frac{1 - q^2}{(1 - q^3)} &= lim_{q \to 1} \frac{(1 - q^2)'}{(1 - q^3)'} \\ &= lim_{q \to 1} \frac{-2q}{-3q^2} \\ &= \frac{2}{3} \end{aligned}$$

So, for fixed M, as $q \to 1$, we get

$$\mathfrak{B} = \frac{GM}{4\pi a_1 a_2 a_3} \int_s r^2 d\omega \tag{162}$$

Now,

$$x_1 = r \sin\theta \cos\chi \tag{163}$$

$$x_2 = r \sin\theta \sin\chi \tag{164}$$

$$x_3 = r \cos\theta \tag{165}$$

But,

$$\begin{aligned} 1 &= \sum_{i=1}^{3} \left(\frac{x_i^2}{a_i^2} \right) \\ &= \frac{x_1^2}{a_1^2} + \frac{x_2^2}{a_2^2} + \frac{x_3^2}{a_3^2} \\ &= \frac{r^2 \cos^2\theta}{a_3^2 + r^2 \sin^2\theta} \left(\frac{\cos^2\chi}{a_1^2} + \frac{\sin^2\chi}{a_2^2} \right) \end{aligned}$$

$$\therefore \quad \frac{1}{r^2} = \frac{\cos^2\theta}{a_3^2} + \sin^2\theta \left(\frac{\cos^2\chi}{a_1^2} + \frac{\sin^2\chi}{a_2^2} \right) \tag{166}$$

$$\tag{167}$$

We make the substitution : $t = \tan\chi$

with,

$$dt = \sec^2\chi d\chi$$

$$t^2 = \frac{\sin^2\chi}{\cos^2\chi}$$

$$d\chi = \cos^2\chi dt$$

We can then write :

$$d\chi\left[\frac{\cos^2\theta}{a_3^2} + \sin^2\theta\left(\frac{\cos^2\chi}{a_1^2} + \frac{\sin^2\chi}{a_2^2}\right)\right]^{-1}$$

$$= \quad dt\left[\frac{\cos^2\theta}{\cos^2\chi.a_3^2} + \sin^2\theta\left(\frac{1}{a_1^2} + \frac{\sin^2\chi}{\cos^2\chi.a_2^2}\right)\right]^{-1}$$

$$= \quad dt\left[(\sin^2\theta + \cos^2\theta)\frac{\cos^2\theta}{\cos^2\chi.a_3^2} + \left(\frac{\sin^2\theta}{a_1^2} + t^2.\frac{\sin^2\theta}{a_2^2}\right)\right]^{-1}$$

$$= \quad dt\left[\frac{\sin^2\theta}{a_1^2} + \frac{\cos^2\theta}{a_3^2} + t^2\left(\frac{\sin^2\theta}{a_2^2} + \frac{\cos^2\theta}{a_3^2}\right)\right]^{-1}$$

Now, with $0 \leq \chi \leq \pi$ and $0 \leq \theta \leq \pi$, we have :

$$\int_S r^2 d\omega = 8 \int_0^{\frac{\pi}{2}} \int_0^{\frac{\pi}{2}} \frac{\sin\theta d\theta d\chi}{\frac{\cos^2\theta}{a_3^2} + \sin^2\theta \left(\frac{\cos^2\chi}{a_1^2} + \frac{\sin^2\chi}{a_1^2} \right)} \tag{168}$$

Making the substitution, $t = \tan\chi$, we get by symmetry:

$$\int_S r^2 d\omega = 8 \int_0^{\frac{1}{2}} \int_0^{\frac{\pi}{2}} d\theta \sin\theta \frac{dt}{\left[\frac{\sin^2\theta}{a_1^2} + \frac{\cos^2\theta}{a_3^2} + t^2 \left(\frac{\sin^2\theta}{a_2^2} + \frac{\cos^2\theta}{a_3^2} \right) \right]} \tag{169}$$

But,

$$\int_0^{\infty} \frac{dx}{a^2 + x^2} = \frac{\pi}{2a}$$

so,

$$\int_0^{\infty} \frac{dx}{a^2 + b^2 x^2} = \frac{\pi}{2ab}$$

$$\therefore \int_S r^2 d\omega = 4\pi \int_0^{\frac{\pi}{2}} \frac{\sin\theta d\theta}{\left[\left(\frac{\sin^2\theta}{a_1^2} \right)^{\frac{1}{2}} + \frac{\cos^2\theta}{a_3^2} \times \left(\frac{\sin^2\theta}{a_2^2} + \frac{\cos^2\theta}{a_3^2} \right)^{\frac{1}{2}} \right]} \tag{170}$$

Then, multiplying the RHS by $\frac{\left(\frac{1}{\cos^2\theta}\right)}{\left(\frac{1}{\cos^2\theta}\right)}$, we get :

$$\int_S r^2 d\omega = 4\pi \int_0^{\frac{\pi}{2}} \frac{\left(\frac{1}{\cos^2\theta}\right)\sin\theta d\theta}{\left[(a_1a_3)^{-1}\left(\tan^2\theta a_3^2 + a_1^2\right)^{\frac{1}{2}} \times (a_2a_3)^{-1}\left(\tan^2\theta a_3^2 + a_2^2\right)^{\frac{1}{2}}\right]} \tag{171}$$

Now, we take the transformation :

$$u = a_3^2 \tan^2\theta$$

with,

$$\begin{aligned} du &= 2a_3^2 \tan\theta \sec^2\theta d\theta \\ &= 2a_3^2 \sin\theta \sec^3\theta d\theta \end{aligned}$$

Hence,

$$\int_S r^2 d\omega = 2\pi a_1 a_2 \int du \left[\sec\theta.\left(a_1^2 + u\right)^{\frac{1}{2}} + \left(a_2^2 + u\right)^{\frac{1}{2}}\right)^{-1} \tag{172}$$

Now,

$$\sec\theta = \left(1 + \tan^2\theta\right)^{\frac{1}{2}}$$

$$a_3 \sec\theta \;=\; \left(a_3^2+u\right)^{\frac{1}{2}}$$

Then,

$$\int_S r^2 d\omega \;=\; 2\pi a_1 a_2 a_3 \int_0^\infty du \left[\left(a_1^2+u\right)^{\frac{1}{2}} \times \left(a_2^2+u\right)^{\frac{1}{2}} \times \left(a_3^2+u\right)^{\frac{1}{2}}\right]^{-1}$$

$$= \; 2\pi a_1 a_2 a_3 \int_0^\infty \frac{du}{\Delta} \tag{173}$$

where,

$$\Delta^2 = \left[\left(a_1^2+u\right)\left(a_2^2+u\right)\left(a_3^2+u\right)\right] \tag{174}$$

or

$$\int_S r^2 d\omega = 2\pi L \tag{175}$$

with

$$L = a_1 a_2 a_3 \int_0^\infty \frac{du}{\Delta} \tag{176}$$

Now, we introduce $l_i (i = 1, 2, 3)$, which are the direction cosines of the radius vector **r** joining the centre of the ellipsoid to a point on its surface, with :

$$\sum_{i=1}^{3} l_i^2 \;=\; 1 \tag{177}$$

$$
\begin{aligned}
l_i &= cos\alpha_i && (178)\\
&= \frac{x_i - x_i'}{d} && (179)\\
d &= \left[\sum_{i=1}^{3}(x_i - x_i')^2\right]^{\frac{1}{2}} && (180)
\end{aligned}
$$

Next we consider, $\int_S r^2 l_i^2 d\omega$.

Taking $i = 3$ first, we get :

$$
\begin{aligned}
\int_S r^2 l_3^2 d\omega &= \int_S r^2 \cos^2\theta d\omega \\
&= 2\pi a_1 a_2 a_3 \int_0^\infty \frac{\cos^2\theta d\omega}{\Delta}
\end{aligned}
$$

But,

$$
\begin{aligned}
\cos^2\theta = \frac{1}{\sec^2\theta} &= \left(1 + \tan^2\theta\right)^{-1} \\
&= a_3^2\left(a_3^2 + u\right)^{-1}
\end{aligned}
$$

So,

$$
\begin{aligned}
\int_S r^2 l_3^2 d\omega &= 2\pi a_1 a_2 a_3 \int_0^\infty \frac{a_3^2 du}{\Delta\left(a_3^2 + u\right)} \\
&= 2\pi a_3^2 A_3 && (181)
\end{aligned}
$$

where

$$A_3 = a_1 a_2 a_3 \int_0^\infty \frac{du}{\Delta\left(a_3^2 + u\right)} \tag{182}$$

By symmetry we can generalise.

$$\therefore \int_S r^2 l_i^2 d\omega = 2\pi a_i^2 A_i \tag{183}$$

with

$$A_i = a_1 a_2 a_3 \int_0^\infty \frac{du}{\Delta\left(a_i^2 + u\right)} \tag{184}$$

But,

$$\int_S r^2 d\omega \;\; = \sum_{i=1}^{3} \int_S r^2 l_i^2 d\omega \;\; = 2\pi L$$

$$\therefore \sum_{i=1}^{3} a_i^2 A_i = L \tag{185}$$

Now,

$$\frac{\partial L}{\partial a_3} \;\; = \;\; \frac{\partial}{\partial a_3}\left[a_1 a_2 a_3 \int_0^\infty \frac{du}{\Delta}\right]$$

$$= \quad a_1 a_2 \int_0^\infty \frac{du}{\Delta} \; + \; a_1 a_2 a_3 \left[\frac{\partial}{\partial a_3} \int_0^\infty \frac{du}{\Delta} \right] \tag{186}$$

But,

$$\Delta \quad = \quad \left[\left(a_1^2 + u\right)^{\frac{1}{2}} \left(a_2^2 + u\right)^{\frac{1}{2}} \left(a_3^2 + u\right)^{\frac{1}{2}} \right]$$

$$\therefore \frac{\partial}{\partial a_3} \int_0^\infty \frac{du}{\Delta} \quad = \quad \int_0^\infty du \frac{\partial}{\partial a_3} \left[\left(a_1^2 + u\right)^{-\frac{1}{2}} \left(a_2^2 + u\right)^{-\frac{1}{2}} \left(a_3^2 + u\right)^{-\frac{1}{2}} \right]$$

$$= \quad \int_0^\infty du \left(a_1^2 + u\right)^{-\frac{1}{2}} \left(a_2^2 + u\right)^{-\frac{1}{2}} \left(-\frac{1}{2}\right) \left(a_3^2 + u\right)^{-\frac{3}{2}} (2a_3) \tag{187}$$

Thus,

$$\frac{\partial L}{\partial a_3} \quad = \quad a_1 a_2 \int_0^\infty \frac{du}{\Delta} \; - a_1 a_2 a_3^2 \int_0^\infty \frac{du}{\Delta \left(a_3^2 + u\right)}$$

$$= \quad a_1 a_2 \int_0^\infty \frac{du}{\Delta} \; - a_3 A_3 \tag{188}$$

We can then write

$$A_3 = -\frac{1}{a_3}\frac{\partial L}{\partial a_3} + \frac{a_1 a_2}{a_3}\int_0^\infty \frac{du}{\Delta}$$

$$= -\frac{1}{a_3}\frac{\partial L}{\partial a_3} + \frac{L}{a_3^2} \tag{189}$$

$$\tag{190}$$

This can be generalised to :

$$A_i = \frac{L}{a_i^2} - \frac{1}{a_i}\frac{\partial L}{\partial a_i} \tag{191}$$

So,

$$\sum_{i=1}^{3} \frac{1}{(a_i^2 + u)} = \frac{2}{\Delta}\frac{d\Delta}{du} \tag{192}$$

We have

$$\sum_{i=1}^{3} A_i = \sum_{i=1}^{3} \left(a_1 a_2 a_3 \int_0^\infty \frac{du}{\Delta\,(a_i^2 + u)} \right)$$

$$= 2a_1 a_2 a_3 \int_0^\infty \frac{d\Delta}{\Delta^2}$$

$$= \left[\frac{-2a_1a_2a_3}{\Delta}\right]_0^\infty$$

But we can write

$$\Delta = a_1a_2a_3\left[\left(1+\frac{u}{a_1^2}\right)\left(1+\frac{u}{a_2^2}\right)\left(1+\frac{u}{a_3^2}\right)\right]^{\frac{1}{2}}$$

Since $\frac{u}{a_1^2} \geq 0$ we have $\Delta_{min} = a_1a_2a_3$. Then,

$$\begin{aligned}\left[\frac{-2a_1a_2a_3}{\Delta}\right]_0^\infty &= \left[0 - \frac{-2a_1a_2a_3}{\Delta}\right] \\ &= 2 \qquad (193)\end{aligned}$$

i.e.

$$\sum_{i=1}^{3} A_i = 2 \qquad (194)$$

we have

$$\int_S r^2 d\omega = 2\pi L$$

Differentiating w.r.t. a_i, we get

$$\int_s r\left(\frac{\partial r}{\partial a_i}\right)d\omega = \pi\left(\frac{\partial L}{\partial a_i}\right) \qquad (195)$$

Now,

$$\frac{1}{r^2} = \frac{\cos^2\theta}{a_3^2} + \sin^2\theta\left(\frac{\cos^2\chi}{a_1^2} + \frac{\sin^2\chi}{a_1^2}\right)$$

$$= \frac{l_3^2}{a_3^2} + \frac{l_1^2}{a_1^2} + \frac{l_2^2}{a_2^2}$$

$$\therefore \frac{1}{r^2} = \sum_j^3 = \frac{l_j^2}{a_j^2} \tag{196}$$

Differentiating w.r.t a_i gives

$$-\frac{2}{r^3}\left(\frac{\partial r}{\partial a_i}\right) = -\frac{2l_i^2}{a_i^2}$$

$$\therefore \left(\frac{\partial r}{\partial a_i}\right) = \left(\frac{1}{a_i^3}\right) r^3 l_i^2 \tag{197}$$

Substituting

$$\int_S \left(\frac{1}{a_i^3}\right) r^4 l_i^2 d\omega = \pi\left(\frac{\partial L}{\partial a_i}\right)$$

$$\therefore \int_S r^4 l_i^2 d\omega = \pi a_i^3 \left(\frac{\partial L}{\partial a_i}\right) \tag{198}$$

The standard incomplete integrals are

for the first kind

$$E\left(\psi,\chi\right) \;=\; \int_0^{\chi}\left(1-\sin^2\psi\ \sin^2\chi\ \right)^{\frac{1}{2}}d\chi \tag{199}$$

and for the second kind

$$F\left(\psi,\chi\right) \;=\; \int_0^{\chi}\left(1-\sin^2\psi\ \sin^2\chi\ \right)^{-\frac{1}{2}} \tag{200}$$

with the definitions :

$$\sin\psi \;=\; \left(\frac{a_1^2-a_2^2}{a_1^2-a_3^2}\right)^{\frac{1}{2}} \tag{201}$$

$$cos\chi \;=\; \frac{a_3}{a_1}=\left(1-e^2\right)^{\frac{1}{2}} \tag{202}$$

where $e=\left(1-\frac{a_3^2}{a_1^2}\right)^{\frac{1}{2}}$

We can also write :

$$\cos\psi \;=\; \left(\frac{a_2^2-a_3^2}{a_1^2-a_3^2}\right)^{\frac{1}{2}} \tag{203}$$

and

$$\sin\chi \;=\; \left(1-\frac{a_3^2}{a_1^2}\right)^{\frac{1}{2}} = e \tag{204}$$

Now,

$$A_1 \;=\; \frac{2a_2a_3}{a_1^2\sin^3\chi\ \sin^2\psi}\ \left[F\left(\psi,\chi\right)-E\left(\psi,\chi\right)\right] \tag{205}$$

$$A_2 \;=\; \frac{2a_2a_3}{a_1^2\sin^3\chi\ \sin^2\psi\ \cos^2\psi}\left[E\left(\psi,\chi\right)-F\left(\psi,\chi\right)\cos^2\psi-\frac{a_3}{a_2}\sin^2\psi\ \sin\chi\right] \tag{206}$$

$$A_3 \;=\; \frac{2a_2a_3}{a_1^2\sin^3\chi\ \ \cos^2\psi}\left[\frac{a_2}{a_3}\ \sin\chi-E\left(\psi,\chi\right)\right] \tag{207}$$

For the special; case $a_1=a_2>a_3$, we have $A_1=A_2$

i.e.

$$(F-E) = \left(\frac{1}{\cos^2\psi}\right)\left[E - F\cos^2\psi - \frac{a_3}{a_1}\sin^2\psi\ \sin\chi\right] \quad (208)$$

$$\iff \cos^2\psi\,(F-E) = \left[E\left(\cos^2\psi+\sin^2\psi\right) - F\cos^2\psi - \frac{a_3}{a_1}\sin^2\psi\ \right]$$

$$= -(F-E)\cos^2\psi + \left[E - \left(1-e^2\right)^{\frac{1}{2}} e\right]\sin^2\psi$$

$$\iff 2\cos^2\psi\,(F-E) = \sin^2\psi\left[E - \left(1-e^2\right)^{\frac{1}{2}} e\right]$$

$$\therefore\ (F-E) = \left(\frac{1}{2}\right)\frac{\sin^2\psi}{\cos^2\psi}\left[E - \left(1-e^2\right)^{\frac{1}{2}} e\right] \quad (209)$$

Hence,

$$A_1 = \frac{(a_3/a_1)}{\sin^3\chi}\left(\frac{1}{\cos^2\psi}\right)\left[E - \left(1-e^2\right)^{\frac{1}{2}} e\right]$$

$$= \frac{\left(1-e^2\right)^{\frac{1}{2}}}{e^3}\cdot\left(\frac{1}{\cos^2\psi}\right)\left[E - \left(1-e^2\right)^{\frac{1}{2}} e\right]$$

$$\therefore A_1 \;=\; \left[E.\frac{(1-e^2)^{\frac{1}{2}}}{e^3} - \frac{(1-e^2)}{e^2}\right]\left(\frac{1}{\cos^2\psi}\right) \tag{210}$$

We next wish to find the potential of a homogeneous ellipsoid at an interior point. We first construct an elementary cone of solid angle $d\omega$ with its vertex at x_i The contribution to the potential at x_i by the matter included between the generators of the cone is given by :

$$d\mathfrak{B} = \tfrac{1}{2}G\rho\left(R_1^2 + R_2^2\right)d\omega$$

where R_1 and R_2 are the heights of the two half-cones diverging from x_i.

Integrating over all solid angles, noting that each elementary cone will be counted twice, we get :

$$\mathfrak{B} = \frac{1}{4}G\rho\int\left(R_1^2 + R_2^2\right)dw \tag{211}$$

If the apex of the cone is at x_i then the axis of the cone intersects the ellipsoid at :

$x_i + l_i R_1$ and $x_i + l_i R_2$

where l_i are the direction cosines of the radius vector $\mathbf{r}$, drawn from the centre of the ellipsoid parallel to the elementary cone considered.

Since these points lie on the ellipsoid, it is clear that R_1 and R_2 are the roots of the equation :

$$\sum_{i=1}^{3} \left(\frac{x_i + l_i R}{a_i} \right)^2 = 1 \tag{212}$$

i.e. $R^2 \sum_{i=1}^{3} \frac{l_i^2}{a_i^2} + 2R \sum_{i=1}^{3} \frac{x_i l_i}{a_i^2} + \left(\sum_{i=1}^{3} \frac{x_i^2}{a_i^2} - 1 \right) = 0$

so, we get on multiplying by r^2 :

$$aR^2 + bR + c = 0 \tag{213}$$

where we have written :

$$\begin{aligned} a &= 1 \\ b &= 2r^2 \sum_{i=1}^{3} \frac{x_i l_i}{a_i^2} \\ c &= r^2 \left(\sum_{i=1}^{3} \frac{x_i^2}{a_i^2} - 1 \right) \end{aligned}$$

The roots of this equation are R_1 and R_2.

So,

$$\begin{aligned}(R_1 + R_2) &= -\frac{b}{a} \\ &= -b \\ &= -2r^2 \left(\sum_{i=1}^{3} \frac{x_i l_i}{a_i^2} - 1 \right)\end{aligned}$$

substituting for each of the roots in the quadratic equation above gives :

$$\begin{aligned}R_1^2 + bR_1 + c &= 0 \\ R_2^2 + bR_2 + c &= 0\end{aligned}$$

Adding we get :

$$R_1^2 + R_2^2 + b\left(R_1 + R_2\right) + 2c = 0$$

Substituting for $(R_1 + R_2)$:

$$\begin{aligned}\left(R_1^2 + R_2^2\right) - b^2 + 2c &= 0 \\ \therefore R_1^2 + R_2^2 &= b^2 - 2c \\ &= 4r^4 \left(\sum_{i=1}^{3} \frac{x_i l_i}{a_i^2} \right)^2 + 2r^2 \left(1 - \sum_{i=1}^{3} \frac{x_i^2}{a_i^2} \right)\end{aligned}$$

Then, we can write :

$$\mathfrak{B} = \frac{1}{2}G\rho \int_s \left[2r^4 \left(\sum_{i=1}^{3} \frac{x_i l_i}{a_i^2} \right)^2 + r^2 \left(1 - \sum_{i=1}^{3} \frac{x_i^2}{a_i^2} \right) \right] d\omega$$

Now, $\int r^2 d\omega = 2\pi L$

and $\int r^4 l_i^2 d\omega = \pi a_i^3 \frac{\partial L}{\partial a_i}$

So,

$$\begin{aligned} \mathfrak{B} &= \frac{1}{2}G\rho \int_s \sum_{i=1}^{3} \left[\left(2r^4 l_i^2\right) \left(\frac{x_i^2}{a_i^4} \right) + r^2 - \frac{r^2}{a_i^2} x_i^2 \right] \\ &= \frac{1}{2}G\rho \sum_{i=1}^{3} \left[\left(\pi a^3 \frac{\partial L}{\partial a_i} \right) \left(\frac{2x_i^2}{a_i^4} \right) + (2\pi L) - \left(\frac{2\pi L}{a_i^2} \right) x_i^2 \right] \\ &= \pi G\rho \{ \sum_{i=1}^{3} \left[x_i^2 \left(\frac{1}{a_i} \frac{\partial L}{\partial a_i} - \frac{L}{a_i^2} \right) \right] + L \} \end{aligned}$$

But $A_i = \frac{L}{a_i^2} - \frac{1}{a_i} \left(\frac{\partial L}{\partial a_i} \right)$

So, $\mathfrak{B} = \pi G\rho \left[L - \sum_{i=1}^{3} A_i x_i^2 \right]$

Now by definition,

$\mathfrak{W}_{ij} = \int_v \rho x_i \frac{\partial \mathfrak{B}}{\partial x_j} d\mathbf{x}$

We have

$$\frac{\partial \mathfrak{B}}{\partial x_j} = \frac{\partial}{\partial x_j}\left[\pi G\rho\left(L - \sum_{l=1}^{3} A_l x_l^2\right)\right] \tag{214}$$

$$= \pi G\rho(-2)\sum_{j=1}^{3} A_l x_l \delta_{lj} \tag{215}$$

$$= -2\pi G\rho \sum_{j=1}^{3} A_j x_j \tag{216}$$

Then,

$\frac{\mathfrak{W}}{\pi G\rho} = -2\int_v \rho \sum_{j=1}^{3} A_j x_j d\mathbf{x}$

But,

$I_{ij} = \int_v \rho x_i x_j d\mathbf{x}$

Consequently,

$$\frac{\mathfrak{W}_{ij}}{\pi G\rho} = -2A_i I_{ij} \tag{217}$$

B Table of Symbols

Symbol	Meaning	Page reference
Ω	angular velocity	1
ϵ	ellipticity	3
ξ	vorticity	6
r_{sec}	secular instability limit	11
E	energy	12
J	angular momentum	12
z	cylindrical polar coordinate z	29
ρ	cylindrical polar coordinate ρ	29, Ch.2 only
	density(of fluid star)	40, except Ch. 2
m_{NS}	mass of neutron star	43
m_{NS}	mass of black hole	41
r_{NS}	radius of neutron star	28
R	distance from BH to (fluid element of) star	41
P	pressure (at a point on fluid star)	41
ϕ	gravitational potential	28
ϕ_{NS}	gravitational potential of neutron star	28
ϕ_{BH}	gravitational potential of black hole	40

Symbol	Meaning	Page reference
x	position vector of fluid element	41
$\mathfrak{B}$	gravitational potential	41
$\mathfrak{W}$	potential energy associated with the gravitational potential energy	45
u	velocity of fluid element	41
I	moment of inertia	44
$\mathfrak{I}$	kinetic energy of system	44
p	mass ratio $p = \frac{m_{NS}}{m_{BH}}$	31
Q	mass ratio $Q = \frac{1}{p} = \frac{m_{BH}}{m_{NS}}$	31
q	ratio of radii $q = \frac{r_1}{r_2}$	135
a_i	semi-axes of ellipsoid	134
ω	solid angle dω of an elementary cone with its vertex at the centre	135
r	radius of body	6
G	Universal Gravitational Constant	29
z_c	Critical radius	**??**

C Abbreviations Used

Abbreviation	Meaning
BBH	Binary Black Hole
BH	Black Hole
BHNS	Black Hole - Neutron Star
BNS	Binary Neutron Star
DNS	Double Neutron Star
ELF	Extremely Low Frequency (Band)
EOS	Equation of State
GR	General Relativity
GRB	Gamma-Ray Bursts
GW	Gravitational Wave
HF	High-Frequency (Band)
ISCO	Innermost Stable Circular Orbit
LF	Low-Frequency (Band)
LIGO	Laser Interferometer Gravitational Wave Observatory
LISA	Laser Interferometer Space Antenna
NS	Neutron Star
NSBH	Neutron Star - Black Hole
VLF	Very Low Frequency (Band)

D Journal Abbreviations

Abbreviation	Journal
arXiv	ArXiv e-prints
astro.ph	ArXiv Astrophysics e-prints
gr.qc	ArXiv General Relativity and Quantum Cosmology e-prints
A&A	Astronomy and Astrophysics
ApJ	Astrophysical Journal
ApJS	Astrophysical Journal Supplement Series
ApL	Astrophysical Letters
CQGra	Classical and Quantum Gravity
IJMPD	International Journal of Modern Physics D
MNRAS	Monthly Notices of the Royal Astronomical Society
NIMPA	Nuclear Instruments and Methods in Physics Research A
PNAS	Proceedings of the National Academy of Science
PhRvD	Physical Review D
PhRvL	Physical Review Letters
PNAS	Proceedings of the National Academy of Science
PThPh	Progress of Theoretical Physics
PASJ	Publications of the Astronomical Society of Japan

List of Figures

List of Tables

References

Abramovici, A., et al., 1992. LIGO: The Laser Interferometer Gravitational-Wave Observatory. *Science*, **256**(5055), 325.

Aizenman, M. L., 1968. The Equilibrium and the Stability of the Roche-Riemann Ellipsoids. *ApJ.*, **153**, 511.

Arun, K. G., 2006. Parameter estimation of coalescing supermassive black hole binaries with LISA. *PhRvD*, **74**, 024025.

Baade, W. and Zwicky, F., 1934. Cosmic rays from super-novae. *PNAS*, **20**, 259.

Baker, J.G., Centrella, J., Choi, D.I., Koppitz, M. and van Meter, J., 2006. Binary black hole merger dynamics and waveforms. *PhRvD*, **73**, 104002.

Baker, J., Campanelli, M., Lousto, C. O. and Takahashi, R., 2002. Modeling gravitational radiation from coalescing binary black holes. *PhRvD*, **65**, 124012.

Baker, J., Brügmann, B., Campanelli, M., Lousto, C. O. and Takahashi,R., 2001. Plunge Waveforms from Inspiralling Binary Black Holes *PhRvL*, **87**, 121103.

Baumgarte, T. W., 2000. Innermost stable circular orbit of binary black holes. *PhRvL*, **62**(2), 024018.

Baumgarte, T. W., Cook, G. B., Scheel, M. A., Shapiro, S. L. and Teukolsky, S. A. 1997. Binary Neutron Stars in General Relativity: Quasiequilibrium Models. *PhRvL*, **79**(7), 1182.

Baumgarte, T. W., Cook, G. B., Scheel, M. A., Shapiro, S. L. and Teukolsky, S. A. 1998a. Stability of relativistic neutron stars in binary orbit. *PhRvD*, **57**, 6181.

Baumgarte, T. W., Cook, G. B., Scheel, M. A., Shapiro, S. L. and Teukolsky, S. A. 1998b. General relativistic models of binary neutron stars in quasiequilibrium. *PhRvD*, **57**, 7299.

Baumgarte, T. W. and Shapiro, S. L. 2003. Numerical Relativity and Com-

pact Binaries. *Physics Report*, 376, 41.

Baumgarte, T. W., Skoge, M. L. and Shapiro, S. L. 2004. Black hole-neutron star binaries in general relativity: Quasiequilibrium formulation. *PhRvD*, **70**, 064040.

Belczynski, K., and Bulik, T., 1999. The effect of supernova natal kicks on compact object merger rate. *A&A*, **346**, 91.

Bethe, H. and Brown, G., 1998. Evolution of Binary Compact Objects That Merge. *ApJ*, **506**(2), 780.

Berti, E., Iyer, S. and Will, C. M., 2007. A post-Newtonian diagnosis of quasiequilibrium configurations of neutron star-neutron star and neutron star-black hole binaries. eprint arXiv:0709.2589.

Berti, E., Iyer, S. and Will, C. M., 2006. Eccentricity content of binary black hole initial data. *PhRvD*, **74**, 061503.

Bildsten, L. and Cutler, C., 1992. Tidal Interactions of Inspiraling Compact Binaries. *ApJ*, **400**, 175.

Bishop, N. T., Gómez, R., Lehner, L., Maharaj, M. and Winicour, J., 2005. Characteristic initial data for a star orbiting a black hole. *PhRvD*, **72**, 024002.

Blanchet, L., Damour, T., Iyer, B. R., Will, C. M. and Wiseman, A. G., 1995. Gravitational radiation damping of compact binary systems to second post- Newtonian order. *PhRvL*, **74**(18), 3515.

Blanchet, L., 2002. Innermost circular orbit of binary black holes at the third post-Newtonian approximation. *PhRvD*, **65**(12), 4009.

Bonazzola, S., Gourgoulhon, E. and Marck, J.-A., (1998). Numerical approach for high precision 3D relativistic star models. *PhRvD*, **58**(10), 104020.

Bonazzola, S., Gourgoulhon, E. and Marck, J.-A., 1999. Numerical Models of Irrotational Binary Neutron Stars in General Relativity. *PhRvL*, **82**(5), 892.

Bradaschia, C. et al., 1990. The VIRGO Project: A wide band antenna for gravitational wave detection. *NIMPA*, **289**(3), 518.

Buonanno, A., Cook, G. B. and Pretorius, F., 2007. Inspiral, merger, and ring-down of equal-mass black-hole binaries. *PhRvD*, **75**, 124018.

Buonanno, A. Damour, T., 2000. Transition from inspiral to plunge in binary black hole coalescences. *PhRvD*, **62**, 064015.

Campanelli, M., Lousto, C.O., Marronetti, P. and Zlochower, Y., 2006. Accurate Evolutions of Orbiting Black-Hole Binaries without Excision. *PhRvL*, **96**, 111101.

Carter, B. and Luminet, J. P. 1982. Pancake detonation of stars by black holes in galactic nuclei. *Nature*, **296**, 211.

Carter, B. and Luminet, J.-P. 1983. Tidal compression of a star by a large black hole. I Mechanical evolution and nuclear energy release by proton capture. *A&A*, **121**(1), 97.

Carter, B. and Luminet, J.-P. 1985. Mechanics of the affine star model. *MNRAS*, **212**, 23.

Carter, B. and Luminet, J.-P. 1986. Dynamics of an affine star model in a black hole tidal field. *ApJS*, **61**, 219.

Caudill, M., Cook, G. B., Grigsby, J. D. and Pfeiffer, H. P., 2006. Circular orbits and spin in black-hole initial data. *PhRvD*, **74**, 064011.

Chandrasekhar, S., 1932. Some remarks on the state of matter in the interior of Stars. *Zeitschrift für Astrophysik*, **5**(5), 321.

Chandrasekhar, S., 1963. The virial theorem in general relativity in the post newtonian approximation. *PNAS*, **49**(5), 608.

Chandrasekhar, S., 1965. The post newtonian Equation of hydrodynamics in general relativity. *ApJ*, **142**(4), 1488.

Chandrasekhar, S., 1967. *An Introduction to the Study of Stellar Structure*. New York: Dover

Chandrasekhar, S., 1969. *Ellipsoidal Figures of Equilibrium*. New Haven: Yale University Press.

Cook, G. B. 1994. Three-dimensional initial data for the collision of two black holes. II. Quasicircular orbits for equal-mass black holes. *PhRvD*, **50**(8), 5025.

Cutler, C. et al., 1993. The last three minutes: Issues in gravitational-wave measurements of coalescing compact binaries. *PhRvL*, **70**(20) 2984.

Damour, T., 2007. Black Hole and Neutron Star Binaries: Theoretical Challenges. eprint arXiv:0705.3109v1.

Jaranowski, P. and Schäfer, G., 2000. On the determination of the last stable orbit for circular general relativistic binaries at the third post-Newtonian approximation. *PhRvD*, **62**, 084011.

Davies, M.B., Levan, A.J. and King, A., 2005. The ultimate outcome of black hole - neutron star mergers. *MNRAS*, **356**(1), 54.

de Freitas Pacheco, J.A., Regimbau, T., Vincent, S., and Spallicci, A., 2006. Expected Coalescence Rates of Ns - Ns Binaries for Laser Beam Interferometers. *IJMPD*, **15**, 235.

Duez, M. D., Baumgarte, T.W., Shapiro, S. L., Shibata, M. and Uryū, K., 2002. Comparing the inspiral of irrotational and corotational binary neutron stars. *PhRvD*, **65**, 024016.

Eriguchi, Y. and Hachisu, I., 1983. Gravitational Equilibrium of a Multi-Body Fluid System. *PThPh*, **70**(6), 1534.

Faber, J. A., Baumgarte, T. W., Shapiro, S. L. and Taniguchi, K., 2006. General Relativistic Binary Merger Simulations and Short Gamma-Ray Bursts. *ApJ*, **641**(2), L93.

Faber, J. A., Baumgarte, T. W., Shapiro, S. L., Taniguchi, K. and Rasio, F. A., 2006. Dynamical evolution of black hole-neutron star binaries in general relativity: Simulations of tidal disruption. *PhRvD*, **73**, 024012.

Faber, J. A., Grandclément, P. and Rasio, F. A., 2004. Mergers of irrotational neutron star binaries in conformally flat gravity. *PhRvD*, **69**, 124036.

Faber, J. A., Grandclément, P., Rasio, F. A. and Taniguchi, K., 2002. Measuring Neutron-Star Radii with Gravitational-Wave Detectors. *PhRvL*, **89**, 231102.

Faber, J. A.and Rasio, F. A., 2002. Post-Newtonian SPH calculations of binary neutron star coalescence. III. Irrotational systems and gravitational wave spectra. *PhRvD*, **65**, 084042

Faber, J. A.and Rasio, F. A., 2000. Post-Newtonian SPH calculations of binary neutron star coalescence: Method and first results. *PhRvD*, **62**(6), 064012.

Fishbone, L.G., 1973. The Relativistic Roche Problem. I. Equilibrium Theory for a Body in Equatorial, Circular Orbit around a Kerr Black Hole. *ApJ*, **185**, 43.

Gourgoulhon, E., Grandclément, P., Taniguchi, K., Marck, J.-A. and Bonazzola, S., 2001. Quasiequilibrium sequences of synchronized and irrotational binary neutron stars in general relativity: Method and tests. *PhRvD*, 63, 064029.

Gourgoulhon, E., Grandclément, P. and Bonazzola, S. 2002. Quasiequilibrium sequences of synchronized and irrotational binary neutron stars in general relativity: Method and tests. *PhRvD*, 65, 044020.

Grandclément, P., Gourgoulhon, E. and Bonazzola, S., 2002. Binary black holes in circular orbits. II. Numerical methods and first results. *Phys. Rev. D*, 65, 044021.

Grandclément, P., 2006. Accurate and realistic initial data for black hole - neutron star binaries. *PhRvD*, **74**, 124002, [Erratum-ibid. 2007. D **75**, 129903].

Hachisu I., 1986. A versatile method for obtaining structures of rapidly rotating stars. II - Three-dimensional self-consistent field method. *ApJS*, **62**, 461.

Hachisu I. and Eriguchi Y., 1984a. Fission of dumbbell equilibrium and binary state of rapidly rotating polytropes. *PASJ*, **36**, 239.

Hachisu I. and Eriguchi Y., 1984b, Binary fluid star *PASJ*, **36**, 259.

Hilditch, R. W., 2001. *An introduction to close binary stars.* Cambridge: Cambridge University Press.

Hulse, R.A., and Taylor, J.H., 1975. Discovery of a pulsar in a binary system.

PhRvL, 195, L51.

Ishii, M., Shibata, M. and Mino, Y., 2005. Black hole tidal problem in the Fermi normal coordinates. *PhRvD*, 71, 044017.

Ivanov, P.B. and Novikov, I.D., 2001. A New Model of a Tidally Disrupted Star. *ApJ*, **549**, 467.

Kalogera, V., Kim, C., Lorimer, D. R., Burgay, M., D'Amico, N., Possenti, A., Manchester, R. N., Lyne, A. G., Joshi, B. C., McLaughlin, M. A., Kramer, M., Sarkissian, J. M. and Camilo, F., 2004. The Cosmic Coalescence Rates for Double Neutron Star Binaries *ApL*, **601**, L179.

Kalogera, V., Narayan, R., Spergel, D.N., and Taylor, J.H., 2001. The Coalescence Rate of Double Neutron Star Systems. *ApJ*, **556**, 340.

Kidder, L. E., Will C. M. and Wiseman A. G., 1992. Innermost stable orbits for coalescing binary systems of compact objects. *CQGra*, **9**(9), L125.

Kidder, L. E., Will C. M. and Wiseman A. G., 1993. Coalescing binary systems of compact objects to (post)$^{\frac{5}{2}}$-Newtonian order. III. Transition from

inspiral to plunge. *PhRvD*, **47**,(8), 3281.

Kippenhahn,R. and Weigert, A., 1991. *Stellar structure and evolution.* Berlin: Springer.

Kluzniak, W. and Lee, W.H., 1998.Simulations of Binary Coalescence of a Neutron Star and a Black Hole. *ApJ*, **494**, L53.

Kochanek, C. S., 1992. Coalescing binary neutron stars. *ApJ*, **398**, 234.

Kopal, Z., 1959. *Close Binary Systems.* London: Chapman and Hall.

Kopal, Z., 1978. *Dynamics of Close Binary Systems.* Dordrecht: Reidel.

Kosovichev, A. G. and Novikov, I. D., 1992. Non-linear effects at tidal capture of stars by a massive black hole. I - Incompressible affine model. *MNRAS*, **258**(4), 715.

Lai, D., 1996. Tidal Stablization of Neutron Stars and White Dwarfs. *PhRvL*, **76**(26), 4878.

Lai D., Rasio F. A. and Shapiro S. L., 1993a. Hydrodynamic instability and coalescence of close binary systems. *ApJ*, **406**(2), L63.

Lai D., Rasio F. A. and Shapiro S. L., 1993b. Ellipsoidal figures of equilibrium - Compressible models. *ApJS*, **88**, 205.

Lai D., Rasio F. A. and Shapiro S. L., 1994a. Hydrodynamic instability and coalescence of binary neutron stars. *ApJ*, **420**, 811.

Lai D., Rasio F. A. and Shapiro S. L., 1994b. Equilibrium, stability, and orbital evolution of close binary systems. *ApJ*, **423**, 344.

Lai, D., Rasio, F.A. and Shapiro, S.L., 1994c. Hydrodynamics of rotating stars and close binary interactions: Compressible ellipsoid models. *ApJ*, **437**, 742.

Lai, D. and Wiseman, A.G., 1996. Innermost stable circular orbit of inspiraling neutron-star binaries: Tidal effects, post-Newtonian effects, and the neutron-star equation of state. *PhRvD*, **D54**(6), 3958.

Lattimer, J. M. and Schramm, D. N., 1976. The tidal disruption of neu-

tron stars by black holes in close binaries. *ApJ*, **210**, L549.

Lee, W.H., 2000. Newtonian hydrodynamics of the coalescence of black holes with neutron stars - III. Irrotational binaries with a stiff equation of state. *MNRAS*, **318**(2), 606.

Lee, W.H., 2001. Newtonian hydrodynamics of the coalescence of black holes with neutron stars - IV. Irrotational binaries with a soft equation of state *MNRAS*, **328**(2), 583.

Lee, W.H. and Kluzniak, W., 1999. Newtonian Hydrodynamics of the Coalescence of Black Holes with Neutron Stars. I. Tidally Locked Binaries with a Stiff Equation of State. *ApJ*, **526**(1), 178.

Lee, W.H. and Kluzniak, W., 1999. Newtonian hydrodynamics of the coalescence of black holes with neutron stars - II. Tidally locked binaries with a soft equation of state. *MNRAS*, **308**(3), 780.

Lipunov, V., Postnov, K., and Prokhorov, M., 1997. Formation and coalescence of relativistic binary stars: the effect of kick velocity. *MNRAS*, **288**(1), 245.

Löffler, F., Rezzolla, L. and Ansorg, M., 2006. Numerical evolutions of a black hole-neutron star system in full general relativity: Head-on collision. *PhRvD*, **74**, 104018.

Lombardi J. C., Rasio F. A. and Shapiro S. L., 1997. Post-Newtonian models of binary neutron stars. *PhRvD*, **56**(6), 3416.

Luminet, J.-P. and Carter, B., 1986. Dynamics of an affine star model in a black hole tidal field. *ApJS*, **61**, 219.

Marronetti, P., Mathews, G. J. and Wilson, J. R., 1998. Binary neutron-star systems: From the Newtonian regime to the last stable orbit. *PhRvD*, **58**, 107503.

Mashhoon, B., 1975. *ApJ*, On tidal phenomena in a strong gravitational field. **197**, 705.

Miller, M., 2001. General Relativistic Initial Data for the Binary Black Hole / Neutron Star System in Quasicircular Orbit. eprint arXiv:gr-qc/0106017v1.

Misner, C.W., Thorne, K.S. and Wheeler, J.A., 1973. *Gravitation.* San Francisco: Freeman.

Mora, T. and Will, C. M., 2002. Numerically generated quasiequilibrium orbits of black holes: Circular or eccentric? *PhRvD*, **66**, 101501(R).

Mora, T. and Will, C. M., 2004. Post-Newtonian diagnostic of quasiequilibrium binary configurations of compact objects. *PhRvD*, **69**, 104021.

Motl, P.M., Tohline, J.E. and Frank, J., 2002. Numerical Methods for the Simulation of Dynamical Mass Transfer in Binaries. *ApJS*, **138**(1), 121.

Narayan, R., Piran, T. and Shemi, A., 1991. Neutron star and black hole binaries in the Galaxy. *ApJ*, **379**(2), L17.

Narlikar, J.V., 1993. *Introduction to Cosmology.* Cambridge: Cambridge University Press.

Narlikar, J.V., 1996. *The Lighter Side of Gravity.* Cambridge: Cambridge University Press.

Nelemans, G., Portegies Zwart, S.F., Verbunt, F., and Yungelson, L.R., 2001. Population synthesis for double white dwarfs. II. Semi-detached systems: AM CVn stars. *A&A*, **368**, 939.

Nduka, A., 1971. The Roche Problem in an Eccentric Orbit. *ApJ*, **170**, 131.

Ori, A. and Thorne, K.S., 2000. Transition from inspiral to plunge for a compact body in a circular equatorial orbit around a massive, spinning black hole. *PhRvD*, **62**(12), 124022.

O'Shaughnessy, R., Kim, C., Fragos, T., Kalogera, V., and Belczynski, K., 2005. ConstrainingPopulation Synthesis Models via the Binary Neutron Star Population. *ApJ.*, **633**, 1076.

Padmanabhan, T., 1993. *Structure Formation in the Universe.* Cambridge: Cambridge University Press.

Paczyńsky B., 1986. Gamma-ray bursters at cosmological distances *ApJ*, **308**(2), L43.

Paczyńsky B. and P. J. Wiita, 1980. Thick accretion disks and supercritical luminosities. *A&A*, **88**, 23.

Pfahl, E., Podsiadlowski, P. and Rappaport, S. 2005. Relativistic Binary Pulsars with Black Hole Companions. *ApJ*, **628**, 343.

Pfeiffer, H.P. Teukolsky, S.A. and Cook, G.B., 2000. Quasicircular orbits for spinning binary black holes. *PhRvD*, **62**, 104018.

Poisson, E. and Will, C.M., 1995. Gravitational waves from inspiraling compact binaries: Parameter estimation using second-post-Newtonian waveforms. *PhRvD*, **52**(2), 848.

Portegies Zwart, S.F., 1998. Gamma-Ray Binaries: Stable Mass Transfer from a Neutron Star to a Black Hole. *ApJ*, **503**, L53.

Portegies Zwart, S.F. and Yungelson, L.R., 1998. Formation and evolution of binary neutron stars. *A&A*, **332**, 173.

Postnov, K.A. and Yungelson, L.R., 2006. The Evolution of Compact Binary Star Systems. *Living Reviews in Relativity*, **9**(6).

Pretorius, F., 2006. Simulation of binary black hole spacetimes with a harmonic evolution scheme. *CQGra*, **23**, S529.

Pretorius, F., 2005. Evolution of Binary Black-Hole Spacetimes. *PhRvL*, **95**(12) 121101.

Price, R.H. and Pullin, J., 1994. Colliding black holes: The close limit. *PhRvL*, **72**(21), 3297.

Rantsiou, E., Kobayashi, S., Laguna, P. and Rasio, F., 2007. Mergers of Black Hole - Neutron Star binaries. I. Methods and First Results. eprint arXiv:astro.ph/0703599.

Rasio, F. A. and Shapiro S. L., 1994. Hydrodynamics of binary coalescence. 1: Polytropes with stiff equations of state. *ApJ*, **432**, 242.

Rasio F. A. and Shapiro S. L., 1996. in Compact Stars in Binaries, proceedings of IAU Symposium 165, eds. van Paradijs J., van den Heuvel E. P. J., Kuulkers E., Dordrecht: Kluwer Academic Publishers.

Rosswog, S., 2005. On the viability of neutron star black hole binaries as central engines of gamma-ray bursts. eprint arXiv:astro-ph/0505007v1.

Rosswog, S., Speith,R. and Wynn, G. A., 2004. Accretion dynamics in neutron star - black hole binaries. *MNRAS*, **351**,(4), 1121.

Shapiro S. L. and Teukolsky S. A., 1983. *Black Holes, White Dwarfs and Neutron Stars*. New York: Wiley.

Shibata, M., 1996. Relativistic Roche-Riemann Problems around a Black Hole. *PThPh*, **96**,(5), 917.

Shibata M., 1997. Numerical study of synchronized binary neutron stars in the post-Newtonian approximation of general relativity. *PhRvD*, **55**,(10), 6019.

Shibata, M. and Sasaki, M., 1998. Innermost Stable Circular Orbits around Relativistic Rotating Stars. *PhRvD*, **58**, 104011.

Shibata, M. and Taniguchi, K., 2007. Merger of black hole and neutron star in general relativity: Tidal disruption, torus mass, and gravitational

waves. *PhRvD*, submitted, [preprint: arXiv:0711.1410].

Shibata, M. and Taniguchi, K., 2006. Merger of binary neutron stars to a black hole: Disk mass, short gamma-ray bursts, and quasinormal mode ringing. *PhRvD*, **73**, 064027.

Shibata, M., Taniguchi, K. and Uryu, K., 2005. Merger of binary neutron stars with realistic equations of state in full general relativity. *PhRvD*, **71**(8), 084021.

Shibata, M. and Uryū, K. 2007. Merger of black hole neutron star binaries in full general relativity. *CQGra*, **24**(12) S125.

Shibata, M. and Uryū, K., 2006. Merger of black hole-neutron star binaries: Nonspinning black hole case. *PhRvD*, **74**, 121503(R).

Shibata, M. and Uryū, K. 2001. Computation of gravitational waves from inspiraling binary neutron stars in quasiequilibrium circular orbits: Formulation and calibration. *PhRvD*, **64**, 104017.

Sopuerta, C. F., Sperhake, U. and Laguna, P. 2006. Hydro-without-hydro

framework for simulations of black hole neutron star binaries. *CQGra*, **23**,(16), S579.

Stairs, I.H., 2004. Pulsars in Binary Systems: Probing Binary Stellar Evolution and General Relativity. *Science*, **304**(5670), 547.

Taniguchi, K., Baumgarte, T. W., Faber, J. A. and Shapiro, S. L., 2007a. Relativistic black hole-neutron star binaries in quasiequilibrium: effects of the black hole excision boundary condition. *PhRvD*, submitted, [preprint arXiv:0710.5169v1].

Taniguchi, K., Baumgarte, T. W., Faber, J. A. and Shapiro, S. L., 2007b. Quasiequilibrium black hole-neutron star binaries in general relativity. *PhRvD*, **75**, 084005.

Taniguchi, K., Baumgarte, T. W., Faber, J. A. and Shapiro, S. L., 2006. Quasiequilibrium sequences of black hole - neutron star binaries in general relativity. *PhRvD*, **74**, 041502(R).

Taniguchi, K., Baumgarte, T. W., Faber, J. A. and Shapiro, S. L., 2005. Black hole-neutron star binaries in general relativity: Effects of neutron star

spin. *PhRvD*, **72**, 044008.

Taniguchi K. and Nakamura T., 1996. Innermost Stable Circular Orbit of Coalescing Neutron Star-Black HoleBinary. *PThPh*, **96**,(4), 693.

Taniguchi, K. and Nakamura, T., 2000a. Almost Analytic Solutions to Equilibrium Sequences of Irrotational Binary Polytropic Stars for $n = 1$. *PhRvL*, **84**,(4), 581.

Taniguchi, K. and Nakamura, T., 2000b. Equilibrium sequences of irrotational binary polytropic stars: The case of double polytropic stars. *PhRvD*, **62**, 044040.

Taniguchi, K. and Shibata, M., 1997. Solving the Darwin problem in the first post-Newtonian approximation of general relativity *PhRvD*, **56**, 798.

Taylor, J. H. and Weisberg, J. M., 1982. A new test of general relativity - Gravitational radiation and the binary pulsar PSR 1913+16. *ApJ*, **253**(1), 908.

Taylor, J. H. and Weisberg, J. M., 1989. Further experimental tests of rela-

tivistic gravity using the binary pulsar PSR 1913 + 16. *ApJ*, **345**(1), 434.

Todhunter, I., 1873. *A History Of The Mathematical Theories Of Attraction And The Figure Of The Earth From The Time Of Newton To That Of Laplace*. London: MacMillan and Company.

Tsokaros, A.A. and Uryū, K., 2007. Numerical method for binary black hole/neutron star initial data: Code Test. *PhRvD*, **75**(4), 044026.

Tutukov, A. V. and Yungelson, L. R., 1993. The merger rate of neutron star and black hole binaries. *MNRAS*, **260**(3), 675.

Uryū, K. and Eriguchi, Y., 1996. Existence of non-axisymmetric polytropes sustained by internal motions. *MNRAS*, **282**(2), 653.

Uryū, K. and Eriguchi, Y., 1998a. Stationary structures of irrotational binary systems: Models for close binary systems of compact stars. *ApJ*, **118**(2), 563.

Uryū, K. and Eriguchi, Y., 1998b. Stationary states of irrotational binary neutron star systems and their evolution as a result of gravitational wave emission. *MNRAS*, **296**(1), L1.

Uryū, K. and Eriguchi, Y., 1998c. Incompressible fluid binary systems with internal flows - models of close binary neutron star systems with spin. *MNRAS*, **299**(2), 575.

Uryū, K. and Eriguchi, Y., 1999. Newtonian Models for black hole-gaseous star close binary systems. *MNRAS*, **303**(2) 329.

Uryū, K. and Eriguchi, Y., 2000. New numerical method for constructing quasiequilibrium sequences of irrotational binary neutron stars in general relativity. *PhRvD*, **61**, 124023.

Uryū, K., Shibata, M. and Eriguchi, Y., 2000. Properties of general relativistic, irrotational binary neutron stars in close quasiequilibrium orbits: Polytropic equations of state. *PhRvD*, **62**, 104015.

Usui, F., Uryū, K. and Eriguchi, Y., 2000. New numerical scheme to compute three-dimensional configurations of quasiequilibrium compact stars in general relativity: Application to synchronously rotating binary star systems. *PhRvD*, **61**, 024039.

Vallisneri, M., 2000. Prospects for Gravitational - Wave Observations of Neutron - Star Tidal Disruption in Neutron Star - Black Hole Binaries. *PhRvL*, **84**(16), 3519.

van den Heuvel, E.P.J. and Lorimer D.R., 1996. On the galactic and cosmic merger rate of double neutron stars. *MNRAS*, **283**, L37.

Voss, R., and Tauris, T.M., 2003. Galactic distribution of merging neutron stars and black holes - Prospects for short gamma-ray burst progenitors and LIGO/VIRGO. *MNRAS*, **342**, 1169.

Wiggins, P and Lai, D., 2000. Tidal Interaction between a Fluid Star and a Kerr Black Hole in Circular Orbit. *ApJ*, **532**, 1.

Wilson, J. R. and Mathews, G. J., 1995. Instabilities in Close Neutron Star Binaries. *PhRvL*, **75**, 4161.